Beyond photon pairs

Yorulmaz, S.Ç.

Beyond photon pairs

Saime Çiğdem Yorulmaz

Beyond photon pairs

PROEFSCHRIFT

ter verkrijging van
de graad van Doctor aan de Universiteit Leiden,
op gezag van Rector Magnificus prof. mr. C. J. J. M. Stolker,
volgens besluit van het College voor Promoties
te verdedigen op dinsdag 10 juni 2014
klokke 13:45 uur

door

Saime Çiğdem Yorulmaz

geboren te Denizli, Turkije
in 1983

Promotiecommissie:

Promotor:	Prof. dr. E. R. Eliel	
Co-promotor:	Dr. M. J. A. de Dood	
Leden:	Prof. dr. K. S. E. Eikema	(Vrije Universiteit Amsterdam)
	Dr. S. F. Pereira	(Technische Universiteit Delft)
	Prof. dr. J. M. van Ruitenbeek	
	Prof. dr. G. Nienhuis	
	Dr. M. P. van Exter	

The research reported in this thesis was conducted at the 'Leids Instituut voor Onderzoek in de Natuurkunde' (LION). This work is a part of the research program of the 'Stichting voor Fundamenteel Onderzoek der Materie' (FOM), which is financially supported by the Netherlands Organization for Scientific Research (NWO).

An electronic version of this dissertation is available at the Leiden University Repository (https://openaccess.leidenuniv.nl).

Casimir PhD series, Delft-Leiden 2014-11
ISBN: 978-90-8593-186-7

Contents

CHAPTER 1

Introduction

1.1 Quantum states of light

The quantum nature of light is commonly treated by introducing the *photon*, quanta of the radiation field that can be thought of as individual particles with well-defined energy and momentum. The wave or coherence properties of the photon are incorporated in its quantum-mechanical wave function. Because light fields generally contain more than a single photon, a description in terms of multi-particle states is introduced that reflects the relevant statistical properties of the light [1]. In all cases, the quantum state of the light can be expressed as a sum over states with a different number of photons.

Possibly the easiest, non-trivial, quantum state of light is that of a photonic qubit containing only a single photon. Such a qubit can be created if the photon can exist in two distinct states, labeled as '0' and '1'. Note that we limit the discussion here to optical implementations of qubits, although analogous systems have been realized using e.g. the electron spin stored in the excited states of an atom or ion [2]. For photon-based qubits, a common implementation is to use the polarization of light, where two orthogonal polarizations, for instance horizontal and vertical, are used to define the '0' and '1'. The polarization degree of freedom is appealing as it gives an insightful binary system that is accessible in experiments by the use of conventional polarization optics and photon detectors.

The distinctive feature of qubits, or quantum bits, over classical bits is that they also can exist in a quantum-mechanical superposition of the states '0'

and '1'. In that case, the state of the qubit is given by $\Psi = \alpha|0\rangle + \sqrt{1-\alpha^2}|1\rangle$, where α is the probability amplitude of the particle being in the state $|0\rangle$. As a consequence, a single qubit contains much more (quantum) information than the corresponding classical bit. While the classical bit has two possible realizations, the quantum state of the qubit is described by a vector in a two-dimensional Hilbert space.

1.2 High-dimensional quantum states

The practical applications of individual qubits are perhaps limited to quantum cryptography, which relies on the projection postulate of quantum mechanics. Simply, this postulate states that a measurement of a quantum state necessarily projects the quantum state onto an eigenstate of the system. More interesting quantum states can be created by coupling two (or more) qubits together. Most notably, two qubits can be joined to create an entangled state. This entangled state is a two-particle superposition that has no classical counterpart. The persistence of correlations between the two particles in different measurement basis has been used to verify the validity of quantum mechanics by a violation of Bell's inequalities [3].

The fields of quantum information processing and quantum computation put considerable effort in extending quantum states beyond the notion of a single qubit, and in using quantum information and entanglement as a resource. In quantum computation, multiple qubits are coupled together using quantum logical gates to define a system of n coupled qubits. Quantum computation focuses almost exclusively on qubits and two-qubit gates as this system is believed to lead to a scalable implementation [4]. The resulting quantum system of n coupled qubits should be described by a 2^n-dimensional Hilbert space and computations can be realized by a projection of this quantum state by using the process of measurement.

A different line of research tries to expand the information carrying capacity of indivudual particles by extending the number of possible states for a single particle to *more than two states*. Instead of employing a qubit, one uses a quNit, i.e. a quantum state with N possible modes that resides in an N-dimensional Hilbert space. The creation of two entangled quNits creates a quantum system that should be described by a N^2-dimensional Hilbert space. Such high-dimensional two-quNit states can be created by exploiting e.g. the

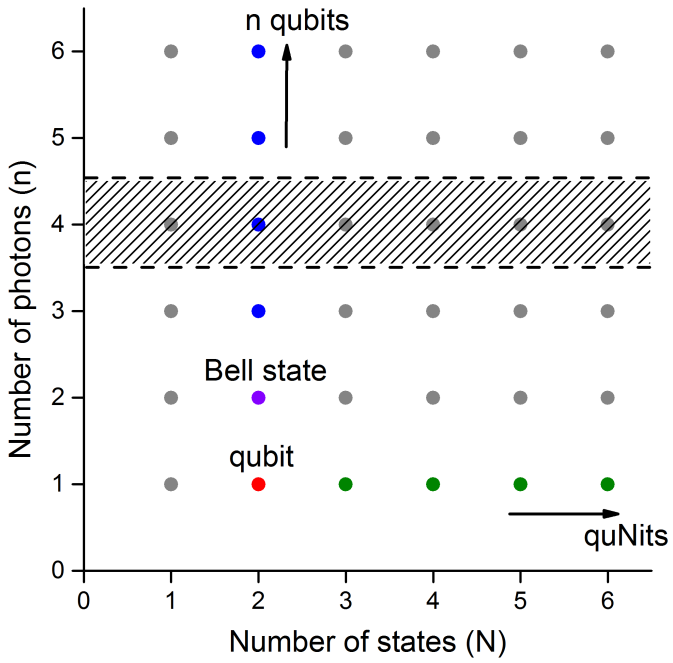

Figure 1.1: Schematic classification of high-dimensional quantum states. The number of photons n is shown on the vertical axis, while the number of states N, available to each photon, is on the horizontal axis. In this thesis we explore the shaded area of four-photons combined with variety of states per photon.

temporal [5], frequency [6] or spatial [7] properties of an optical field.

Both approaches, that of multiple qubits [8, 9] as well as that of two quNits [10–12] have been studied experimentally in various implementations. Figure 1.1 brings these two approaches together by showing a classification of all possible implementation of high-dimensional quantum systems. The blue and green dots in the vertical and horizontal direction of the Fig. 1.1 indicate the commonly explored systems of n-coupled qubits and two coupled quNits, respectively. Red and purple dots correspond to a single qubit and Bell state. This thesis will explore the relatively uncharted territory of multiple (more than two) high-dimensional particles. This territory is

indicated by the shaded area in Fig.1.1. In the case of photons, these high-dimensional multi-particle states can be created by stimulated parametric down-conversion in a non-linear crystal.

1.3 Spontaneous parametric down-conversion

Spontaneous parametric down-conversion (SPDC) is a second-order nonlinear process, that can be utilized to create entangled photon pairs [13]. In this process, a blue pump photon spontaneously splits into two red photons, called signal and idler photons for historical reasons. The two photons have a combined energy and momentum equal to the energy and momentum of the pump photon. The process of SPDC cannot be explained by the classical theories of three wave mixing because the average input field strength at the signal and idler frequency is zero. In a description where the radiation field is quantized, SPDC occurs in the nonlinear crystal as random vacuum fluctuations initiate the down-conversion of the pump photon [14].

The experimental results presented in this thesis are based on parametric down-conversion (PDC), an extension of SPDC that allows to create not just single photon pairs but also double pairs, triple pairs, etc. The number of pairs produced in either SPDC or PDC depends critically on the phase mismatch ΔkL between the pump and down-converted photons, where L is the crystal length. Thus, it is important to understand this phase matching in detail. However, the yield in parametric down-conversion is always very low, it is much more attractive to analyze and study phase matching in the reverse process, where two low-frequency photons join up to create a single photon at the sum energy. This is the process of second-harmonic generation (SHG), well known from classical nonlinear optics. Below, we will work out phase matching for SHG with the awareness that we can apply all that we have learned to PDC. Note that in SHG, the energy and momentum of the photon at the second-harmonic frequency are fixed because the energy and momentum of the two pump photons are given. This simplifies the description of second-harmonic generation and allows a treatment where the momentum of the photons can be treated as a scalar quantity. In the following section, we will discuss phase matching in second-harmonic generation in a periodically-poled KTP crystal. Note that the experimental data presented below are obtained by using a 2 mm long periodically-poled KTP crystal that

is identical to the crystal used to observe SPDC in the remaining chapters of this thesis.

1.4 Second-harmonic generation in PPKTP

Second-harmonic generation is a nonlinear process that is most commonly described in two steps. In the first step, the nonlinearity is treated as a perturbation, and a nonlinear polarization as a function of position is calculated, that is proportional to the square of the strength of the applied electric field of the pump wave multiplied by a nonlinear coefficient d_{eff}. The nonlinear polarization emits radiation, which is propagated to the exit face of the crystal and coherently added. This second step only yields a large contribution if all radiation is in phase. The nonlinear process is then said to be 'phase-matched'. Because of the important role of phase matching, we will go in more detail for the periodically-poled KTP crystals used in this thesis.

1.4.1 Phase matching

In this section we consider phase matching by calculating the phase difference for the relatively simple geometry of collinear SHG. The phase difference or phase mismatch is given by the difference in wavevector Δk at the pump and second harmonic frequency, multiplied by the crystal length L. In most cases, the dispersion in the refractive index of the nonlinear material gives rise to a non-zero value of $\Delta kL = (k_{2\omega} - 2k_{\omega})L$ as depicted in Fig. 1.2.

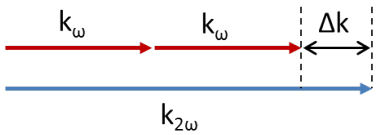

Figure 1.2: The wave-vector mismatch for collinear second harmonic generation as a result of dispersion in the refractive index of the nonlinear material. Note that for most materials the refractive index for blue wavelengths is larger than the refractive index for red wavelengths.

In order to achieve optimum SHG, Δk should be zero. The wavevector

mismatch as a result of index dispersion is given by

$$\Delta k = k_{2\omega} - 2k_{\omega} = \frac{2\omega}{c}(n(2\omega) - n(\omega)) \tag{1.1}$$

where $n(2\omega)$ and $n(\omega)$ represent the refractive index of the nonlinear material at frequencies 2ω and ω, respectively. For materials that display normal dispersion, the phase mismatch is always positive. A solution of practical relevance is the use of birefringence to compensate for the difference in refractive index by angle tuning of the crystal. This birefringent phase-matching scheme is limited to a certain wavelength range related to the optical properties of the crystal. For instance, for KTP it is impossible to achieve phase matching for SHG for pump wavelength shorter than $\sim$ 1000 nm.

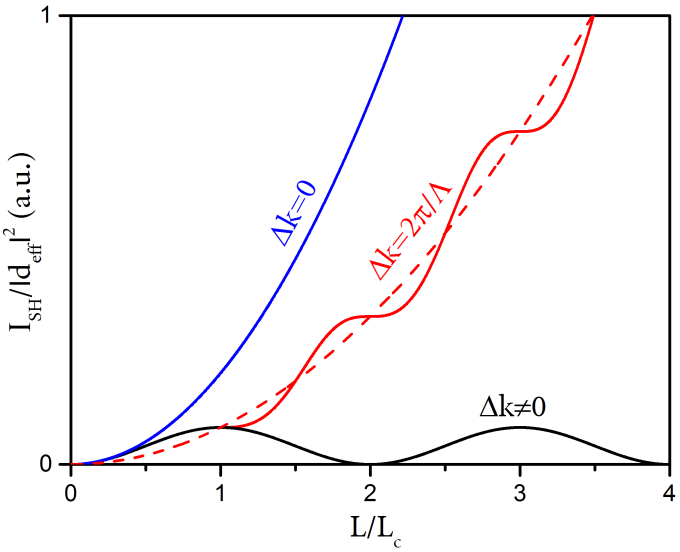

Figure 1.3: Calculation of the second-harmonic intensity for perfect phase matching $\Delta k = 0$ (blue line), quasi-phase matching $\Delta k = (2\pi)/\Lambda$ (red line) and non-phase matched $\Delta k \neq 0$ (black line) configurations, as a function of number of coherence lengths (L/L_c) along the propagation direction. Dashed line corresponds to $\Delta k = 0$ condition with periodic poling.

The second-harmonic intensity as a function of phase mismatch is given by

$$\frac{I_{SH}(L)}{|\, d_{\text{eff}}\,|^2} \propto L^2 \text{sinc}^2\left(\frac{1}{2}L\Delta k\right), \tag{1.2}$$

where d_{eff} is the nonlinear coefficient of the material and L corresponds to the length of the medium. Note that we have divided the intensity by the nonlinear coefficient $\mid d_{\text{eff}} \mid^2$ to facilitate a comparison between different materials and/or angles. The second harmonic intensity is maximum for a phase-matched configuration where $\Delta k = 0$. When the phase mismatch is nonzero ($\Delta k \neq 0$), the second harmonic intensity grows until a crystal length equal to the coherence length $L_c = \pi/\Delta k$. Beyond this point, the nonlinear polarization generates second harmonic which is out of phase with the already existing field and causes a drop in the intensity of second harmonic field for crystals longer than L_c. This behavior is shown in Fig. 1.3 by the black line. For comparison, the blue line shows the quadratic increase of the second harmonic intensity as a function of crystal length for the same crystal when it is properly phase-matched, i.e. $\Delta k = 0$.

1.4.2 Quasi-phase matching

When birefringent phase matching is not feasible one may use a periodic poling process to realize what is called quasi-phase matching. The idea behind this poling process is that the crystal direction and thereby the sign of the nonlinear coefficient is inverted after every coherence length L_c of the crystal. This introduces a periodic π phase shift in the nonlinear polarizability that ensures that the second-harmonic radiation is in phase at the output facet of the crystal and thus interferes constructively there. The resulting second harmonic from a periodically poled crystal as a function of length is indicated by the red line in Fig. 1.3. Compared to birefringent phase-matching schemes, periodic poling has the added advantage that the largest nonlinear coefficient of the material can be used.

The effect of periodic inversion (poling) of the nonlinear coefficient on the phase-matching conditions is more conveniently described using Fourier analysis. Periodic poling results in adding an appropriate reciprocal lattice vector $2\pi m/\Lambda$ to the wavevector mismatch, where m is an integer and Λ the poling period. The resulting intensity is given by

$$\frac{I_{SH}(m,L)}{\mid d_{eff} \mid^2} \propto L^2 \left(\frac{2}{\pi m}\right)^2 \text{sinc}^2 \left(\frac{1}{2} L \left(\Delta k - \frac{2\pi m}{\Lambda}\right)\right). \tag{1.3}$$

The pre-factor $(2/\pi m)^2$ is related to the Fourier coefficient of the m-th harmonic of the periodic poling function, assumed to be "square wave". The

second-harmonic intensity as a function of crystal length predicted by Eq. 1.3 is indicated by the red dashed line in Fig. 1.3. When comparing Eqns. 1.2 and 1.3, periodic poling induces a shift of the *sinc*-function along the Δk-axis.

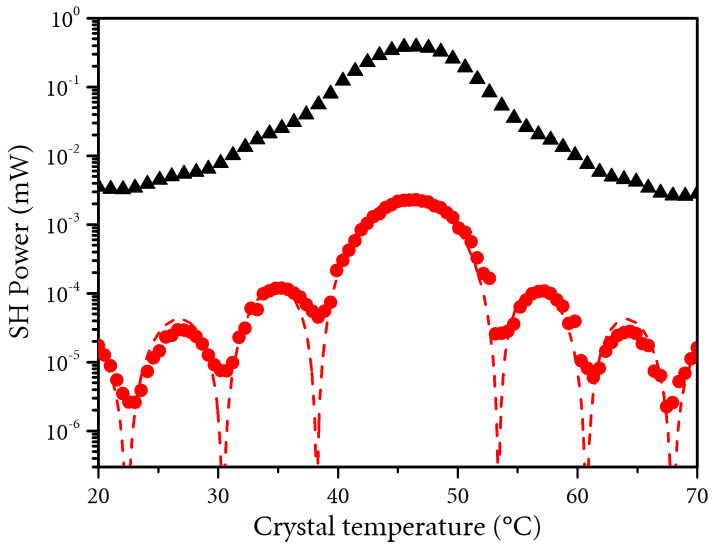

Figure 1.4: Measured second harmonic power obtained from a 2 mm PPKTP crystal as a function of crystal temperature. Data are shown for the PPKTP crystal pumped by a continuous wave Ti:Sapphire laser at the wavelength of 826.4 nm (red circles) and for a pulsed laser producing 2 ps pulses (black triangles). The red dashed line corresponds to a fit of the phase matching expressed by Eq.1.2 using a Taylor expansion of the temperature dependent refractive index of KTP.

In order to compare these calculations with experiments, we need to change the value of Δk while keeping the frequency of the input beam fixed (for convenience). This can be achieved by changing the temperature of the PPKTP crystal, the refractive index of PPKTP is temperature dependent [15]. As an example, Fig. 1.4 shows the measured second-harmonic signal generated in a 2 mm long PPKTP crystal with poling period $\Lambda = 3.675$ μm as a function of temperature. The data shown in Fig. 1.4 corresponds to measurements using a continuous wave Ti:Sapphire laser operating at 826.4 nm (red circles). These data illustrate the concept of phase matching. The dashed line is a fit through the data using a second order Taylor expansion of the refractive index as a function of temperature. For comparison, data are shown for

a pulsed laser with the same average power producing 2 ps pulses (black triangles). The second harmonic generated by the pulsed laser is enhanced by almost 3 orders of magnitude due to the high peak power associated with pulsed operation. The characteristic minima of the phase-matching function have disappeared because of the spread in pump wavelength of the 2 ps duration pulses.

So far we have discussed phase matching in SHG as entirely equivalent to phase matching in parametric down-conversion. There is, however, an essential difference. In SHG the frequencies and wave vectors of the two input fields are fixed, which together fix the frequency of the second harmonic and the wavevector of the non-linear polarization field. The phase mismatch is then fixed (for a given temperature and crystal setting). In PDC, however, only one frequency and wavevector are prescribed by the input field and there is thus much more freedom to achieve phase matching by choosing the emission directions of signal and idler. Nevertheless, the concept of phase matching is still useful but the phase mismatch is now defined for the case of degenerate signal and idler waves propagating along the pump direction.

1.5 Two-photon field of parametric down-conversion

In this thesis, we consider frequency degenerate Type-I parametric down-conversion in a periodically poled KTP crystal with an effective nonlinearity $d_{\text{eff}} = (2/\pi)d_{33}$=9.8 pm/V [15, 16]. The crystals are pumped at a wavelength of 413.2 nm and produce pairs at 826.4 nm that are strongly correlated in their spatial degrees of freedom.

To illustrate the role of phase matching in PDC, we consider the quantum state and corresponding two-photon amplitude created by continuous-wave pumping, when the pump beam has a waist w_p. The quantum state of the signal-idler pair can be written as [17]

$$|\Psi\rangle = \int \mathrm{d}\mathbf{q_s}\mathrm{d}\mathbf{q_i}\mathcal{E}_\mathbf{p}(\mathbf{q_s}+\mathbf{q_i})\mathcal{V}(\mathbf{q_s}-\mathbf{q_i})|\mathbf{q_s}\rangle|\mathbf{q_i}\rangle, \tag{1.4}$$

where the integrand represents the two-photon field as a product of the angular spectrum of the pump $\mathcal{E}_\mathbf{p}(\mathbf{q_s}+\mathbf{q_i})$ and the phase-matching function $\mathcal{V}(\mathbf{q_s}-\mathbf{q_i})$.

The vectors $\mathbf{q_s}$ and $\mathbf{q_i}$ in Fig. 1.5 represent the transverse components of the signal and idler wavevector, respectively.

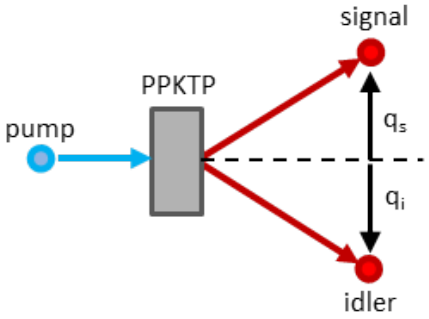

Figure 1.5: Illustration of the spontaneous parametric down-conversion (SPDC) process in a PPKTP crystal. The blue pump photon splits into signal and idler photons with transverse momenta q_s and q_i.

The angular spectrum of the pump is given by

$$\mathcal{E}_{\mathbf{p}}(\mathbf{q_s}+\mathbf{q_i}) \propto \frac{1}{\sqrt{\pi}w_p}\exp\left[-\frac{w_p^2}{4}|\mathbf{q_s}+\mathbf{q_i}|^2\right], \tag{1.5}$$

while the phase-matching function can be written as

$$\mathcal{V}(\mathbf{q_s}-\mathbf{q_i}) \propto \sqrt{\frac{k_p}{\pi L}}\mathrm{sinc}\left[-\frac{L}{4k_p}|\mathbf{q_s}-\mathbf{q_i}|^2\right], \tag{1.6}$$

where L is the length of the crystal and k_p is the magnitude of the pump wavevector. Note that we use the paraxial approximation where $|\mathbf{q_s}|/k_p \ll 0$ and $|\mathbf{q_i}|/k_p \ll 0$.

An important property of the quantum state is the associated Schmidt number K, which is useful measure for the number of optical modes involved. This number can be found via a Schmidt decomposition of the two-photon field. For our situation, this decomposition can be found in a closed form if the phase-matching function is approximated by a Gaussian function [18]. This results in a Schmidt number given by

$$K = \frac{1}{2}\left(\sqrt{\frac{L}{w_p^2 k_p}}+\sqrt{\frac{w_p^2 k_p}{L}}\right)^2. \tag{1.7}$$

This number quantifies the effective number of modes and is a measure of the amount of quantum information that can be carried by the system. The number of states determines the relative importance of the spontaneous and stimulated parametric down-conversion process and is thus an important quantity for the work described here.

1.6 Thesis outline

In this thesis we explore spatial quantum correlations of high-dimensional multi-photon states. These states are produced using the process of parametric down-conversion and are experimentally explored by measuring correlations with only two detectors. Compared to earlier investigations of multi-photon states, the correlations in this thesis are created in the spatial domain instead of the temporal domain. This has a distinct experimental advantage because it is much easier to measure the emission direction compared to a measurement of the arrival time of the photons.

- **Chapter 2** contains an experimental characterization of the far-field distribution of down-converted photons created in periodically-poled KTP crystals using a pulsed laser. The phase matching conditions relevant to the pulsed down-conversion process are made explicit. The difference in group velocity for the pump and down-converted photons limits the useful length to a group velocity walk-off length set by the combination of pulse duration and the group index of the PPKTP crystal. Chapter 2 provides the calculated intensity distributions of pulsed and cw SPDC light and shows the role of group velocity walk-off length.
- **Chapter 3** presents a novel method to obtain a highly correlated four-photon state produced by stimulated pair emission in non-collinear parametric down-conversion with a picosecond pulse. The method distinguishes the four-photon state from independent double pairs produced by spontaneous pair emission. We introduce the visibility of four-photon state as the ratio of contributions from stimulated and spontaneous events. The visibility of four-photon state observed in this Chapter reaches a value of 25%.
- **Chapter 4** focuses on the visibility of the four-photon state introduced in Chapter 3. We analyze the effect of pump beam size used to cre-

ate down-converted light. A characteristic mode size is introduced that captures the effect of different focussing conditions and paves the way for a universal expression of the visibility. By narrow spectral and spatial filtering of PDC light, the visibility is increased up to 80%.

- **Chapter 5** introduces a quadruple photon state where all four photons are emitted in the same spatial mode in a collinear parametric down-conversion geometry. This state is obtained as a result of the creation of a second pair stimulated by both photons of the initial pair in the same optical mode. The extra coincidences due to the stimulated emission of pairs in combination with the detectors produce a distinct peak in the measurements.

Bibliography

[1] R. Loudon, *The quantum theory of light*, Oxford University Press, Oxford, 1973.

[2] C. Cirac and P. Zoller, *Quantum computations with cold trapped ions*, Phys. Rev. Lett. **74**, 4091 (1995).

[3] P. Lougovski and S. J. van Enk, *Strengthened Bell inequalities for entanglement verification*, Phys. Rev. A **80**, 034302 (2009).

[4] E. Knill, R. Laflamme, and G. J. Milburn, *A scheme for efficient quantum computation with linear optics*, Nature **409**, 46 (2001).

[5] R. T. Thew, A. Acín, H. Zbinden, and N. Gisin, *Bell-type test of energy-time entangled qutrits*, Phys. Rev. Lett. **93**, 010503 (2004).

[6] X. Li, L. Yang, X. Ma, L. Cui, Z. Y. Ou, and D. Yu, *All-fiber source of frequency-entangled photon pairs*, Phys. Rev. A **79**, 033817 (2009).

[7] A. J. H. van der Torren, S. C. Yorulmaz, J. J. Renema, M. P. van Exter, and M. J. A. de Dood, *Spatially entangled four-photon states from a periodically poled potassium-titanyl-phosphate crystal*, Phys. Rev. A **85**, 043837 (2012).

[8] W. Dür, G. Vidal, and J. I. Cirac, *Three qubits can be entangled in two inequivalent ways*, Phys. Rev. A **62**, 062314 (2000).

[9] T. H. Yang and M. Nevascues, *Robust self-testing of unknown quantum systems into any entangled two-qubit states*, Phys. Rev. A **87**, 050102(R) (2013).

[10] S. P. Walborn, D. S. Lemelle, D. S. Tasca, and P. H. S. Ribeiro, *Schemes for quantum key distribution with higher-order alphabets using single-photon fractional Fourier optics*, Phys. Rev. A **77**, 062323 (2008).

[11] G. Molina-Terriza, A. Vaziri, R. Ursin, and A. Zeilinger, *Experimental quantum coin tossing*, Phys. Rev. Lett. **94**, 040501 (2005).

[12] S. D. Huver, C. F. Wildfeuer, and J. P. Dowling, *Entangled Fock states for robust quantum optical metrology, imaging and sensing*, Phys. Rev. A **78**, 063828 (2008).

[13] C. K. Hong, Z. Y. Ou, and L. Mandel, *Measurement of subpicosecond time intervals between two photons by interference*, Phys. Rev. Lett. **59**, 2044 (1987).

[14] C. Cohen-Tannoudji, J. Dupont-Roc, and G. Grynberg, *Atom-photon interactions*, Wiley-Interscience, Canada, 1992.

[15] W. H. Peeters and M. P. van Exter, *Optical characterization of periodically-poled $KTiOPO_4$*, Optics Express **16**, 7344 (2008).

[16] M. V. Pack, D. J. Armstrong, and A. V. Smith, *Measurement of the χ^2 Tensors of $KTiOPO_4$, $KTiOAsO_4$, $RbTiOPO_4$ and $RbTiOAsO_4$ Crystals*, Appl. Opt. **43**, 3319 (2004).

[17] A. T. Avelar and S. P. Walborn, *Genuine tripartite continuous-variable entanglement with spatial degrees of freedom of photons*, Phys. Rev. A **88**, 032308 (2013).

[18] C. K. Law and J. H. Eberly, *Analysis and interpretation of high transverse entanglement in optical parametric down conversion*, Phys. Rev. Lett. **92**, 127903 (2004).

CHAPTER 2

Characterization of pulsed parametric down-conversion in PPKTP crystals

We experimentally characterize sources of frequency degenerate down-converted photons at 826.4 nm generated in 2 mm, 5 mm and 10 mm long periodically-poled KTP crystals. The crystals are pumped by 413.2 nm laser pulses with 2 ps duration. The dispersion D=1.5 ps/mm puts a limit to the length over which phase matching is efficient for a 2 ps pulse and provides a lower limit for the angular width of SPDC in the far-field. We investigate the far-field distribution of SPDC produced by periodically-poled KTP crystals and compare this with the calculated intensity distribution and find good agreement with theory. We also discuss the performance of PPKTP in terms of nonlinearity and group velocity walk-off compared to other available materials.

S. Cigdem Yorulmaz and Michiel J.A. de Dood, *Characterization of parametric down-conversion in periodically poled KTP crystals with a picosecond pump*, Proc. SPIE 8440, 84400G (2012).

2.1 Introduction

Spontaneous parametric down-conversion (SPDC) is a second order nonlinear process that converts a high energy pump photon into two highly correlated signal and idler photons at lower energy. Because of the strong correlations between the photons, SPDC is a good candidate for creating entangled photons. Sources of polarization [1, 2], frequency [3, 4], time-bin [5, 6] and spatially [7–9] entangled photons all have been demonstrated.

Here we consider spatially entangled photons with the same polarization, which can be described by the transverse photon momentum. Generating such spatially entangled single photon pairs has been demonstrated using continuous wave lasers as a pump. However, in order to create spatially entangled multi-photon states, the photons should be generated within a coherence time of the photon pairs set by either a bandpass filter or the intrinsic width of the down-conversion. Since these coherence times are typically in the 10-1000 fs range, the use of short laser pulses is a requirement to observe multi-photon events.

In this Chapter, we present an experimental characterization of SPDC sources created using periodically-poled KTP (PPKTP) crystals with different length pumped by a picosecond pulsed laser. We discuss the effect of group velocity walk-off in PPKTP using the group velocity mismatch. To compare the characteristics of the pulsed SPDC source, we compare our results to the calculated intensity distribution of a continuous wave pumped SPDC source based on PPKTP. We also discuss the efficiency for pulsed SPDC of different crystal types such as PPLN, BBO, LBO and $LiIO_3$ compared to PPKTP crystal.

2.2 Phase matching in pulsed down-conversion

In a parametric down-conversion process, energy is conserved, and therefore the frequencies of the photons are related via $\omega_p = \omega_s + \omega_i$ where p, s and i correspond to pump, signal and idler photons, respectively. For an efficient process, photons are expected to satisfy the phase matching condition $\mathbf{k_p} = \mathbf{k_s} + \mathbf{k_i}$, where $\mathbf{k_p}, \mathbf{k_s}, \mathbf{k_i}$ represent the wavevector of the pump, signal and idler photons. Here we consider a frequency-degenerate type-I SPDC process in a PPKTP crystal, where pump, signal and idler photons have the same polarization, while signal and idler photons have the same frequency

($\omega_p = 2\omega_s = 2\omega_i$). To simplify the notation, we use $k_{2\omega}$ and k_ω for the wavenumber of the pump and SPDC photons.

Phase matching of down-conversion generated by continuous-wave (cw) pumping is well known and has been extensively described for PPKTP crystals [10]. For a pump beam polarized in the z-direction and propagating in the x-direction of the crystal, the transverse wavevector mismatch in the $y-z$ plane is approximately zero i.e. ($q_s \approx -q_i$), while the longitudinal wavevector mismatch is non-zero due to the temperature-dependence of the refractive index of the PPKTP crystal. Hence, the temperature of the PPKTP crystal determines the geometry of the SPDC light in the $y-z$ plane, and the far-field intensity distribution can be either an open ring shape (non-collinear) or a disk shape (collinear).

The far-field intensity distribution of SPDC light generated by a plane-wave, cw pump beam can be written as [10]

$$I(q,T) \propto \mathrm{sinc}^2\left(\frac{L}{2k_\omega}q_\omega^2 + \varphi(T)\right) \tag{2.1}$$

where q_ω and k_ω are the transverse momentum and wavenumber of the down-converted photon, L is the crystal length and $\varphi(T)$ is a temperature-dependent longitudinal phase mismatch. Collinear SPDC corresponds to $\varphi(T) = 0$ and occurs only for a specific crystal temperature.

We consider frequency-degenerate down-conversion generated by picosecond laser pulses in the same PPKTP crystal. Since a pulsed pump has a nonzero spectral width, the phase matching condition should be modified to contain the effect of this spectral width of the pump. We use a first order Taylor expansion of the wavevector mismatch for frequency-degenerate SPDC to include the effect of dispersion on the phase matching condition [11]

$$\Delta k(\Omega) \approx (k_{2\omega} - 2k_\omega) + D\Omega. \tag{2.2}$$

Here D is the dispersion that contains the group velocity mismatch between pump and down-converted photons and is defined as $D = 1/v_g(2\omega) - 1/v_g(\omega) = (n_g(2\omega) - n_g(\omega))/c$ with v_g and n_g the group velocity and group index. The frequency Ω is the detuning of the pump frequency relative to the center frequency of the pump. Note that to arrive at Eq. (2.2), we have used the fact that pump and down-converted photons all have the same polarization [11], and that we neglect the relatively small phase-mismatch due to differences in the frequency of the SPDC

photons. This second simplification corresponds to a typical experimental situation where the SPDC light is filtered by a narrow bandpass filter with a bandwidth much smaller than the natural bandwidth of the source. For comparison, the natural phase matching bandwidth for a 2 mm PPKTP crystal is around 40 nm, while the bandpass filter has a FWHM width of 1 nm, which selects SPDC light close to frequency degeneracy. For the UV pulsed pump (λ=413.2 nm) used in the experiment, the difference in group index is $n_g(2\omega) - n_g(\omega) = 0.4564$ for the PPKTP crystal at a temperature of 300 K and the corresponding group velocity dispersion D = 1.5 ps/mm [12]. In the calculation, we assume a plane-wave pump beam with a Gaussian envelope function to represent the frequency content of the pulsed pump. The intensity distribution for pulsed down-converted photons generated in PPKTP can then be written as

$$I(q,T) \propto \frac{1}{\sigma\sqrt{2\pi}} \int_{\Omega} d\Omega \exp\left(-\frac{1}{2}(\Omega/\sigma)^2\right) \times \operatorname{sinc}^2\left(\frac{L}{2k_\omega} q_\omega^2 + \varphi(T) + \frac{1}{2} D\Omega L\right) \tag{2.3}$$

where σ is defined as the standard deviation of the intensity distribution in the angular-frequency domain and τ_p is the duration of the pulse defined at FWHM [13]. The corresponding time-bandwidth product for a transform-limited gaussian pulse is defined by $\sigma\tau_p \approx 1.18$. For efficient conversion of all spectral components in the pulse, the condition of $DL < \tau_p$ has to be satisfied. Thus, the group velocity walk-off length $L_w = \tau_p / D$ is a typical length over which the SPDC process is efficient. For crystals longer than this walk-off length, the pulse duration of the SPDC light is significantly broadened compared to the pump pulse [14].

In order to visualize the role of group velocity walk-off in the pulsed down-conversion process, we calculate the angular width of the collinear SPDC light as a function of crystal length for both cw (Eq. 2.1) and pulsed laser pump (Eq. 2.3). The calculation is performed assuming a transform-limited gaussian pulse with 2 ps duration, which has an angular frequency bandwidth $\sigma = 0.59$ rad/ps. Fig.2.1 shows the calculated width (FWHM) of the far-field intensity distribution for collinear SPDC for continuous-wave (red solid line) and a pulsed pump (black solid line) as a function of crystal length on a log-log scale. The inset of Fig.2.1 shows the calculated angular intensity distribution of SPDC light for cw pumping (red solid line) and

for pulsed pumping (black solid line) considering a group velocity walk-off length $L_w = 1.3$ mm. At this length, the pulsed nature of the pump removes the distinct local minima of the sinc function while the width of the peak is comparable. As can be seen in Fig.2.1 for cw pumping, the angular width decreases inversely proportional to $\sqrt{L}$ while the angular width of pulsed SPDC light starts saturating when the crystal is longer than walk-off length L_w. For short crystals ($L \lesssim 0.3$ mm), the effect of dispersion can be ignored and the phase matching conditions for cw and pulsed SPDC become identical.

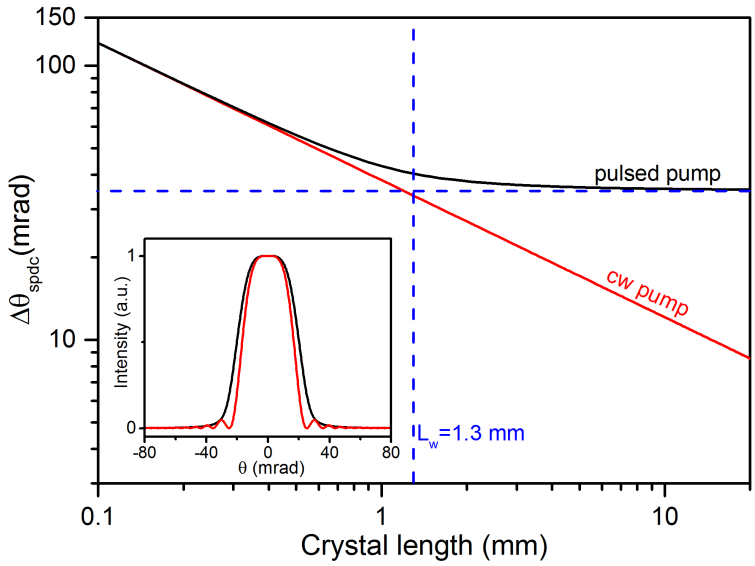

Figure 2.1: Calculation of the angular width (FWHM) of collinear ($\varphi = 0$) down-converted light as a function of crystal length for both cw (red solid line) and pulsed (black solid line) SPDC process. The pulsed pump is assumed to be a transform limited gaussian pulse with a spectral width $\sigma = 0.59$ rad/ps for a 2 ps pulse. The horizontal dashed line indicates the limit of angular width where the width saturates for a pulsed pump. This occurs for crystal lengths longer than the walk-off length of 1.3 mm (vertical dashed line). The inset shows the calculated normalized intensity versus angle of collinear SPDC light generated by cw (red solid line) and pulsed (black solid line) laser for a crystal length of 1.3 mm.

2.3 Experimental characterization of a pulsed SPDC source

In our experiment, we use periodically-poled KTP crystals (potassium titanyl phosphate (KTiOPO4)) designed for type-I phase matching by temperature tuning of the crystal. The crystals of various lengths are pumped by a weakly focussed (w_p =100 μm) linearly polarized pulsed laser propagating along the x-axis of the crystal. The length of the crystals are 2 mm, 5 mm and 10 mm in the x-direction and all crystals have a width of 2 mm and a height of 1 mm. The poling period of the PPKTP crystal $\Lambda_0 = 3.675$ μm is designed to enable collinear phase matching at a crystal temperature of 50°C to generate vertically polarized SPDC light at the frequency degenerate wavelength of 826.4 nm.

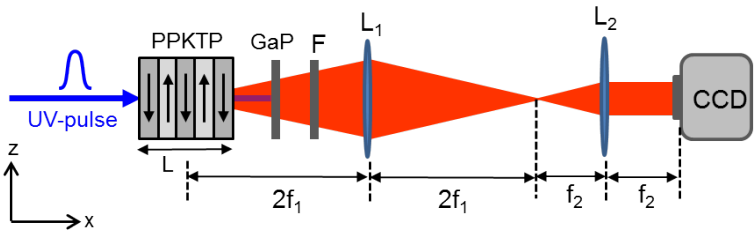

Figure 2.2: Schematic of the experimental setup to record far-field images of down-converted light. A periodically poled KTP crystal is pumped by 413.2 nm frequency-doubled Ti:Sapphire laser producing 2 ps pulses at a repetition rate of 80 MHz. The pump light is removed from down-converted light using anti-reflection coated GaP wafer. A bandpass filter F centered around 826.4 nm with a bandwidth of 1 nm is used to collect frequency degenerate SPDC light. The lenses L_1 ($f_1 = 50$ mm) and L_2 ($f_2 = 25$ mm) create a far-field image that is recorded by a CCD camera.

Figure 2.2 illustrates the experimental setup to obtain far-field images of the generated SPDC light. UV pulses at a wavelength of 413.2 nm with a duration of $\tau_p \approx 2$ ps are produced by frequency-doubling a Ti:Sapphire laser are focussed into a PPKTP crystal to create frequency degenerate down-converted photons at 826.4 nm. The average power of the UV pulses is kept constant at 170 mW. A GaP wafer that is anti-reflection coated for 826 nm is used to block the residual pump light in the experiment. In order to detect only frequency degenerate photons ($\omega_s \simeq \omega_i$), we use a narrow bandpass filter centered at 826.4 nm with a bandwidth of 1 nm which is much

narrower than phase-matching bandwidth of SPDC light (40 nm for a 2 mm PPKTP crystal). The two lenses with focal distances of 50 mm and 25 mm are used to create a far-field image of the down-converted light on the CCD camera. The temperature of the PPKTP crystal is controlled via a Peltier element with a PID controller, which keeps the temperature constant within 10 mK. Temperature-dependent far-field images of the SPDC source are recorded by a CCD camera for the temperature range of 10-50°C.

The temperature dependence of the refractive index of the PPKTP crystal determines the angular distribution of the generated SPDC light in the far-field through the temperature dependent phase-mismatch $\varphi(T)$. Fig. 2.3 (a), (b) and (c) show CCD images of the far-field intensity distribution of SPDC light at temperatures of 10°C, 30°C and 50°C generated in a 2 mm long PPKTP crystal. The pixel numbers were converted to far-field angles using the known size of the pixels of the CCD camera and focal length of the second lens f=25 mm that generates the far-field image. The down-converted photon emission is close to collinear phase matching ($\varphi \approx 0$) at the crystal temperature of 50°C, while at 10°C, the collected SPDC photons in the far-field form an open ring corresponding to a negative phase mismatch ($\varphi < 0$). In comparison to cw SPDC light, the intensity distribution of collinear SPDC has a shape that can be described by a Gaussian rather than the typical sinc shape of Eq. 2.1 for cw pump.

We recorded the intensity distribution of SPDC photons at 826.4 nm in the far-field from 2 mm, 5 mm and 10 mm long PPKTP crystals as a function of temperature between 10 and 50°C. In order to find the width (FWHM) and radius of the SPDC ring, each image is first converted to polar coordinates around its approximate center and then azimuthally averaged to obtain a radial distribution. We perform a numerical search that calculates the radial distribution as a function of center position to find the exact center that maximizes the peak intensity and minimizes the width. The radial intensity distribution obtained from the CCD images (a), (b) and (c) in Fig. 2.3 are shown in (d), (e) and (f), respectively. To determine the temperature dependent phase mismatch $\varphi(T)$, the radial intensity distribution for each crystal and all temperatures are fitted to Eq. (2.3) with ϕ, σ and an overall amplitude as fit parameters. Typical examples of the fit are shown by the solid lines in Fig. 2.3.

Fig. 2.4 shows the temperature dependence of the phase mismatch $\varphi(T)$,

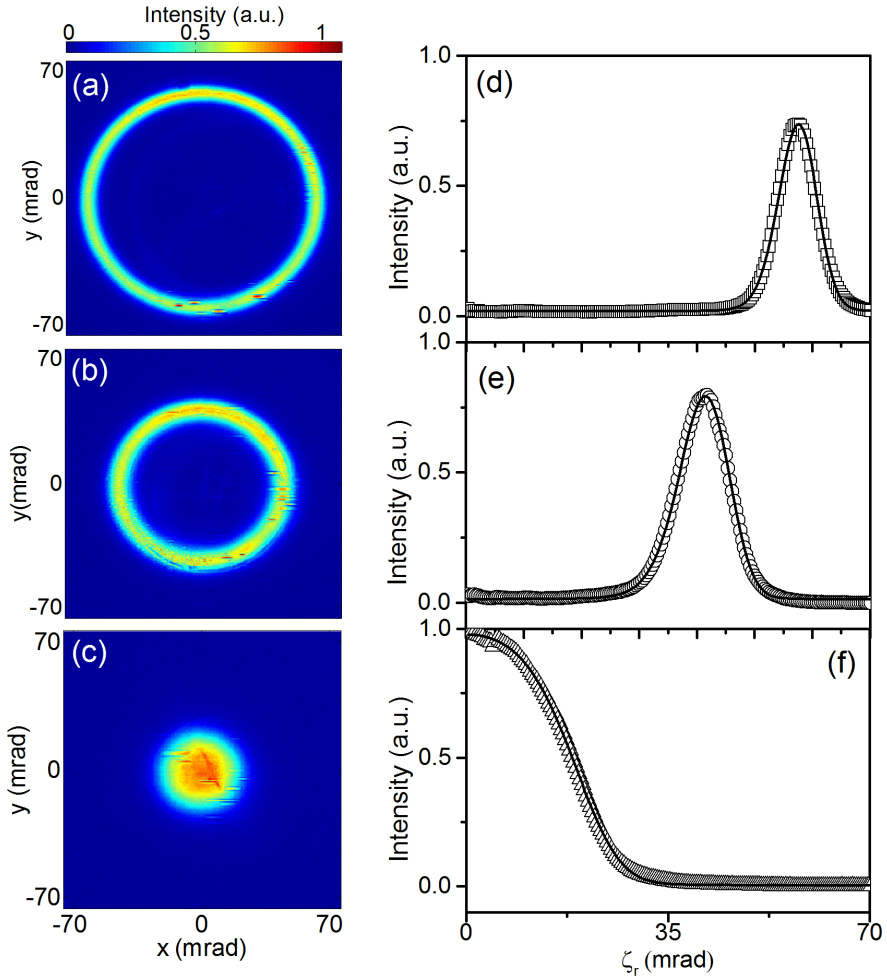

Figure 2.3: CCD images of the far-field distribution of SPDC light at 826.4 nm from a 2 mm PPKTP crystal pumped by 2 ps laser pulses at 413.2 nm and filtered by a 1 nm FWHM bandpass filter are shown for different temperatures of the crystal (a) T=10°C (b) T=30°C (c) T=50°C. (d), (e) and (f) correspond to radially integrated intensity of recorded far-field images as a function of far-field angle of the SPDC light. Solid lines are fits of Eq. (2.3) to the data (see text). Collinear phase matching is obtained close to a crystal temperature of 50°C.

which is related to the known temperature-dependent refractive index of PPKTP crystal [10, 15]. In order to describe the results in Fig. 2.4 and com-

pare them to literature, we introduce a Taylor expansion for the temperature dependent phase mismatch around a reference temperature of $T_r = 25^oC$ and find the coefficients α and β of the linear and quadratic temperature dependence.

$$\varphi(T) = \varphi(T_r) + \frac{1}{2}k_{2\omega}L[\alpha(T - T_r) + \beta(T - T_r)^2] \tag{2.4}$$

For non-collinear SPDC, the negative phase-mismatch provides a measure of the opening angle of the SPDC ring. Fig. 2.4 shows the phase-mismatch values extracted from the fit for the 2 mm (square), 5 mm (circles) and 10 mm (triangle) long PPKTP crystals as a function of temperature. The solid lines in Fig. 2.4 correspond to a best fit of Eq. 2.4 to the data.

L (mm)	α ($^\circ C^{-1}$) ($\times 10^{-6}$)	β ($^\circ C^{-2}$) ($\times 10^{-8}$)
2	26.1 ± 0.04	8.2 ± 0.3
5	27.4 ± 0.02	5.9 ± 0.2
10	26 ± 0.1	7.5 ± 0.6
5(cw)*	24.0 ± 0.02	4.8 ± 0.3

Table 2.1: The coefficients of the quadratic temperature dependence of the PPKTP crystal obtained from fitting the experimental results in Fig. 2.4 to Eq. 2.4. *The values of the coefficients obtained by cw pumping of a 5 mm crystal are shown as a reference [10].

The coefficients α and β of the temperature dependence of the PPKTP crystal obtained from the fit are shown in Table 2.1. In literature, an explicit expression for the temperature dependent refractive index of KTP crystal is given [15]. From this expression, the coefficients $\alpha = 23.56 \times 10^{-6}\ ^\circ C^{-1}$ and $\beta = 8.6 \times 10^{-8}\ ^\circ C^{-2}$ are found. Our values of α shown in Table 2.1 are comparable to the literature value, and the value found in experiments with a cw laser source using the exact same crystal [10]. The value of β is somewhat lower than the literature value, but is consistent with previous work for cw pumping using the same crystals as in this study [10]. As shown in Fig. 2.4, it is clear that the 5 mm PPKTP crystal has a slightly different collinear phase matching temperature compared to the 2 mm and 10 mm long crystals. The 2 and 10 mm crystals are grown by the manufacturer (Raicol crystals Ltd.) in a single batch, while the 5 mm crystal was produced by the same manufacturer

on a different date. Hence, we believe that the difference between crystals are due to small variations in crystal growth.

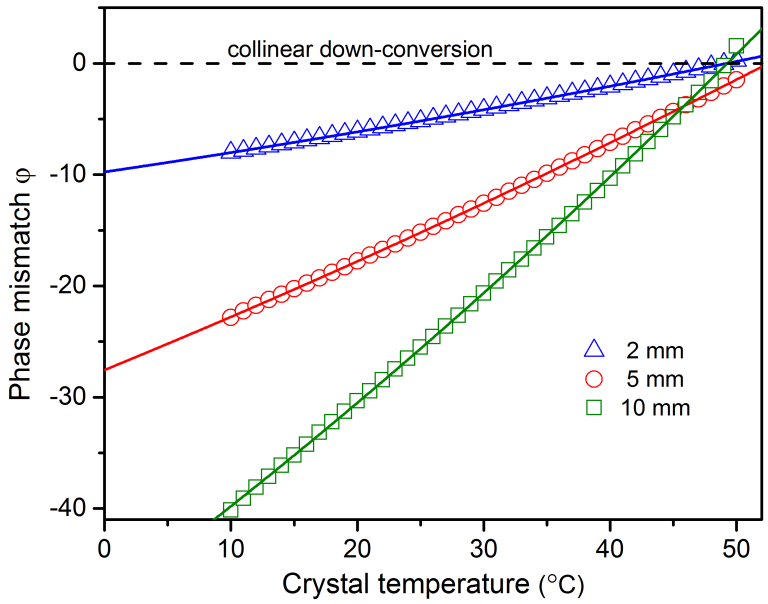

Figure 2.4: Phase-mismatch φ as a function of crystal temperature obtained from fitting the measured radial intensity distribution of SPDC ring pattern with the Eq. (2.3) for 2 mm (blue triangle), 5 mm (red circle) and 10 mm (green square) long PPKTP crystals. The solid lines show fits to the data (see text). The condition for collinear phase matching ($\varphi = 0$) is indicated by the horizontal dashed line.

Fig. 2.5 shows the experimentally determined temperature dependence of the angular width (FWHM) of the SPDC ring in pulsed down-conversion for three different crystal lengths. Data are shown for the 2 mm (blue triangles), 5 mm (red circles) and 10 mm (green squares) PPKTP crystals and are plotted as a function of phase-mismatch by using the temperature dependence of $\varphi(T)$ obtained from Fig. 2.4. The inset shows a false color plot of the radial intensity distribution as a function of phase-mismatch (bottom axis), crystal temperature (top axis) and angle for a 10 mm long PPKTP crystal. This clearly demonstrates the widening of the SPDC ring as the temperature is tuned toward the collinear phase-matching condition $\varphi = 0$. The sharp peak in the width as a function of phase-mismatch occurs at the point where the

intensity in the center equals half the intensity of the maximum and is a direct result of using the FWHM as a measure of the angular width.

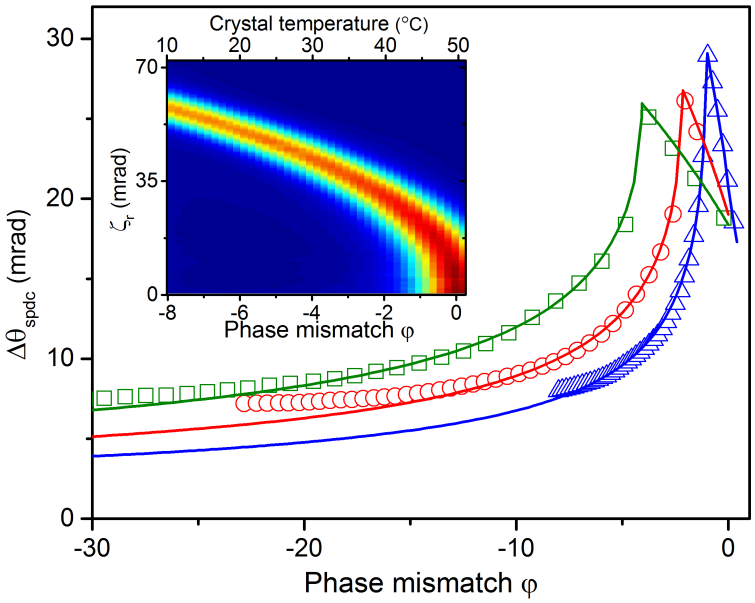

Figure 2.5: Angular width (FWHM) of SPDC ring patterns measured for various values of phase-matching of 2 mm (triangle), 5 mm (circle) and 10 mm (square) long PPKTP crystals obtained from fitting the radial intensity distribution to Eq. (2.3). The corresponding crystal temperature range is $10 - 50°$C for all crystals. The solid lines correspond to the angular width of the pulse predicted by Eq. (2.3) using spectral widths of $\sigma_{2mm} = 0.74$ rad/ps, $\sigma_{5mm} = 0.66$ rad/ps and $\sigma_{10mm} = 0.63$ rad/ps that best describes the data. The inset shows a false color plot of the radial intensity distributions as a function of crystal temperatures (top axis) and phase mismatch (bottom axis) for the 2 mm crystal.

For every crystal and each temperature we fit Eq. (2.3) to the radial intensity distribution and find a value for the spectral width σ that best describes the data. The solid lines in Fig. 2.5 correspond to the calculated angular width (FWHM) as obtained from Eq. (2.3) by setting a constant value for σ for each curve. We use a value σ = 0.74, 0.66 and 0.63 rad/ps for crystal lengths of 2, 5 and 10 mm, respectively. These values of σ are slightly larger than the transform-limited $\sigma = 0.59$ rad/ps for a 2 ps duration pulse as is commonly

observed for an actively mode-locked Ti:sapphire laser producing picosecond pulses [13] *. The fact that the value of σ depends on crystal length is not expected because σ is a property of the laser pulse. We remind the reader that Eq. (2.3) is an approximation for a plane-wave pump. The pump beam waist of 100 μm creates a spread in the pump beam transverse wavevector $\Delta\theta \sim \frac{\lambda_p}{w_p} \approx 4$ mrad. The diffraction limited angular width of the SPDC light is thus close to 8 mrad and explains the saturation of the ring width for large, negative phase mismatch.

Crystal	$n_g(2\omega) - n_g(\omega)$	$D\ (ps/mm)$	$d_{\text{eff}}\ (pm/V)$	$L_w d_{\text{eff}}^2\ (nm^3/V)$
PPKTP	0.456	1.5	9.8	125
PPLN	0.514	1.7	24.3	710
BBO	0.053	0.18	2.0	45
LBO	0.033	0.11	0.8	11
$LiIO_3$	0.154	0.51	3.4	45

Table 2.2: Group index mismatch $n_g(2\omega) - n_g(\omega)$, dispersion D and effective non-linearity d_{eff} for different crystals.

To create an efficient, pulsed source of SPDC light, non-linear crystals with a large second-order non-linearity are desirable. However, for crystals longer than the walk-off length $L_w = \tau/D$, the efficiency of the non-linear process of SPDC is reduced. To create bright sources of single photon pairs or sources that are capable of producing multiple pairs within a pulse it is important to consider the combined effect of the non-linear response and group velocity walk-off. For this purpose Table 2.2 summarizes the group index mismatch, dispersion D in ps/mm and the effective second-order non-linearity d_{eff} in pm/V. As can be seen from the table, the effective non-linearity of the crystals is strongly correlated with the dispersion D. This effect is similar to an empirical correlation between the linear and non-linear susceptibilities, known as Miller's rule [12, 16]. It is highly relevant here, because increase in performance due to a larger non-linearity is canceled by the effect of group velocity walk-off.

For a given spectral bandwidth of the bandpass filter used to collect the

*The manufacturer of our laser (Spectra-Physics) specifies a time-bandwidth product smaller than 1.7 times the Fourier limited time-bandwidth product

SPDC light the total number of photon pairs produced is proportional to the average laser power and the crystal length L. The intensity created by the non-linear process is thus proportional to $L\, d_{\text{eff}}^2$. This is valid for the common experimental situation of not too long crystal where the natural bandwidth of the SPDC light is much larger than the filter bandwidth. For pulsed lasers the useful length is limited to the group velocity walk-off length. Therefore we postulate that a good number to compare the pair production rate from different non-linear crystals is given by $L_w\, d_{\text{eff}}^2$

Table 2.2 compares this number for common non-linear crystals that could be used to create bright pair sources around 800 nm. The numbers in the table show that PPKTP and PPLN crystals are expected to outperform sources based on BBO or $LiIO_3$. It should be noted that the birefringent phase-matching required for BBO, LBO and $LiIO_3$ also introduces a spatial walk-off that depends on the waist of the pump beam. This spatial walk-off could shorten the length over which phase-matching is efficient and the number given in the table should be regarded as an upper limit for these crystals. For BBO the walk-off angle ρ is as large as 66 mrad, limiting the useful length for 100 μm waist of the pump beam in the experiment to only 1.5 mm. The walk-off angle in LBO is only 16 mrad, making the performance of LBO comparable to that of BBO when spatial walk-off becomes important. In contrast, periodically poled crystals such as PPKTP and PPLN do not suffer from spatial walk-off since the polarization of the pump and down-converted photons can be chosen to be identical. This greatly simplifies the design of the source. Given the large non-linearity of PPLN compared to PPKTP and a rather similar value of D, PPLN crystals would be preferred. This is especially true for processes that involve higher photon numbers as the yield of double pairs and triple pairs scales exponentially with the efficiency of the source. With current state-of-the-art poling technology for PPLN crystals sources that produce pairs at 980 nm would be feasible. Sources that operate around 800 nm, being the maximum detection efficiency of Si-based single photon counting detectors, seem to be within reach.

2.4 Conclusion

We have characterized and compared pulsed sources of frequency degenerate photons created by pulsed SPDC in a periodically poled KTP crystals of

different crystal lengths. For pulsed laser sources, group velocity dispersion becomes important and sets a limit to the length over which the SPDC process is efficient. For the 2 ps duration pulse in the experiment we estimate a group velocity walk-off length $L_w \approx 1.3$ mm. The experimentally observed radial intensity distributions as a function of temperature show a characteristic cone shaped emission pattern with an opening angle that increases with decreasing temperature. We find that the width (FWHM) of the open ring saturates at a value of $\sim$8 mrad for the lowest temperatures, independent of the crystal length (either 2, 5 or 10 mm in the experiment).

The radial intensity distribution is well described by a theoretical model that takes into account this group velocity walk-off. From fits of the model to the experimental data we obtain the co-linear phase-mismatch as a function of temperature. The temperature dependent phase-mismatch can be well approximated by a second order polynomial and is comparable to the temperature dependence for the same crystals pumped by a cw pump laser. Compared to literature values of the temperature-dependent refractive index of KTP crystal we find good agreement for the linear term and a small deviation in the quadratic term.

Bibliography

[1] Z. D. Walton, A. V. Sergienko, B. E. A. Saleh, and M. C. Teich, *Generation of polarization-entangled photon pairs with arbitrary joint spectrum*, Phys. Rev. A **70**, 052317 (2004).

[2] M. Fiorentino, G. Messin, C. E. Kuklewicz, F. N. C. Wong, and J. H. Shapiro, *Generation of ultrabright tunable polarization entanglement without spatial, spectral, or temporal constraints*, Phys. Rev. A **69**, 041801(R) (2004).

[3] Z. Y. Ou and L. Mandel, *Violation of Bell's inequality and classical probability in a two-photon correlation experiment*, Phys. Rev. Lett. **61**, 50 (1988).

[4] X. Li, L. Yang, X. Ma, L. Cui, Z. Y. Ou, and D. Yu, *All-fiber source of frequency-entangled photon pairs*, Phys. Rev. A **79**, 033817 (2009).

[5] S. Friberg, C. K. Hong, and L. Mandel, *Measurement of time delays in the parametric production of photon pairs*, Phys. Rev. Lett. **54**, 2011 (1985).

[6] H. D. Riedmatten, V. Scarani, I. Marcikic, A. Acn, W. Tittel, H. Zbinden, and N. Gisin, *Two independent photon pairs versus four-photon entangled states in parametric down conversion*, J. Mod. Opt. **51**, 1637 (2004).

[7] D. V. Strekalov, A. V. Sergienko, D. N. Klyshko, and Y. H. Shih, *Observation of two-photon ghost interference and diffraction*, Phys. Rev. Lett. **74**, 3600 (1995).

[8] C. K. Law and J. H. Eberly, *Analysis and interpretation of high transverse entanglement in optical parametric down conversion*, Phys. Rev. Lett. **92**, 127903 (2004).

[9] A. J. H. van der Torren, S. C. Yorulmaz, J. J. Renema, M. P. van Exter, and M. J. A. de Dood, *Spatially entangled four-photon states from a periodically poled potassium-titanyl-phosphate crystal*, Phys. Rev. A **85**, 043837 (2012).

[10] W. H. Peeters and M. P. van Exter, *Optical characterization of periodically-poled $KTiOPO_4$*, Optics Express **16**, 7344 (2008).

[11] T. E. Keller and M. H. Rubin, *Theory of two-photon entanglement for spontaneous parametric down-conversion driven by a narrow pump pulse*, Phys. Rev. A **56**, 1534 (1997).

[12] W. J. Alford and A. V. Smith, *Wavelength variation of the second-order nonlinear coefficients of $KNbO_3$, $KTiOPO_4$, $KTiOAsO_4$, $LiNbO_3$, $LiIO_3$, $\beta - BaB_2O_4$, HH_2PO_4 and LiB_3O_5 crystals: a test of Miller wavelength scaling*, J. Opt. Soc. Am. B **18**, 524 (2001).

[13] A. E. Siegman, *Lasers*, University Science Books, Sausalito, California, 1986.

[14] S. Wang, V. Pasiskevicius, F. Laurell, and H. Karlsson, *Ultraviolet generation by first-order frequency doubling in periodically poled $KTiOPO_4$*, Optics Letters **23**, 1883 (1998).

[15] S. Emanueli and A. Arie, *Temperature-dependent dispersion equations for $KTiOPO_4$ and $KTiOAsO_4$*, Applied Optics **42**, 33 (2003).

[16] R. C. Miller, *Optical second harmonic generation in piezo- electric crystals*, Appl. Phys. Lett. **5**, 17 (2003).

CHAPTER 3

Spatially entangled four-photon states from a PPKTP crystal

Spatial quantum correlations are an important resource for quantum imaging and future quantum technologies based on high-dimensional entanglement. We experimentally explore spatial correlations in four-photon states generated by a highly efficient parametric down-conversion process in a 2 mm long periodically poled KTP crystal. The four-photon states produced in the crystal contain a contribution due to independent double pairs produced via spontaneous pair emission and a highly correlated four-photon state produced by stimulated emission of a second photon pair. We separate this contribution and introduce a joint spatial density for stimulated pair emission. We observe a maximum visiblity $\chi = 0.25$ of the four-photon state for a 1 nm bandpass filter.

Alexander J. H. van der Torren, S. Cigdem Yorulmaz, Jelmer J. Renema, Martin P. van Exter, and Michiel J. A. de Dood , *Spatially entangled four-photon states from a periodically poled potassium-titanyl-phosphate crystal*, Phys. Rev. A **85**, 043837 (2012).

3.1 Introduction

Photon pairs produced via spontaneous parametric down-conversion (SPDC) in a non-linear crystal give rise to strong nonclassical correlations. The resulting entangled photons are an important resource in quantum information, fundamental tests of quantum mechanics and have been used in experiments that demonstrate the violation of Bell's inequality, quantum teleportation and quantum communication. While most experiments focus on discrete polarization entanglement, quantum states of two particles that are entangled in continuous variables [1] such as frequency [2, 3], time-bin [4–6] or photon momenta [7–10] are also possible, which gives access to high-dimensional entanglement that can be explored by measuring correlations between two photons.

In this chapter, we focus on spatial entanglement using photon momenta as a continuous variable. Unlike other forms of continuous variable entanglement, the quantum correlations in spatial entanglement can be resolved with relative ease and high resolution by using a combination of lenses and apertures only. The low conversion efficiency in non-linear crystals combined with the long coherence time of a continuous wave pump and ultrashort coherence time of the photon pairs ensure that most experiments are well described by two-photon interference of individual pairs [10]. As a consequence, spatial entanglement with more than two photons has remained elusive and spatial correlations beyond independent photon pairs have not been addressed in an experiment [11]. These multi-photon states are of interest since they provide access to non-trivial entanglement between more than two particles [12, 13]. Furthermore, the generation rate of four photon states sets fundamental limits on the visibility achievable in two-photon interference experiments [14] and the maximum attainable key generation rate in quantum key distribution protocols.

Here we investigate events where four spatially entangled photons are generated by SPDC. These four photons can either be two independent pairs, or they may all be in the same set of spatial and temporal modes to create a true four-photon state [5, 6]. The production of these four photon states is enhanced by the physical process of stimulated emission of a second photon pair into the same optical mode as the first pair. In the ideal situation of a single temporal and spatial mode, stimulated emission enhances the pair

production rate by a factor of two compared to the probability to generate four photons in the same mode via two independent spontaneous processes. For a multi-mode situation, the relative importance of the stimulated emission process is given by a "visibility" χ that ranges from 0 to 1.

The distinction between two independent pairs and four-photon states has been addressed in the time-domain using time-bin entanglement with a pulsed laser source [5, 6]. These experiments are restricted to a single spatial mode and therefore do not allow use of spatial degrees of freedom to explore the process of stimulated emission. The total number of modes is then given by the available temporal modes and is directly related to the frequency bandwidth of the SPDC light as compared to the frequency bandwidth of the pulsed laser source [6]. To directly resolve the underlying mode structure requires a measurement of quantum correlations within a single laser pulse. Such a direct measurement of the arrival time would require detectors with high quantum efficiency and sub-picosecond timing resolution, which is well outside reach of current single-photon detector technology [15, 16]. Instead, we use spatially entangled multi-photon states that allow us to resolve the fine structure of stimulated pairs emitted in a single laser pulse in a straightforward way. Using pinholes the momentum resolution in the far-field of the SPDC source may be made arbitrarily high. In an experiment, there is always a trade-off between the size of the pinhole and the collected signal, which sets the time required to measure coincidence rates to a sufficient level of accuracy.

3.2 Stimulated emission of spatially entangled four-photon states

The downconversion process in the PPKTP crystal that generates photon pairs in N spatial modes can be described by an interaction Hamiltonian of the SPDC process given by [17, 18]:

$$H = \kappa \sum_{i=1}^{N} a^{\dagger}_{\mathbf{q_i}} a^{\dagger}_{-\mathbf{q_i}} + \text{h.c.}, \tag{3.1}$$

where $a^{\dagger}_{\mathbf{q_i}}$ is the creation operator that creates a single photon in a spatial mode labeled by the transverse wavevector $\mathbf{q_i}$. In this equation, the summation is done for positive values of the index i and excludes the collinear

direction ($\mathbf{q} = \mathbf{0}$). A detailed discussion of the collinear direction is given in Chapter 5. The operator $a^\dagger_{\mathbf{q_i}} a^\dagger_{-\mathbf{q_i}}$ thus creates a pair of photons that is correlated in their transverse photon momenta and forms the basis for spatial entanglement. The parameter κ describes the strength of the non-linear interactions and contains, among others, the (time-dependent) field of the pump and the effective non-linearity of the PPKTP crystal. For our purpose, where we pump the crystal with an intense pulsed laser, κ can be assumed to be a classical quantity. The corresponding wavefunction of the state generated by SPDC can be directly obtained from the Hamiltonian:

$$|\Psi\rangle = \exp(-iH\frac{t}{\hbar})|0\rangle \approx (1 - \frac{it}{\hbar}H - \frac{t^2}{2\hbar^2}H^2)|0\rangle, \tag{3.2}$$

where we limited the Taylor expansion in the last step to exclude quantum states with more than four photons. The linear term in the Taylor expansion creates a state $|\Psi_2\rangle$ that consists of a superposition of a single photon pair in any of the available spatial modes:

$$|\Psi_2\rangle = \frac{-it}{\hbar}H|0\rangle \approx \frac{-i\kappa t}{\hbar}\sum_{i=1}^{N}|1_{\mathbf{q_i}};1_{-\mathbf{q_i}}\rangle. \tag{3.3}$$

Please note that we use a shorthand notation in which we leave out all spatial modes without a photon. The spatial modes that contain photons are numbered by the number of photons in that mode and the subscript refers to the transverse photon momentum of that mode. The quadratic term gives rise to a state $|\Psi_4\rangle$ with four photons that contains all double pair contributions, which can be represented using the same notation [6] as

$$|\Psi_4\rangle \approx \frac{-\kappa^2 t^2}{2\hbar^2}\left(2\sum_{i=1}^{N}|2_{\mathbf{q_i}};2_{-\mathbf{q_i}}\rangle + \sum_{i=1}^{N}\sum_{j=1,i\neq j}^{N}|1_{\mathbf{q_i}},1_{\mathbf{q_j}};1_{-\mathbf{q_i}},1_{-\mathbf{q_j}}\rangle\right). \tag{3.4}$$

The effect of stimulated emission follows directly from the creation operators and is contained in the extra factor $\sqrt{2}$ when two photon pairs are created in the same spatial mode.

A measurement of a single photon in a particular spatial mode with wavevector $\mathbf{q_i}$ determines the wavevector of the twin photon and corresponds to a state projection: $a_{\mathbf{q_i}}|\Psi\rangle$. The state projection allows us to calculate the probabilities of creating a single photon pair P_2 as well as the probability

P_4 to create a state with four photons in the same mode. For a single spatial and temporal mode, the probability P_4 is exactly equal to P_2^2 and is thus enhanced by a factor 2 compared to stimulated emission of two photon pairs in the same spatial modes. In a situation with more than one spatial mode, which is of interest here, stimulated emission enhances the probability P_4 by a factor $(1+\chi)$, where χ is a "visibility" from 0 to 1 that quantifies the extra contribution to the four photon states due to stimulated emission. The probability to create a four photon state with the photons in the same mode can then be expressed as [6]:

$$P_4 = \frac{P_2^2}{2}(1+\chi). \tag{3.5}$$

3.2.1 Experimental investigation of four-photon quantum correlations

3.2.2 Experiment

Figure 3.1 depicts the setup to explore the spatial quantum correlations due to stimulated emission of pairs in a four-photon state. In order to get a non-negligible rate of double pairs we use a highly efficient, 2 mm long, periodically poled KTP (PPKTP) crystal [19] pumped by ∼100 mW of 413.2 nm pulsed laser light. The pulsed laser in our setup produces 2 ps pulses and is focussed into the PPKTP crystal using a lens $L1$, with a focal length f of 250 mm. The source creates non-collinear, frequency degenerate photon pairs at a wavelength of 826.4 nm that are filtered by a bandpass filter F and collected by lenses $L2$ (f = 270 mm). Three detector assemblies $D1-D3$ are used to collect single photons with a well-defined momentum. Each of these assemblies consists of a lens $L3$ (f_3 = 4.5 mm), an aperture A placed in the far-field to select the photon momentum and a (multi-mode) fiber-coupled single photon counting avalanche photodiode (Perkin-Elmer SPCM-AQ4C). The mode diameter of the fiber used in the experiments is 50 μm and lenses $L2$ and $L3$ provide a 60× magnification factor. Coincidence detection with a ∼1.7 ns coincidence window between the detectors $D1$ and $D3$ (or $D2$ and $D3$) results in a measurement of spatial entanglement of single pairs. The beamsplitter, BS, allows us to record coincidence events between detectors $D1$ and $D2$ that are due to two photons from different pairs. To record the spatial correlations both detector assemblies $D1$ and $D2$ are placed on com-

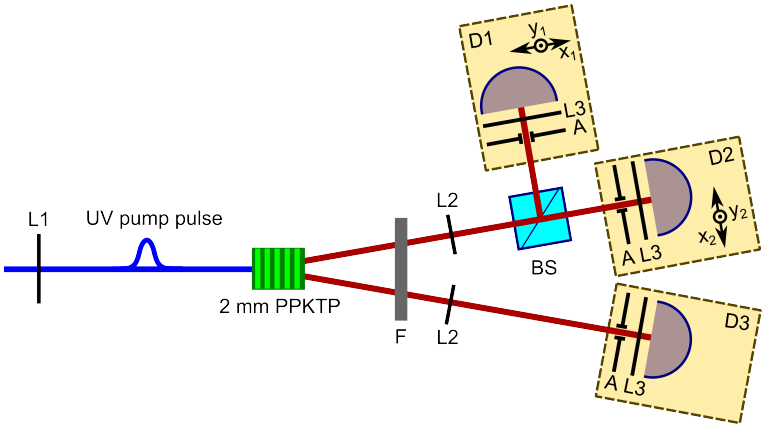

Figure 3.1: Setup to measure spatially entangled four-photon states via parametric downconversion in a 2 mm PPKTP crystal. UV pump pulses from a frequency doubled Ti:Sapphire laser are focused by lens L1 (f_1 = 250 mm). Photons are collected by the lenses $L2$ (f_2 = 270 mm) and detected by the detector assemblies $D1 - D3$ that use photon counting APDs to detect single photons in a particular direction defined by the apertures A placed in the combined focal planes of $L2$ and $L3$ (f_3 = 4.5 mm). The beamsplitter, BS, allows to record if two photons are in the same spatial mode. To this end detector assemblies $D1$ and $D2$ are placed on computer controlled translation stages. Correlations in the coincidence events are due to four-photon states that are created by the process of stimulated emission of photon pairs.

puter controlled translation stages that allow movement in the x and y directions transverse to the optical beam.

The essential feature of the setup is that it allows us to distinguish a genuine four-photon state from two independent pairs by detecting coincidences between two photons in the same arm, as was introduced earlier for four-photon states in the time-domain [6]. In this setup only the four-photon states created by stimulated emission generate strong correlations between detectors $D1$ and $D2$, while double pair states do not create any special correlations.

The length of the 2 ps laser pulse is a compromise between a short laser pulse to select a single temporal mode on the one hand and a somewhat longer laser pulse to retain efficient SPDC on the other hand. For a very short laser pulse the photons are created at a well-defined time, but the SPDC process becomes inefficient due to the broad spectral content of the laser pulse. In our study, the combination of the pulse duration and the bandpass filter se-

lects ∼3 temporal modes, leading to a maximum possible visibility χ=1/3 for a single spatial mode. The choice of the pulse duration and the length of the crystal was motivated by the group velocity walk-off length L_g = 1.5 mm, calculated for transform-limited pulses, being comparable to the crystal length. Under those conditions, the phase-matching in the crystal is only mildly affected by the pulsed laser and all frequency components of the laser pulse contribute to the efficient generation of SPDC light.

3.2.3 Quantum correlations at the two-photon level and number of Schmidt modes

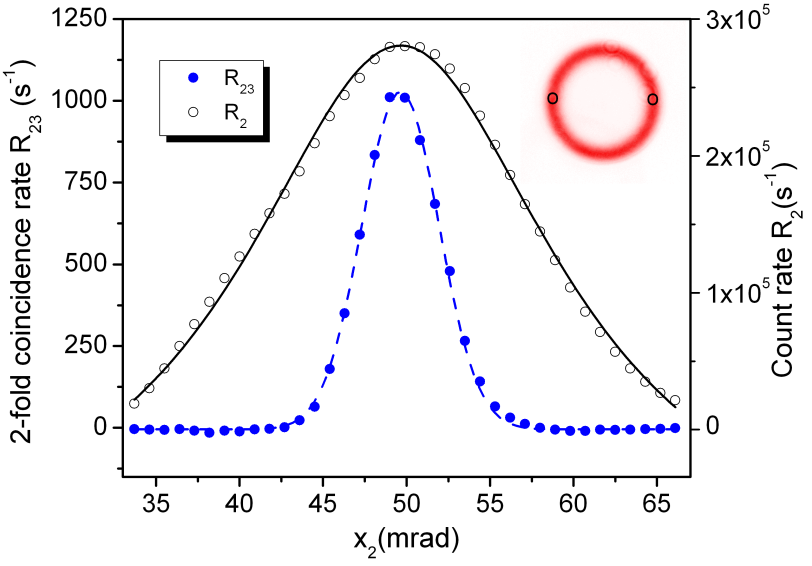

Figure 3.2: Measured single count rates R_2 (open symbols) and 2-fold coincidence rates R_{23} (filled symbols) as a function of position x_2, demonstrating spatial correlations in the two-photon field. The pulsed laser beam was focused in the center of the crystal using a f = 250 mm lens. Data are collected using a 1 nm FWHM bandpass filter and a 1.5 mm aperture in the far-field. The solid and dashed lines indicate Lorentzian and Gaussian fits to the single and coincidence rates, respectively. The inset shows a far field image of the SPDC light emitted by the PPKTP crystal at a temperature of 20 °C. The approximate positions of detectors D2 and D3 are shown by circles on the ring.

Figure 3.2 shows the measured coincidence rate between detectors $D2$ and $D3$ (solid symbols, left axis) as a function of the position x_2 of detector D_2. Detector assembly D_3 is positioned at a fixed position and collects photons at an angle of -50 mrad in the far-field of the source. The measured coincidences, corrected for accidental events, are compared to the measured single count rate on detector $D2$ (open symbols, right axis). The measured single count rate on detector D_3 is $\sim 3 \cdot 10^5\ s^{-1}$ and is constant throughout the experiment.

The single count rate as a function of detector position is well described by a Lorentzian fit (solid line) centered at a position of 50$\pm$5 mrad and a width of 14.9$\pm$0.5 mrad FWHM. The relatively large error bar in the center position is due to the fact that it is difficult to determine the absolute position of lens $L2$ on the optical table. The characteristic minima of the sinc^2 phase-matching curve commonly observed under continuous wave pumping are 'averaged' out by the multiple frequencies available in the spectrum of the picosecond pulsed laser [20]. The measured two-fold coincidence rate as a function of the position x_2 of the detector is well described by a Gaussian (dashed line) with a width (FWHM) of 5.1$\pm$0.1 mrad, and a center position of 50$\pm$5 mrad. The observation that the peak in coincidence rate is much narrower than the measured singles is a clear signature of two-photon correlations in a high-dimensional Hilbert space. The ratio of the width of the singles versus the coincidences is a direct measure of the Schmidt number K_r of the (radial) spatial entanglement generated in the PPKTP crystal [21]. Based on the measured width of the coincidence and singles peak, we estimate a Schmidt number $K_{exp} \approx 2.9 \pm 0.1$ for the pulsed laser. This estimate should be converted to a two-dimensional Schmidt number in order to compare this number to values given in literature for continuous wave pumping.

To this end, we introduce a second azimuthal Schmidt number K_ϕ, being the ratio of the circumference of the SPDC ring, i.e. $2\pi \times 50$ mrad, over the measured width of the coincidence peak. This results in $K_\phi \approx 60 \pm 6$ and a corresponding Schmidt number $K = K_r K_\phi \approx 175 \pm 20$. This number should be compared to calculated values [8] and experimental values obtained for a 5.0 mm crystal pumped by a continuous wave laser [21]. The value of K from ref. [21] for strongly negative phase mismatch (i.e. an open SPDC ring) was scaled to our case by taking into account the differences in pump beam waist and crystal length. Based on this, we expect a two-dimensional Schmidt number of $\sim$125. This value is somewhat lower than the value stated

above, which we attribute to the fact that we neglected the effect of the pulsed laser on the width of the SPDC ring. The pulsed laser contains many pump frequencies which gives a slightly broader ring and consequently causes an overestimate of the value of K_r.

3.2.4 Observation of quantum correlations of four-photon states in the spatial degrees of freedom

To explore the contribution of stimulated emission we measure the coincidence rate R_{21} between detectors $D1$ and $D2$. Coincidences can only be registered if at least four photons are generated by a single photon pulse, since only one-photon in each pair produced by SPDC can be detected. The measured coincidence rate for photons originating from the same pulse contains both stimulated and spontaneous events. To get a measure of the number of coincidences due to spontaneous emission we introduce a tunable electronic delay between detectors $D1$ and $D2$. This allows a measurement of the coincidences in the same laser pulse ($R_{21}^{0\text{ns}}$) as well as the coincidence events between subsequent laser pulses by setting the electronic delay to 12 ns ($R_{21}^{12\text{ns}}$). This latter coincidence rate is dominated by events where a single pair is produced in each of the laser pulses and the coincidence rate $R_{21}^{12\text{ns}}$ thus represents only the coincidence rate due to two spontaneously emitted photon pairs.

The difference in these coincidence rates, normalized by the coincidence rate due to spontaneous events is equal to the "visibility" χ, i.e. $\chi = (R_{21}^{0\text{ns}} - R_{21}^{12\text{ns}})/R_{21}^{12\text{ns}}$ and is a good measure of the extra events due to stimulated emission of four-photon states. The measured visibility as a function of the position of the two detectors, $\chi(x_1, x_2)$, can be interpreted as a joint spatial density of stimulated pair emission. This joint spatial distribution of stimulated pair emission is depicted in Fig 3.3. The false colour image in Fig. 3.3a shows the difference in coincidence rate $(R_{21}^{0\text{ns}} - R_{21}^{12\text{ns}})$ as a function of the position x_1 and x_2 of detectors $D1$ and D_2 using a 5 nm bandpass filter for the SPDC light. The image is centered around the point $x_1 = x_2 = 50$ mrad and clearly shows the expected positive correlation due to stimualted emission of the four-photon state that leads to extra coincidences whenever the two detectors detect photons in the same optical mode, i.e. when $x_1 = x_2$. The width (FWHM) of the peak along the diagonal ($x_1 - x_2 = 0$ mrad) is 11.5 ± 0.3

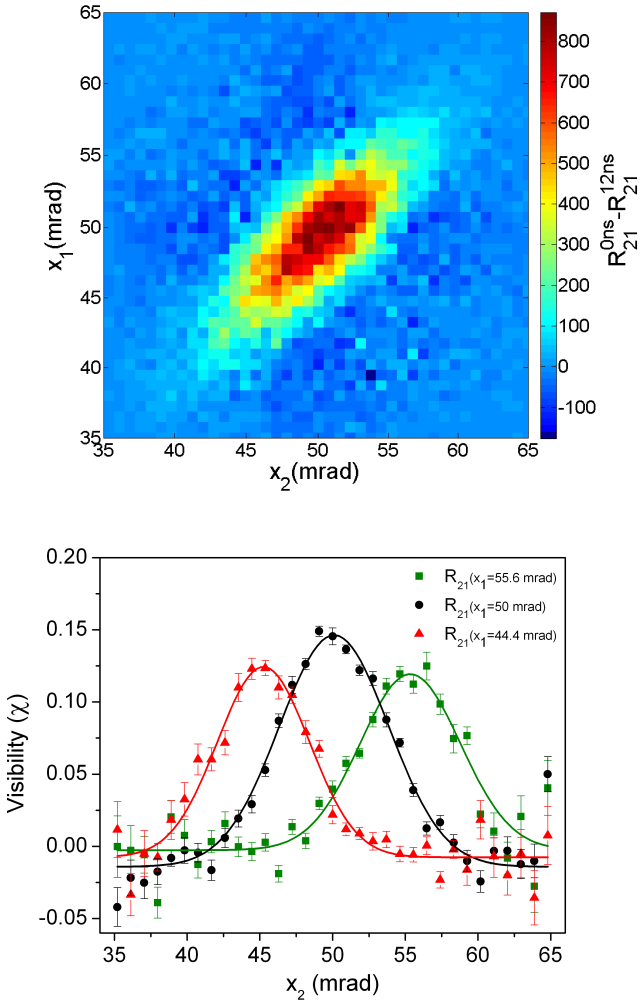

Figure 3.3: Measured joint spatial distribution of stimulated pair emission. (a) False-color plot of the measured difference in coincidence rate $(R_{21}^{0\text{ns}} - R_{21}^{12\text{ns}})$ as a function of the positions x_1 and x_2 of detectors D_1 and D_2. Data are collected with a 5 nm FWHM bandpass filter and a 1.5 mm aperture size. The observed maximum coincidence rate $R_{21}^{0\text{ns}}$ is typically 25,000 s^{-1}. The data clearly demonstrate that stimulated pair emission occurs when the photons are emitted in the same spatial mode, i.e. when $x_1 = x_2$. (b) Visibility χ of the four-photon state as a function of position x_2. The different symbols (triangles, circles, squares) correspond to different positions x_1 (44.4, 50.0, 55.6 mrad) of detector D_1. Data are collected using a 1 nm FWHM bandpass filter and a 1.5 mm aperture. The solid lines through the data are Gaussian fits.

mrad, while the width along the anti-diagonal direction ($x_1 + x_2$ = 100 mrad) is 4.5±0.1 mrad.

Figure 3.3b shows the visibility $\chi(x_1, x_2)$ as a function of position x_2 of detector $D2$ for a fixed position of detector $D1$. The three curves correspond to x_1 = 44.4 mrad (triangles), 50.0 mrad (circles) and 55.6 mrad (squares). These data are taken with a 1 nm bandpass filter for the SPDC light in order to enhance the visibility at the expense of a much lower count rate. The narrow band frequency filter lowers the number of temporal modes involved, but does not affect the spatial modes. The integration time per point was increased by repeated scanning of the detector in the x_2 direction. Because the phase-mismatch of the PPKTP crystal that governs the SPDC process depends weakly on laser power, the long term stability of the laser becomes important. In order to correct for this effect we also monitor the single counts on the detector $D2$ as a function of position x_2 and exclude scans from our analysis where the SPDC ring appears shifted. The solid lines through the data are Gaussian fits to the data with a FWHM width of 8.9±0.3. The peak positions are shifted to the position of detector $D1$, such that the peak of the Gaussian appears at $x_1 = x_2$. The obtained peak visibilities for the three curves are 0.13±0.01, 0.16±0.01 and 0.12±0.01. For a uniform illumination of the aperture one would expect the peak visibility to be independent of the position x_1. This case corresponds to a situation where the width of the SPDC ring, as given by the phase-matching function, is much larger than the shift in position x_1. In our experiment the slightly lower visibility for x_1 = 44.4 and 55.6 mrad is caused by the finite diameter of the 1.5 mm aperture that captures a non-uniform part of the SPDC ring. For larger apertures (data not shown) this decrease in visibility indeed becomes more significant.

The visibility in our experiment is limited by both the number of temporal modes collected as well as by the ratio of the total number of spatial modes available over the number of spatial modes collected by the aperture. The total number of temporal modes generated is given by the frequency bandwidth of the SPDC light as compared to the frequency spread of the pulse. For a Fourier limited pulse shape the frequency bandwidth is related to the pulse duration via $\tau = (2\ln(2)\lambda^2)/(\pi c \Delta\lambda)$, where τ is the pulse duration and $\lambda/\Delta\lambda$ is the relative frequency spread. The 2 ps pulse corresponds to an equivalent spectral width of 0.5 nm, while the 2 mm PPKTP crystal produces SPDC light with a bandwidth of ∼40 nm FWHM. Consequently, the num-

ber of available temporal modes for a PPKTP crystal pumped by a 2 ps laser pulse is potentially ∼80. We use '5 nm' and '1 nm' bandpass filters centered at 826.4 nm to limit the number of temporal modes. The measured FWHM bandwidth of these filters is 4.6 nm and 1.5 nm, which extends the coherence time of the SPDC light and limit the number of temporal modes to ∼9 and ∼3 respectively. Since χ is inversely proportional to the number of available temporal modes [6], this produces upper limits to χ of 0.1 and 0.3 for the two bandpass filters. We stress that shorter pump pulses do not necessarily lead to a higher flux of photons since the phase-matching in the 2 mm PPKTP crystal effectively filters the pump pulse. In our experiments we have carefully chosen the crystal length to maximize conversion efficiency without significantly stretching the pump pulse to avoid a non-factorable structure ('X-entanglement') between spatial and temporal degrees of freedom [22].

Figure 3.4 shows the measured visibility as a function of aperture size for a 5 nm bandpass filter (circles) as compared to a 1 nm bandpass filter (triangles). Measurements were performed by measuring coincidence rates between detectors $D1$ and $D2$ at a fixed position $x_1 = x_2 = 50$ mrad. A measurement of the coincidence rate as a function of the electronic time delay is shown in the inset for a point with a relatively high visibility of 0.25. The extra 50 counts/sec at zero delay are due to stimulated emission of photon pairs. Clearly, the visibility is low and nearly constant for apertures that are larger than 2 mm and rises as the number of available spatial modes is reduced by closing the aperture. In our experiments the visibility saturates at apertures sizes above 2 mm where the aperture size is limited by the finite numerical aperture of the multimode fiber in combination with the focal length of the fiber coupling lens $L3$. The saturation is represented by the horizontal dashed lines.

The visibility χ in the experiment is proportional to the inverse of the number of spatial and temporal modes, i.e. $\chi \propto N_t^{-1} N_{sp}^{-1}$, where N_t and N_{sp} are the number of temporal and spatial modes respectively. Throughout the experiment N_t is determined by the FWHM of the bandpass filter and can be considered constant. We use values of $N_t = 9$ and $N_t = 3$ for the two different bandpass filters. In order to estimate the number of spatial modes collected as a function of aperture size we consider the correlations between two point-

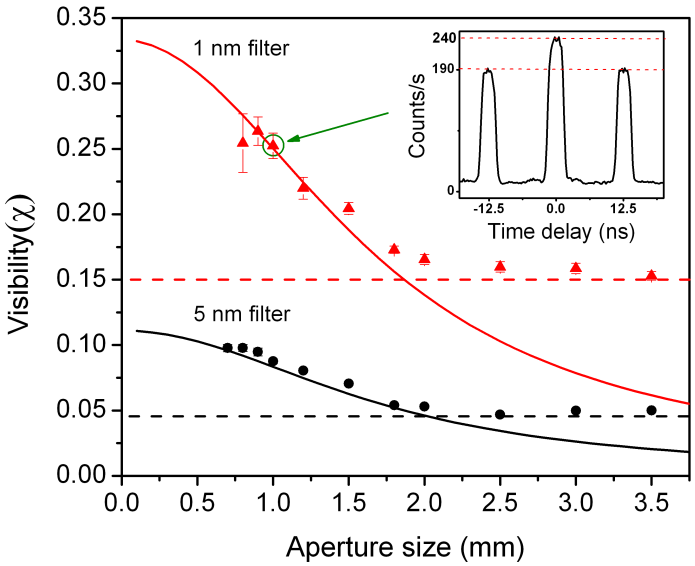

Figure 3.4: Visibility χ of the four-photon state as a function of aperture size using a 1 nm FWHM bandpass filter (triangles) and a 5 nm FWHM bandpass filter (circles). These data are obtained by comparing the measured coincidence rate at a delay of 12 ns with the measured coincidence rate at zero delay, using $\chi \equiv (R_{21}^{0\text{ns}} - R_{21}^{12\text{ns}})/R_{21}^{12\text{ns}}$. Typical single count rates on the detector are 1.4×10^6 and 3×10^5 sec^{-1} for apertures > 2 mm and drop to 5×10^5 and 1×10^5 sec^{-1} for a 1 mm aperture size. The solid lines represent a calculation with no free parameters (see text). For apertures larger than 2 mm, the aperture is limited by lens $L3$ and the numerical aperture of the fiber and the visibility saturates as indicated by the horizontal dashed lines. The inset shows the measured coincidence rate R_{12} as a function of electronic delay for a 1 nm FWHM bandpass filter and a 1 mm aperture size ($\chi = 0.25$), indicated by the arrow.

like apertures at positions $\mathbf{r_1}$ and $\mathbf{r_2}$. The resulting visibility is given by:

$$\chi(\mathbf{r_1}, \mathbf{r_2}) = \exp(-\frac{|\mathbf{r_1} - \mathbf{r_2}|^2}{r_0^2}). \tag{3.6}$$

The characteristic distance $r_0 = (\lambda f_2)/(\pi w_p)$, where f_2 = 270 mm is the focal distance of lens $L2$ that creates the far-field of the SPDC source and w_p is the waist of the pump beam created by focussing the pump beam using lens $L1$. Using the measured waist of the pump beam of 80 μm we find a characteristic distance r_0 = 0.9 mm. The visibility in the experiment due to finite aperture size for two apertures centered at the same position can be found via integration:

$$\chi(a) = \frac{1}{N_t \pi a^4} \iint \chi(\mathbf{r_1}, \mathbf{r_2}) \Theta(a - |\mathbf{r_1}|) \Theta(a - |\mathbf{r_2}|) \mathrm{d}\mathbf{r_1} \mathrm{d}\mathbf{r_2}, \tag{3.7}$$

where the Heaviside step-functions $\Theta(a - |\mathbf{r_1}|)$ and $\Theta(a - |\mathbf{r_2}|)$ represent the sharp edges of the two apertures with equal radius a in the far-field. The solid lines through the data in Fig. 3.4 are the results of calculating the double integral represented by Eq. 3.7 using 3 and 9 temporal modes for the two bandpass filters and the calculated value of r_0 based on the measured beam waist. The agreement between the data and the model with no adjustable parameters is striking for aperture sizes below 2 mm. For apertures above 2 mm the visibility saturates, as indicated by the horizontal dashed lines, at a value determined by lens $L3$ and the numerical aperture of the multimode fiber that limit the beam diameter to $\sim$2 mm. This saturation phenomenon is absent in later measurements presented as Fig. 4.2 in the next chapter, where we replace the lens $L3$ to increase the collected beam diameter to $\sim$5 mm.

3.3 Conclusion

In conclusion, we have demonstrated the existence of spatial correlations between photon pairs in a four-photon state. These correlations are induced via stimulated pair emission. In our experiments we are able to separate the contribution from spontaneous parametric down-conversion and stimulated parametric down-conversion at the level of double pairs. The stimulated emission becomes important when a 2 mm long PPKTP crystal is pumped by a 2 ps pulsed laser at 413.2 nm wavelength to create frequency and polarization degenerate photon pairs at a wavelength of 826.4 nm. The spatial

correlations of the stimulated photon pairs contains a rich structure when using a non-collinear geometry for the down-conversion process, which can be explored with relative ease using apertures in the far-field. In this way we present the first measurements of the joint spatial distribution of stimulated pair emission and discuss the acquired visibility. This technique opens new possibilities to explore the structure of higher-dimensional entanglement by making use of spatial degrees of freedom instead of the temporal degree of freedom. The possibility to distinguish between stimulated and spontaneous processes can be used to explore recent proposals for ghost imaging with thermal and quantum light sources [23, 24].

Bibliography

[1] S. L. Braunstein and P. van Loock, *Quantum information with continuous variables*, Rev. Mod. Phys. **77**, 513 (2005).

[2] Z. Y. Ou and L. Mandel, *Violation of Bell's inequality and classical probability in a two-photon correlation experiment*, Phys. Rev. Lett. **61**, 50 (1988).

[3] X. Li, L. Yang, X. Ma, L. Cui, Z. Y. Ou, and D. Yu, *All-fiber source of frequency-entangled photon pairs*, Phys. Rev. A **79**, 033817 (2009).

[4] S. Friberg, C. K. Hong, and L. Mandel, *Measurement of time delays in the parametric production of photon pairs*, Phys. Rev. Lett. **54**, 2011 (1985).

[5] Z. Y. Ou, J.-K. Rhee, and L. J. Wang, *Observation of four-photon interference with a beam splitter by pulsed parametric down-conversion*, Phys. Rev. Lett. **83**, 959 (1999).

[6] H. D. Riedmatten, V. Scarani, I. Marcikic, A. Acn, W. Tittel, H. Zbinden, and N. Gisin, *Two independent photon pairs versus four-photon entangled states in parametric down conversion*, J. Mod. Opt. **51**, 1637 (2004).

[7] D. V. Strekalov, A. V. Sergienko, D. N. Klyshko, and Y. H. Shih, *Observation of two-photon ghost interference and diffraction*, Phys. Rev. Lett. **74**, 3600 (1995).

[8] C. K. Law and J. H. Eberly, *Analysis and interpretation of high transverse entanglement in optical parametric down conversion*, Phys. Rev. Lett. **92**, 127903 (2004).

[9] J. C. Howell, R. S. Bennink, S. J. Bentley, and R. W. Boyd, *Realization of the Einstein-Podolsky-Rosen paradox using momentum- and position-entangled photons from spontaneous parametric down conversion*, Phys. Rev. Lett. **92**, 210403 (2004).

[10] S. Walborn, C. Monken, S. Pdua, and P. S. Ribeiro, *Spatial correlations in parametric down-conversion*, Physics Reports **495**, 87 (2010).

[11] P.-L. de Assis, M. A. D. Carvalho, L. P. Berruezo, J. Ferraz, I. F. Santos, F. Sciarrino, and S. Pádua, *Control of quantum transverse correlations on a four-photon system*, Optics Express **19**, 3715 (2011).

[12] D. Greenberger, M. Horne, and A. Zeilinger, *Bells theorem, quantum theory and conceptions of the universe*, Kluwer Academics, Dordrecht, The Netherlands, 1989.

[13] W. Dür, G. Vidal, and J. I. Cirac, *Three qubits can be entangled in two inequivalent ways*, Phys. Rev. A **62**, 062314 (2000).

[14] I. Marcikic, H. de Riedmatten, W. Tittel, V. Scarani, H. Zbinden, and N. Gisin, *Time-bin entangled qubits for quantum communication created by femtosecond pulses*, Phys. Rev. A **66**, 062308 (2002).

[15] R. H. Hadfield, *Single-photon detectors for optical quantum information applications*, Nature Photonics **3**, 696 (2009).

[16] M. D. Eisaman, J. Fan, A. Migdall, and S. V. Polyakov, *Single-photon sources and detectors*, Rev. Sci. Instrum. **82**, 071101 (2011).

[17] C. Simon, G. Weihs, and A. Zeilinger, *Optimal quantum cloning via stimulated emission*, Phys. Rev. Lett. **84**, 2993 (2000).

[18] P. Kok and S. L. Braunstein, *Postselected versus nonpostselected quantum teleportation using parametric down-conversion*, Phys. Rev. A **61**, 042304 (2000).

[19] W. H. Peeters and M. P. van Exter, *Optical characterization of periodically-poled $KTiOPO_4$*, Optics Express **16**, 7344 (2008).

[20] T. E. Keller and M. H. Rubin, *Theory of two-photon entanglement for spontaneous parametric down-conversion driven by a narrow pump pulse*, Phys. Rev. A **56**, 1534 (1997).

[21] H. D. L. Pires, C. H. Monken, and M. P. van Exter, *Direct measurement of transverse-mode entanglement in two-photon states*, Phys. Rev. A **80**, 022307 (2009).

[22] A. Gatti, E. Brambilla, L. Caspani, O. Jedrkiewicz, and L. A. Lugiato, *X entanglement: The nonfactorable spatiotemporal structure of biphoton correlation*, Phys. Rev. Lett. **102**, 223601 (2009).

[23] K. W. C. Chan, M. N. O'Sullivan, and R. W. Boyd, *Two-color ghost imaging*, Phys. Rev. A **79**, 033808 (2009).

[24] M. N. O'Sullivan, K. W. C. Chan, and R. W. Boyd, *Comparison of the signal-to-noise characteristics of quantum versus thermal ghost imaging*, Phys. Rev. A **82**, 053803 (2010).

CHAPTER 4

The role of spatial and temporal modes in pulsed parametric down-conversion

We explore spatial correlations created by stimulated pair emission in frequency degenerate parametric down-conversion from a periodically poled KTP crystal pumped by ∼2 ps duration laser pulses. The ratio of stimulated pairs over spontaneous pairs reaches as high 0.8 in the experiment. This ratio is a direct measure of the total number of modes relevant to the down-conversion process. We identify a universal curve for this ratio that accounts for the effect of the focused pump, introducing a coherence diameter r_0 related to the diffraction limited size of the pump beam in the far-field. Measurements of the spatial correlations of the PDC light for longer crystals and tight focusing conditions show that the description given in terms of a universal curve is surprisingly robust and breaks down only for a laser beam focussed to a waist smaller than 40 μm in a 2 mm long PPKTP crystal.

S. C. Yorulmaz, M. P. van Exter, and M. J. A. de Dood , *The role of spatial and temporal modes in pulsed parametric down-conversion*, Optics Express **22**, 5913-5926 (2014).

4.1 Introduction

It is well-known that parametric down-conversion (PDC) produces highly correlated quantum states that consist of pairs of photons. The quantum correlations of the pairs can pertain to the temporal [1–3], polarization [4–7] and/or spatial [8–11] degrees of freedom. Although polarization entanglement provides the paradigmatic system it is somewhat limited because each photon lives in a two-dimensional Hilbert space. In recent years other types of photonic entanglement have become almost as popular because they can provide a dimensionality per photon that is much larger than two. This high-dimensional aspect enhances the information-carrying capacity of the quantum system. As a result, improved security in quantum key distribution [12, 13], quantum coin tossing [14], increased quantum channel capacity [15, 16] and robust quantum imaging [17] have all been proposed and realized.

In parallel, multi-photon states of light have been investigated as they are an interesting resource because they can be used to test quantum mechanics in ways beyond what is possible with two qubits [18, 19]. The generation and control of more than two photons is a minimal requirement for possible future linear-optics quantum-computation [20] and may be useful for quantum communication protocols that are extra secure or robust against photon loss [21].

The combination of higher-dimensional quantum states with more than two photons is difficult to realize and characterize experimentally and has therefore received limited attention. To date, most experimental efforts use photons that are distinguishable in the time-domain and rely on measuring and modifying small differences in arrival time between photons. Spatial entanglement of photons provides an attractive alternative for higher-dimensional entanglement because the quantum correlations can be modified and detected with high (spatial) resolution simply by using lenses and apertures. The dimensionality of a spatially entangled state created by PDC depends on the crystal length and the beam waist of the focused pump [22, 23]. Non-collinear PDC is attractive because the photons within a pair are emitted in distinct directions, which greatly facilitates experiments because the photons can be detected on separate single photon counting detectors. In this way, spatial correlations of two-photon states have been demonstrated in a

variety of experiments, including quantum imaging [8, 24, 25], two-photon speckle [26, 27] and non-local momentum-position correlations [10, 28].

Thus far, most experimental work on spatial entanglement has addressed spatial quantum correlations at the two-photon level using a continuous wave pump laser to create individual photon pairs. Recently, we have explored spatially entangled four-photon states in an experiment with short pump laser pulses [29] and distinguish between double pairs created by spontaneous emission and true four-photon states created by stimulated emission [29]. Analogous to the case of time-bin entanglement [30], we introduced a visibility parameter χ that quantifies the relative importance of the stimulated-emission process. This parameter is a measure of the number of modes involved in the down-conversion process and plays a central role as it determines the photon number statistics of the quantum state created.

Here we explore how the visibility of the four-photon state, and hence the number of modes involved, depends on the focusing conditions and crystal length. By narrow spectral and spatial filtering, we are able to increase the visibility to values as high as 80%. For a constant crystal length, we find a universal curve for the visibility of the four-photon state as a function of the size of the detection aperture that combines all data for different pump beam diameters.

4.2 Properties of four-photon states produced by parametric down-conversion

The regime of parametric down conversion where multiple photon pairs are produced simultaneously is typically achieved using a pulsed, ultraviolet laser as a pump source. Both photon pairs can be generated via the spontaneous parametric down-conversion process. For this independent process the probability to create four photons is predicted by Poisson statistics and the corresponding probability is given by $P_4 = P_2^2/2$, where P_2 is the probability to produce a single pair via spontaneous parametric down-conversion. The process of stimulated parametric downconversion enhances the probability P_4. In an experimental configuration where only a single spatial and temporal mode is available, the process of spontaneous and stimulated emission are indistinguishable and the probability of spontaneous emission of a second pair exactly equals the probability of stimulated pair emission so that

$P_4 = P_2^2$. A visibility parameter χ, ranging between 0 and 1, can be introduced [30] via $P_4 = (P_2^2/2)(1+\chi)$ to quantify the relative importance of stimulated emission. For a single-mode configuration χ is maximum and equal to 1. When multiple spatial and/or temporal modes are involved the visibility is reduced since the probability to create two pairs in the same mode is reduced. Only this contribution from pairs produced in the same mode is enhanced through stimulated emission. As a result, the visibility parameter χ is inversely proportional to the number of modes [29, 30], and the number of spatial and temporal modes available in the down-conversion process are important quantities as they set an upper limit to the experimentally achievable visibility χ.

4.2.1 Estimating the number of modes

Since the parametric down-conversion process generates either independent pairs, or exact copies of the pairs produced in the same mode the corresponding four-photon amplitude can be written as a product of two-photon amplitudes [31] and a description in terms of a two-photon amplitude to find the corresponding number of modes suffices. This number of modes, or Schmidt number, involved in the parametric down-conversion process can be obtained via a Schmidt decomposition of the two-photon field. Estimates of the Schmidt number related to the spatial degrees of freedom are reported in literature for collinear [22] as well as non-collinear [23] geometries. Similarly, the effect of spectral filtering on the number of modes for pulsed PDC in a single spatial mode has been reported [30, 32]. Here we consider an experimental situation for crystals of different length where we include spatial as well as temporal modes. In this limit, analytical expressions can no longer be found. Instead of lengthy numerical computations we approximate the two-photon amplitude and use a two-photon coherence area to find approximate expressions that can be compared to the experiment.

The two-photon probability amplitude $C(\mathbf{q_s}, \mathbf{q_i}, \omega_s, \omega_i)$ for generating a non-collinear photon pair with transverse momenta $\mathbf{q_s}$ and $\mathbf{q_i}$ at frequencies ω_s and ω_i is given by

$$C(\mathbf{q_s}, \mathbf{q_i}, \omega_s, \omega_i) = E_p(\mathbf{q_s} + \mathbf{q_i}; \omega_s + \omega_i) \cdot T(\omega_s) \cdot T(\omega_i) \cdot \mathrm{sinc}(\frac{1}{2}\Delta kL), \quad (4.1)$$

where $E_p(\mathbf{q_s} + \mathbf{q_i}; \omega_s + \omega_i)$ is the electric field amplitude of the pump pulse,

and $T(\omega_s)$ and $T(\omega_i)$ are the transmission profiles of the spectral filters in the signal and idler beams, respectively. The term $\mathrm{sinc}(\frac{1}{2}\Delta kL)$ is the phase-matching function. The phase mismatch $\Delta kL/2$ can be approximated using a Taylor expansion that includes the effect of index dispersion, and is given by

$$\frac{1}{2}\Delta k(\omega)L = b^2|\mathbf{q_s} - \mathbf{q_i}|^2 + \varphi_0 + \eta(\delta\omega_s + \delta\omega_i), \tag{4.2}$$

where the first two terms are the phase mismatch for the center wavelength with a collinear phase mismatch φ_0, and parameter $b^2 = L/(4k_p)$, where $k_p = \omega_p n/c$ is the length of the wavevector at the center wavelength of the pump. The quantities $\delta\omega_s$ and $\delta\omega_i$ are the detuning of the angular frequency of the signal and idler frequency relative to the center frequency of the signal and idler beams. The phase mismatch φ_0 controls the opening angle of the cone of down-converted light and can be tuned in the experiment through temperature tuning of the PPKTP crystal [33, 34].

The parameter $\eta = (DL)/2$ with $D = 1/v_g(\omega_p) - \frac{1}{2}(1/v_g(\omega_s) + 1/v_g(\omega_i))$ is the difference in inverse group velocities v_g at the pump, signal and idler frequency [34, 35]. This term quantifies the difference in arrival time of pump and down-converted photons, and vanishes for small η (small D and/or L), where this walk-off is not important. We note that the group-delay dispersion D as introduced here is only valid for type-I down-conversion where both down-converted photons have the same polarization [34, 35]. This is appropriate for the PPKTP crystals used in this study where pump and down-converted photons are all ordinarily polarized.

In order to address a more specific, experimentally relevant situation, and to allow for simple solutions, we introduce Gaussian approximations of the various factors in Eq. (4.1). We express the pump amplitude $E_p(\mathbf{q_s} + \mathbf{q_i}; \omega_s + \omega_i)$ as the product of two Gaussian functions

$$E_p(\mathbf{q_s} + \mathbf{q_i}; \omega_s + \omega_i) \propto \exp(-|\mathbf{q_s} + \mathbf{q_i}|^2/\sigma^2)\ \exp(-\tau^2(\delta\omega_s + \delta\omega_i)^2/2) \tag{4.3}$$

where $\sigma = 2/w_p$ is the inverse spatial width of the pump profile and $\tau = \tau_p/1.18$ characterizes the duration of the pump pulse, and τ_p is the duration of the pump pulse expressed as FWHM. We express the filter functions as $T(\omega_{s,i}) = \exp(-(\delta\omega_{s,i}/2\mathcal{F})^2)$, where $\mathcal{F}$ is the filter bandwidth (FWHM), which is assumed to be much smaller than the natural bandwidth of the Type-I PDC process.

To approximate the phase-matching function by a Gaussian we use $\mathrm{sinc}[\Delta k_z L/2] \approx \exp[-(1/4)(\Delta k_z L/2)^2]$. The phase-mismatch given by Eq. (4.2) shows that the spectral and spatial properties of PDC light are generally mixed. This implies that the color of the PDC light changes with emission angle. For colinear PDC this leads to non-separable 'X'-entanglement [36] that becomes noticeable when a large frequency bandwidth of PDC light is collected. For non-colinear PDC, that we consider in this article, the correlations are transformed into a separable structure [37]. In addition, we collect only a small fraction of PDC light by using narrow frequency filters in the detection. Under those conditions the phase-matching function can be approximated as a separable product of two Gaussian functions to keep the analysis simple. The total two-photon probability amplitude of a pulsed pump can then be written as

$$\begin{aligned} C(\mathbf{q_s}, \mathbf{q_i}, \omega_s, \omega_i) \propto\ & \mathrm{e}^{-(\eta)^2(\delta\omega_s+\delta\omega_i)^2} \times \\ & \mathrm{e}^{-(\tau^2/2)(\delta\omega_s+\delta\omega_i)^2} \mathrm{e}^{-(1/(2\mathcal{F}))^2(\delta\omega_s^2+\delta\omega_i^2)} \times \\ & \mathrm{e}^{-(b^2|\mathbf{q_s}-\mathbf{q_i}|^2+\varphi_0)^2} \mathrm{e}^{-(1/\sigma)^2|\mathbf{q_s}+\mathbf{q_i}|^2}. \end{aligned} \tag{4.4}$$

Despite the various approximations, the Schmidt decomposition of the two photon field of Eq. (4.4) has to be computed numerically. In this section we follow a different approach and estimate the visibility χ measured in the experiment as a function of the diameter of the pump beam, the length of the crystal, and the size of the aperture placed in the far field to collect the down-converted light.

Inspired by Eq. (4.4), we assume that the effect of the temporal modes, spatial modes and walk-off can be factorized so that their influence can be separated, i.e. $\chi = \chi_t \chi_s \chi_w$. This assumption is based on the fact that the spatio-temporal correlations of non-colinear PDC are separable and that second-order terms in the Taylor expansion of phase mismatch $\Delta kL/2$ are small. These terms give rise to additional mixing of spatial and temporal degrees of freedom and can be safely neglected for crystal lengths that are shorter than τ/D [37]. For the PPKTP crystals and the pulse duration in this study this length equals 1.3 mm and the neglecting the contribution of these terms is thus not strictly valid.

By treating the different degrees of freedom separately, we can use known expressions for the different visibilities. The visibility χ_t, for PDC light filtered by a spectral filter with a bandwidth that is much more narrow than

the natural bandwidth of the process, is given by [30, 32]

$$\chi_t = \frac{1}{\sqrt{1+(\tau\mathcal{F})^2}} \tag{4.5}$$

The influence of walk-off, characterized by the visibility χ_w can be estimated based on the two-photon field given by Eq. (4.4) and expressions found in literature for the Schmidt number of spatial modes for collinear [22] and non-collinear PDC [23] geometries. We write the dependence of the visibility on walk-off as

$$\chi_w = \frac{1}{\sqrt{1+\left(\frac{L}{2L_0}\right)^2}}, \tag{4.6}$$

where L_0 is the total walk-off length as a result of both transverse and group-velocity walk-off.

The visibility χ_s can be determined by considering the correlations of two points at positions $\mathbf{r_1}$ and $\mathbf{r_2}$ in the far field, which are

$$\chi_s(\mathbf{r_1},\mathbf{r_2}) = \exp(-|\mathbf{r_1}-\mathbf{r_2}|^2/r_0^2). \tag{4.7}$$

A coherence diameter $r_0 = \lambda f/\pi w_p$ has been introduced [29] as a measure for the diffraction limited momentum spread of the pump. Here λ is the wavelength of the down-converted light and f is the focal length of the lens used to create the far-field of the PDC source. To postulate these correlations, we have assumed that the coherence diameter r_0 is smaller than the width of the PDC ring. To keep a consistent notation we note that the quantity r_0 introduced here and the quantity σ used in Eq. (4.4) are related via $r_0 = 2\sigma f/k_p$.

In the experiment, photons are collected through a finite aperture with a diameter a. Therefore the observed visibility of the four-photon state with two detectors is obtained by integration over the apertures, resulting in:

$$\chi_s(a) = \frac{1}{\pi^2 a^4}\iint \chi_s(\mathbf{r_1},\mathbf{r_2})\Theta(\frac{a}{2}-|\mathbf{r_1}|)\Theta(\frac{a}{2}-|\mathbf{r_2}|)\mathrm{d}\mathbf{r_1}\mathrm{d}\mathbf{r_2}, \tag{4.8}$$

where the Heaviside step-functions $\Theta(\frac{a}{2}-|\mathbf{r_1}|)$ and $\Theta(\frac{a}{2}-|\mathbf{r_2}|)$ represent the sharp edges of the two apertures with equal radius $a/2$ in the far-field. When both apertures are centered at the same position, the calculation of the visibility resembles that of efficient collection of two-photon states from a PDC source and the integral can be simplified to [38]:

$$\chi_s(a) = \frac{1}{\pi}\int_0^1 \left(\arccos(x) - x\sqrt{1-x^2}\right)\exp(-(xa/r_0)^2)\mathrm{d}x. \tag{4.9}$$

4.3 Experiment

The experimental setup to measure the visibility of the four-photon state is sketched in Fig. 4.1. UV pulses are produced by frequency doubling the pulses of a tunable mode locked Ti:sapphire laser operating at 826.4 nm wavelength. This results in $\sim$ 2 ps long pulses at 80 MHz repetition rate, with approximately 180 mW average laser power at a wavelength of 413.2 nm. Lens L_1 focusses the pulsed laser beam to a diameter w_p into a periodically poled KTP (PPKTP) crystal that generates non-collinear, frequency degenerate photon pairs at a wavelength of 826.4 nm [34]. To this end the PPKTP crystal is temperature controlled, and stabilized within 20 mK, to adjust the phase-matching conditions. Typically, we set a constant temperature of $T = 25°$C of the PPKTP crystal to create an opening angle $\theta \approx 40$ mrad for the down-converted light.

The PDC light is collected by lens L_2 with a 270 mm focal distance and is filtered by a bandpass filter F with a bandwidth of either 1.0 nm or 0.4 nm FWHM. The photons are split by a beamsplitter BS and are then spatially filtered by the apertures A and collected into a 50 μm core multi-mode fiber using lens L_3 (f_3 = 11 mm). The photons are then detected by fiber-coupled single photon counting modules. The combination of aperture, lens and fiber acts as a bucket detector and is mounted on a motorized translation stage to scan the detection unit in x and y-directions in the far field of the PDC source created by the lens L_2. In the experiment we convert the position of the detector in the far-field to an angle by dividing by the focal length of the lens. This angle, denoted as q, corresponds to the transverse momentum $\mathbf{q}$ normalized to the wavevector of the PDC light, i.e. $q = 2|\mathbf{q}|/k_p$.

An electronic time delay of either 0 ns or 12 ns is introduced between detectors D_1 and D_2 to record coincidence events in the same pulse (R^{0ns}) and between subsequent pulses (R^{12ns}). For count rates small compared to the laser repetition rate the contribution from more than two pairs to the coincidence rates can be neglected. The coincidence rate R^{12ns} is due to two independent pairs produced in the two different laser pulses, and is given by

$$R^{12ns} = N_P(\frac{\eta}{2})^2\frac{P_2^2}{2}, \tag{4.10}$$

where N_P is the laser repetition rate, P_2 is the probability to create a single photon pair via spontaneous PDC, and $\eta/2$ is the photon detection efficiency

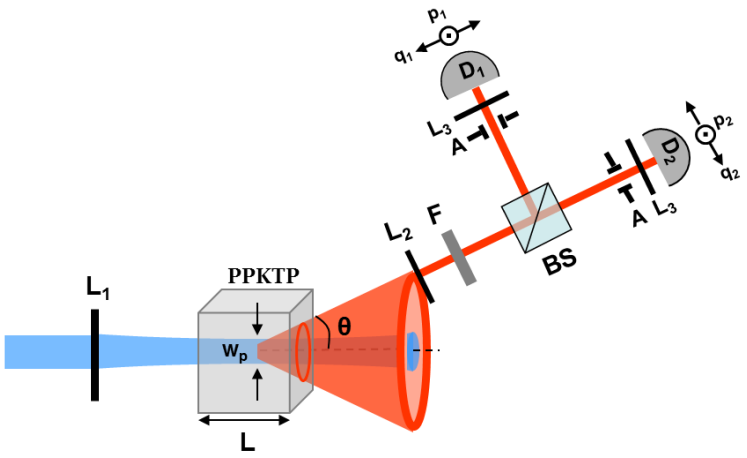

Figure 4.1: Experimental setup for generating and characterizing spatially entangled four-photon states. UV pump pulses from a frequency doubled Ti:Sapphire laser are focused by lens L_1 in a PPKTP crystal. Down-converted photons are collected by the lens L_2 ($f_2 = 270$ mm) and filtered by a bandpass filters F at a wavelength of 826.4 nm with 1 nm or 0.4 nm FWHM bandwidths. Photons are split by a beam splitter (BS) and detected by fiber-coupled APDs D_1 and D_2 placed on computer controlled translation stages. Spatial-mode selection occurs by means of tunable detector apertures (A) and a lens L_3 mounted on a translation stage. Photon counts and coincidences are recorded as a function of the angular positions q (horizontal direction) and p (vertical direction) of the detectors in the far-field.

that contains an extra factor two to accounts for the beamsplitter. Similarly, the coincidence count rate R^{0ns} contains a contribution due to stimulated emission and is given by

$$R^{0ns} = N_P(\frac{\eta}{2})^2 \frac{P_2^2}{2}(1+\chi), \tag{4.11}$$

In the experiment we find the visibility parameter as $\chi = (R^{0ns} - R^{12ns})/R^{12ns}$ [29], assuming that contributions to the coincidence rate from quantum states with more than 4 photons remain small in the experiment. Since the setup collects photons from one side of the PDC ring, two signal photons created by stimulated emission (the corresponding two idler photons are located on the other side of the ring) are split on the beam splitter and detected in the far field by detectors D_1 and D_2. Only

photon states produced by stimulated emission give rise to the correlations that register as coincidences. Hence, this setup with two detectors suffices to monitor the correlations of a four-photon state [29, 30].

4.4 Results and Discussion

4.4.1 Four-photon visibility in the spatial and temporal domain

Figure 4.2 shows the measured visibility of the four-photon state as a function of aperture size for a 2 mm long PPKTP crystal and a pump beam focused to a waist $w_p = 85 \pm 10$ μm. Measurements are shown for a 1 nm and 0.4 nm FWHM bandpass filter. The transmission spectra of the two bandpass filters are shown in the inset. The different symbols in the figure correspond to different measurement series. As can be seen, the visibility increases for smaller aperture size and more narrow bandpass filters. The solid lines through the data are calculations based on numerical integration of Eq. (4.8) using a fixed coherence diameter $r_0 = 0.84 \pm 0.1$ mm, which is calculated from the independently measured beam waist. The shaded areas in Fig. 4.2 show the outcome of similar calculations based on a realistic range of beam diameters of $w_p = 75 - 95$ μm in the experiment. Spectral filtering with the 0.4 nm FWHM bandpass filter yields a twice higher visibility ($\chi = 0.8$) than filtering with the 1 nm FWHM bandpass filter, consistent with the dependence of χ_t on filter bandwidth.

4.4.2 Universal expression for visibility

The far-field size of a spatial mode, and thus the coherence area r_0, increase for tighter focusing conditions. The diameter and width of the PDC ring remain constant as long as the Rayleigh range of the focused beam is significantly larger than the crystal length. As a consequence, an area on the PDC ring selected by an aperture with diameter a in the far field is expected to yield a higher visibility of four-photon states when created with a tighter focus.

The measured visibility of the four-photon states as a function of aperture size for three different focusing conditions ($w_p = 55 \pm 5$ μm (black symbols), $w_p = 85 \pm 5$ μm (red symbols) and $w_p = 155 \pm 5$ μm (blue symbols)) is shown in Fig. 4.3(a), where the different symbols refer to different measure-

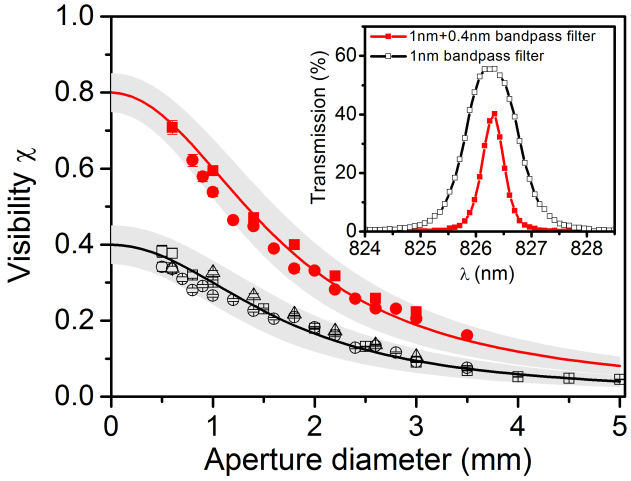

Figure 4.2: Variation of the visibility χ of the four-photon state as a function of aperture size. The PDC light is generated in a 2 mm PPKTP crystal and detected using 1 nm FWHM bandpass filter (black open symbols) and 0.4 nm FWHM bandpass filter in combination with the 1 nm FWHM filter (red solid symbols) at 826.4 nm wavelength. The solid lines (with shaded areas) correspond to calculations based on Eq. (4.8) with pump beam diameter of 85±10 μm for each of the bandpass filters. The inset shows the measured transmission spectra of the filters.

ment runs. Photons are created in a 2 mm long PPKTP crystal and filtered by a 1 nm FWHM bandpass filter centered at 826.4 nm. In the experiment we ensure that light is collected from the same area on the PDC ring by maximizing the coincidence rate and the visibility.

The solid lines in Fig. 4.3(a) indicate the calculated visibility as a function of detector aperture size a obtained by numerical evaluation of Eq. (4.8). This calculation contains no free parameters other than the number of temporal modes, determined by the 1 nm bandpass filter, which limits the maximum visibility to χ_t=0.4. The value of r_0 calculated from the measured beam diameter for the different focussing conditions is $r_0 = 1.42 \pm 0.14$ mm, 0.84 ± 0.08 mm and 0.46 ± 0.05 mm for a pump beam waist of 55±5, 85±5 and 155±5 μm, respectively. As can be seen, the model is in excellent agreement with the experimental data.

The similarity of the curves in Fig. 4.3(a) and the prominent role of r_0

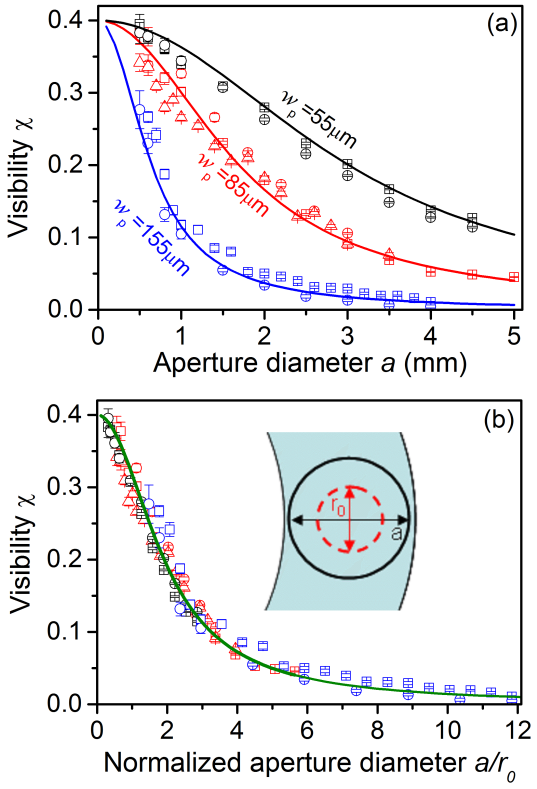

Figure 4.3: (a) Visibility χ of four-photon states obtained using different pump beam diameters equal to $w_p = 55 \pm 10\ \mu$m (black symbols), $w_p = 85 \pm 10\ \mu$m (red symbols) and $w_p = 155 \pm 10\ \mu$m (blue symbols) as a function of the diameter of the detector aperture. Photon pairs are created in a 2 mm long PPKTP crystal and filtered by a 1 nm FWHM bandpass filter. (b) Universal curve for visibility of four-photon states as a function of the normalized aperture diameter a/r_0. The inset illustrates one side of the PDC ring with an area selected by an aperture of diameter a together with the characteristic diameter $r_0 = \lambda f/(\pi w_p)$ determined by the diameter of the pump beam w_p.

suggest the existence of a universal relationship for the four-photon visibility. This universal curve is expressed in integral form by Eq. (4.9), which contains the ratio a/r_0. Figure 4.3(b) shows the same data rescaled by plotting the visibility as a function of the ratio of aperture and coherence diameter a/r_0.

All measurements now fall onto the same curve for the visibility as a function of the dimensionless parameter a/r_0. We note that the universal curve in Fig. 4.3(b) can only be valid as long as the detector aperture is smaller than the width of the PDC ring (see the inset of Fig. 4.3(b)), so that the coherence expressed by Eq. (4.8) remains independent of the width of the PDC ring. Hence, for a given combination of aperture size and pump beam diameter only part of the curve can be recovered.

4.4.3 Spatial and temporal walk-off

The measured visibility also depends on the length of the crystal through walk-off. This walk-off makes the stimulated emission process less probable since different sections of the crystal function as independent sources. The corresponding visibility of the four-photon states is reduced and should be inversely proportional to the crystal length for crystals that are much longer than the walk-off length.

We limit the discussion to a transverse walk-off and a transit-time difference walk-off because birefringent walk-off is not present in this study that uses a PDC source based on PPKTP crystals where all photons have the same polarization. The transit-time difference walk-off is related to the transit-time dispersion D =1.5 ps/mm [35] and puts a limit to the crystal length over which the down conversion is efficient [34]. This walk-off becomes important when the delay between pump and down-converted pulses is comparable to the pulse duration τ. The corresponding group velocity walk-off length is defined as $L_g = \tau/D$. For the $\sim$2 ps laser pulses used here we estimate a walk-off length 1.3 mm.

For non-collinear PDC, an additional transverse walk-off is present because the down-converted photon beams propagate at an angle relative to the pump beam. The transverse walk-off length is defined via $L_t = w_p n/\theta_0$, where w_p is the beam diameter of the pump beam, n is the (ordinary) refractive index of the crystal and $\theta_0 \approx 40$ mrad is the external opening angle of the PDC light. The corresponding transverse walk-off length for a realistic beam waist of 100 μm is $L_t \approx 4.3$ mm, i.e. a factor 3 larger than the group-velocity walk-off length L_g.

Figure 4.4 shows the measured visibility as a function of crystal length for three different focussing conditions obtained by measuring the extra co-

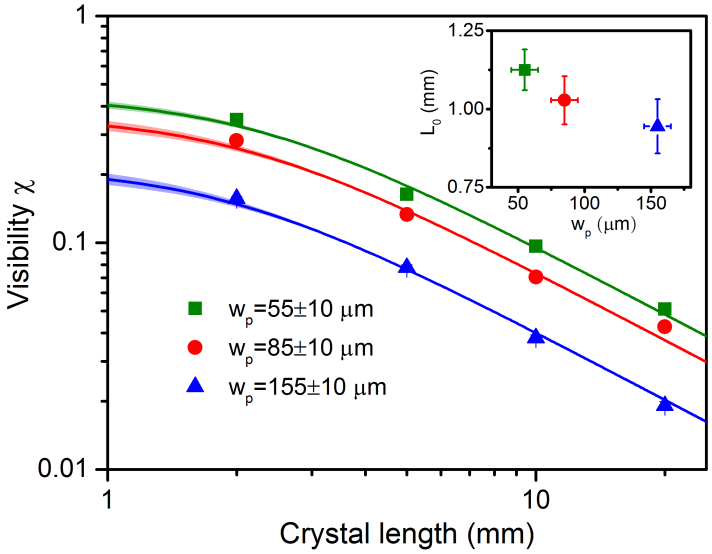

Figure 4.4: Measured visibility χ of the four-photon state generated with pump beam diameters equal to $w_p = 55$ μm (blue triangles), $w_p = 85$ μm (red circles) and $w_p = 155$ μm (green squares). The data are shown as a function of crystal length, using an aperture diameter of 1 mm and a 1 nm FWHM bandpass filter. The solid lines represent fits to the data (see text). The shaded areas indicate the confidence interval of the fit taking into account a ± 10 μm uncertainty in the beam diameter w_p. The inset shows the walk-off length obtained from the fit of Eq. (4.6) to the data.

incidence events for crystal lengths of 2, 5, 10 and 20 mm. The solid lines in Fig. 4.4 correspond to a best fit of the visibility χ given by Eq. (4.6) with only L_0 as a fit parameter to the data. The shaded areas indicate a range of realistic fit curves incorporating a range of beam diameters based on a ± 10 μm uncertainty in the measured beam diameter. In the fit procedure, we reduce the number of fit parameters by considering the contribution to the visibility due to walk-off χ_w, temporal modes χ_t and spatial modes χ_s independently, i.e. by using $\chi = \chi_w \chi_t \chi_s$. The value of χ_t = 0.4 follows from the 1.0 nm spectral bandwidth of the filter used. The value of χ_s can be estimated from Fig. 4.3 using the known aperture diameter $a = 1$ mm and the value of w_p. We estimate χ_s=(1/1.03), (1/1.23) and (1/2.07) for w_p=55 μm, 85 μm, 155 μm, respectively.

All measurements are in good agreement with the model given by

Eq. (4.6) and can be described by a walk-off length $L_0 \approx 1.0 \pm 0.1$ mm that is comparable to the group-velocity walk-off length L_g and is independent of the pump beam waist w_p. The inset of Fig. 4.4 shows the walk-off length as a function of the pump beam waist obtained form a best fit with error bars as a result of experimental uncertainty in beam diameter. These data suggests a trend of decreasing walk-off length L_0 with beam diameter, which is surprising as we would expect a weak increase of the walk-off length with beam diameter because spatial walk-off becomes less important for larger beam diameters. We suggest that the reason for this deviation are terms that mix temporal and spatial degrees of freedom in the two-photon amplitude. These correlations between the frequency of PDC light and transverse momentum will indeed become more apparent in the experiment for smaller r_0, i.e. for larger pump beam diameters.

4.4.4 Joint spatial distribution of four-photon states

The model for the spatial visibility χ_s as expressed by Eqns. 4.7 and 4.8 is valid when the intensity of the down-converted source can be assumed constant over the PDC ring. Strictly speaking this condition is difficult to achieve in an experiment since the sizes of the aperture a, the parameter r_0 as well as the width of the PDC ring in the far field are of the same order of magnitude. It is thus rather surprising that the model works so well and that a universal curve as a function of dimensionless aperture size describes our data. This raises questions how far the visibility model with a simple coherence area can be used outside the range for which it was designed and what are the features of experiments where this model starts to break down.

To investigate this question and to probe the limits of the validity of the model, we measure the coincidence rates as a function of the angular position (transverse momentum in the horizontal (x) direction) (q_1, q_2) of the two apertures in the far field created by lens L_2, for different focussing conditions. From these measurements the excess coincidence rate as $(R^{0ns} - R^{12ns})$ can be determined. Compared to the visibility this quantity is easier to measure for points at the edge of the PDC ring with a low coincidence rate, and we refer to this measurement as a joint spatial distribution of stimulated pair emission [29]. To convert these values to a visibility the rate should be divided by the rate R^{12ns}.

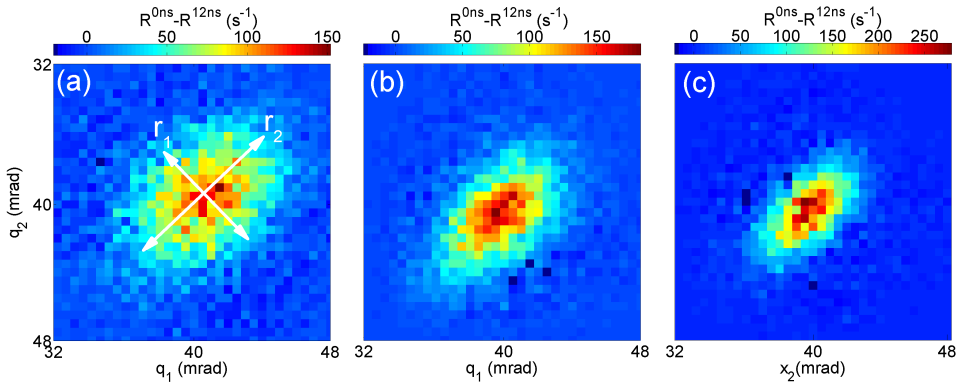

Figure 4.5: Measured joint spatial distribution of genuine four-photon states as a function of the angular positions of q_1 and q_2 of the detectors D_1 and D_2 in the far-field using a 1 nm FWHM bandpass filter and a 1.5 mm aperture size at f = 270 mm. Down-converted photons are created by a pump beam diameter of (a) $w_p = 35 \pm 5$ μm (b) $w_p = 45 \pm 5$ μm (c) $w_p = 85 \pm 5$ μm.

The false color images in Fig. 4.5 show the measured excess coincidences for a pump beam diameter equal to $w_p = 35 \pm 5$ μm (a), $w_p = 45 \pm 5$ μm (b) and $w_p = 80 \pm 5$ μ (c). Data are represented as a function of the angular position q_1 and q_2 of the two scanning detectors D_1 and D_2. To perform these measurements a spectral filter with a 1.0 nm bandwidth and an aperture with a diameter a = 1.5 mm are chosen as a compromise between getting a sufficiently high visibility and a reasonable coincidence count rate. This allows to measure the complete spatial correlations within 4 hours using a point-by-point scan, before realignment of the setup is necessary.

The data in Fig. 4.5 clearly shows an ellipsoidal feature in the excess coincidences with the long axis aligned along the diagonal direction. This diagonal direction corresponds to two detectors looking at the same position in the far field of the PDC source, where strong correlation produced by a stimulated pair emission are expected. To compare the measurements to the model expressed by Eq. (4.8), we need to normalize the measured difference in coincidence rate by the accidental rate R^{12ns}. To this end, we fit both the corrected coincidence rate and the accidental coincidence rate to a 2-D Gaussian distribution. These fits yield characteristic sizes r_1 and r_2 for the excess coincidences, as indicated in Fig. 4.5(a), and a single size r_a for the accidental

rate. We use the fitted values of r_1, r_2 and r_a to compute the size of the correlations in the visibility. The spatial visibility χ_s is also ellipsoidal, with sizes r_1' and r_2'. These sizes are defined via $\left(\frac{1}{r_{1,2}}\right)^2 = \left(\frac{1}{r_{1,2}'}\right)^2 + \left(\frac{1}{r_a}\right)^2$ and are larger than the sizes visible in Fig. 4.5.

Table 4.1: The experimental and calculated values of characteristic diameter r_1' and the visibility $\chi_t\chi_s$ (see text).

		experiment		theory	
w_p (μm)	r_0 (mrad)	r_1' (mrad)	$\chi_s\chi_t$	r_1' (mrad)	$\chi_t\chi_s$
35 ± 5	7.5 ± 1.1	11.2 ± 0.5	0.21 ± 0.08	9.4 ± 1.3	0.35 ± 0.02
45 ± 5	5.8 ± 0.6	7.8 ± 0.3	0.31 ± 0.08	7.6 ± 0.7	0.32 ± 0.02
85 ± 5	3.3 ± 0.2	5.8 ± 0.3	0.22 ± 0.05	5.2 ± 0.2	0.23 ± 0.01

Table 4.1 summarizes the values of r_1' as well as the visibility $\chi_t\chi_s$ deduced from the experiment for the different pump beam waists. The value of r_0 is included as a reference. The error bars on r_1' follow from error propagation using the fitted values r_1 and r_a. The value of $\chi_t\chi_s$ in the experiment was determined by calculating the average value along the diagonal in Fig. 4.5. The experimental values should be compared to a theoretical expression, similar to Eq. (4.8) modified so that the integration runs over the two apertures that are no longer centered at the origin. This model predicts that the visibility is independent of $q_1 + q_2$ and therefore predicts r_2' to be infinite. This is consistent with the data for the 85 μm pump beam size where the width of the accidental coincidences and the extra coincidences is identical within the error bar. For tighter focussing conditions the value of r_2' deduced from the experiment is finite.

The calculated values for the visibility $\chi_t\chi_s$ and r_1' are summarized in table 4.1, where the error bars are calculated taking into account the uncertainty on the measured pump beam waist. Good agreement with the experiment is found for the 45 and 80 μm pump beam waist. For the strongest pump beam focus, the calculated visibility and size r_1' do not agree with the experiment. Our interpretation is that the assumptions underpinning the model of Eq. (4.8) break down. For the strongest focussing conditions, the spread in wavevector of the pump affects the phase-matching conditions as the crystal

length becomes comparable to the Rayleigh range of the beam. This leads to a PDC ring that is broadened in the far-field due to the focussed pump beam. Using the notation of Law and Eberly [22], this corresponds to the regime where $b\sigma > 1$. In this regime the number of Schmidt modes increases and the visibility χ_s is reduced. This decrease in visibility for very tight focussing is not contained in Eqns. 4.7 and 4.8, that predict a monotonous increase with decreasing pump-beam waist, i.e. an increase in the far-field mode size r_0.

4.5 Conclusion

We have characterized four-photon spatial correlations created via stimulated parametric down-conversion in a non-collinear geometry. High visibility of the four-photon state up to 80% is observed by narrow spectral and spatial filtering of the down-converted light. This demonstrates that single (spatial and temporal) mode operation can be achieved under suitable experimental conditions.

Data for different focussing conditions can be combined to a single, universal expression for the visibility of the four-photon state. This universal expression does not depend on material properties and contains only the ratio of the aperture size a and a spatial coherence diameter r_0 set by the divergence of the pump beam. Our experimental results are consistent with this universal expression of the visibility. By varying the size r_0 using different focusing conditions we ensure that the aperture size a remains smaller than the width of the PDC ring. This allows to explore the expression for visibility over a significantly larger range of the parameter a/r_0 than what is possible in a single experiment.

For longer crystals pumped by a picosecond pulsed pump laser, the combination of the crystal length and opening angle of the PDC cone introduces a spatio-temporal walk-off effect. We have explored this effect by measuring the visibility for different focussing conditions as a function of crystal length. The experimental data can be described by a walk-off length of 1.0 ± 0.1 mm for a 2 ps long pulse. This walk-off length is comparable to the group velocity walk-off length, estimated to be 1.3 mm. Transverse walk-off effects were found to be relatively unimportant.

The detailed structure of the spatial correlations expressed as a joint spatial distribution of the four-photon state show that the model and the uni-

versal curve break down for tight focussing. The tight-focussing condition mixes the spatial and temporal degrees of freedom. For a 2 mm long PPKTP crystal, this becomes apparent for a laser beam waist smaller than 40 μm.

Bibliography

[1] S. Friberg, C. K. Hong, and L. Mandel, *Measurement of time delays in the parametric production of photon pairs*, Phys. Rev. Lett. **54**, 2011 (1985).

[2] J. D. Franson, *Bell inequality for position and time*, Phys. Rev. Lett. **62**, 2205 (1989).

[3] R. T. Thew, A. Acín, H. Zbinden, and N. Gisin, *Bell-type test of energy-time entangled qutrits*, Phys. Rev. Lett. **93**, 010503 (2004).

[4] A. Aspect, P. Grangier, and G. Roger, *Experimental tests of realistic local theories via Bell's theorem*, Phys. Rev. Lett. **47**, 460 (1981).

[5] A. Aspect, P. Grangier, and G. Roger, *Experimental realization of Einstein-Podolsky-Rosen-Bohm Gedankenexperiment: A new violation of Bell's inequalities*, Phys. Rev. Lett. **49**, 91 (1982).

[6] P. G. Kwiat, K. Mattle, H. Weinfurter, A. Zeilinger, A. V. Sergienko, and Y. Shih, *New high-intensity source of polarization-entangled photon pairs*, Phys. Rev. Lett. **75**, 4337 (1995).

[7] Y.-X. Gong, X.-B. Zou, X.-L. Niu, J. Li, Y.-F. Huang, and G.-C. Guo, *Generation of arbitrary four-photon polarization-entangled decoherence-free states*, Phys. Rev. A **77**, 042317 (2008).

[8] D. V. Strekalov, A. V. Sergienko, D. N. Klyshko, and Y. H. Shih, *Observation of two-photon ghost interference and diffraction*, Phys. Rev. Lett. **74**, 3600 (1995).

[9] M. I. Kolobov, *The spatial behavior of nonclassical light*, Rev. Mod. Phys. **71**, 1539 (1999).

[10] J. C. Howell, R. S. Bennink, S. J. Bentley, and R. W. Boyd, *Realization of the Einstein-Podolsky-Rosen paradox using momentum- and position-entangled photons from spontaneous parametric down conversion*, Phys. Rev. Lett. **92**, 210403 (2004).

[11] S. Walborn, C. Monken, S. Pdua, and P. S. Ribeiro, *Spatial correlations in parametric down-conversion*, Physics Reports **495**, 87 (2010).

[12] S. P. Walborn, D. S. Lemelle, D. S. Tasca, and P. H. S. Ribeiro, *Schemes for quantum key distribution with higher-order alphabets using single-photon fractional Fourier optics*, Phys. Rev. A **77**, 062323 (2008).

[13] S. P. Walborn, D. S. Lemelle, M. P. Almedia, and P. H. S. Ribeiro, *Quantum key*

distribution with higher-order alphabets using spatially encoded qudits, Phys. Rev. Lett. **96**, 090501 (2006).

[14] G. Molina-Terriza, A. Vaziri, R. Ursin, and A. Zeilinger, *Experimental quantum coin tossing*, Phys. Rev. Lett. **94**, 040501 (2005).

[15] J.-L. Chen, C. Wu, L. C. Kwek, C. H. Oh, and M.-L. Ge, *Violating Bell inequalities maximally for two d-dimensional systems*, Phys. Rev. A **74**, 032106 (2006).

[16] L. Zhang, C. Silberhorn, and I. A. Walmsley, *Secure quantum key distribution using continuous variables of single photons*, Phys. Rev. Lett. **100**, 110504 (2008).

[17] S. D. Huver, C. F. Wildfeuer, and J. P. Dowling, *Entangled Fock states for robust quantum optical metrology, imaging and sensing*, Phys. Rev. A **78**, 063828 (2008).

[18] W. Dür, G. Vidal, and J. I. Cirac, *Three qubits can be entangled in two inequivalent ways*, Phys. Rev. A **62**, 062314 (2000).

[19] T. H. Yang and M. Nevascues, *Robust self-testing of unknown quantum systems into any entangled two-qubit states*, Phys. Rev. A **87**, 050102(R) (2013).

[20] N. Kiesel, C. Schmid, U. Weber, G. Tóth, O. Gühne, R. Ursin, and H. Weinfurter, *Experimental analysis of a four-qubit photon cluster state*, Phys. Rev. Lett. **95**, 201502 (2005).

[21] M. Murao, D. Jonathan, M. B. Plenio, and V. Vedral, *Quantum telecloning and multiparticle entanglement*, Phys. Rev. A **59**, 156 (1999).

[22] C. K. Law and J. H. Eberly, *Analysis and interpretation of high transverse entanglement in optical parametric down conversion*, Phys. Rev. Lett. **92**, 127903 (2004).

[23] M. P. van Exter, A. Aiello, S. S. R. Oemrawsingh, G. Nienhuis, and J. P. Woerdman, *Effect of spatial filtering on the Schmidt decomposition of entangled photons*, Phys. Rev. A **74**, 012309 (2006).

[24] L. A. Lugiato, A. Gatti, and E. Brambilla, *Quantum imaging*, J. Opt. B **4**, S176 (2002).

[25] T. B. Pittman, Y. H. Shih, D. V. Strekalov, and A. V. Sergienko, *Optical imaging by means of two-photon quantum entanglement*, Phys. Rev. A **52**, R3429 (1995).

[26] C. W. J. Beenakker, J. W. F. Venderbos, and M. P. van Exter, *Two-photon speckle as a probe of multi-dimensional entanglement*, Phys. Rev. Lett. **102**, 193601 (2009).

[27] W. H. Peeters, J. J. D. Moerman, and M. P. van Exter, *Observation of two-photon speckle patterns*, Phys. Rev. Lett. **104**, 173601 (2010).

[28] D. S. Lemelle, M. P. Almeida, P. H. S. Ribeiro, and S. P. Walborn, *A simple optical demonstration of quantum cryptography using transverse position and momentum variables*, Am. J.of Phys. **74**, 542 (2006).

[29] A. J. H. van der Torren, S. C. Yorulmaz, J. J. Renema, M. P. van Exter, and M. J. A. de Dood, *Spatially entangled four-photon states from a periodically poled potassium-titanyl-phosphate crystal*, Phys. Rev. A **85**, 043837 (2012).

[30] H. D. Riedmatten, V. Scarani, I. Marcikic, A. Acn, W. Tittel, H. Zbinden, and N. Gisin, *Two independent photon pairs versus four-photon entangled states in parametric down conversion*, J. Mod. Opt. **51**, 1637 (2004).

[31] Z. J. Ou, *Multi-photon quantum interference*, Springer, New York, 2007.

[32] P. R. Tapster and J. G. Rarity, *Photon statistics of pulsed parametric light*, J. Mod. Opt. **45**, 595 (1998).

[33] W. H. Peeters and M. P. van Exter, *Optical characterization of periodically-poled $KTiOPO_4$*, Optics Express **16**, 7344 (2008).

[34] S. C. Yorulmaz and M. J. A. de Dood, *Characterization of pulsed parametric down-conversion in PPKTP crystals*, Proc. SPIE **8440**, 84400G (2012).

[35] T. E. Keller and M. H. Rubin, *Theory of two-photon entanglement for spontaneous parametric down-conversion driven by a narrow pump pulse*, Phys. Rev. A **56**, 1534 (1997).

[36] A. Gatti, E. Brambilla, L. Caspani, O. Jedrkiewicz, and L. A. Lugiato, *X entanglement: The nonfactorable spatiotemporal structure of biphoton correlation*, Phys. Rev. Lett. **102**, 223601 (2009).

[37] L. Caspani, E. Brambilla, and A. Gatti, *Tailoring the spatiotemporal structure of biphoton entanglement intype-i parametric down-conversion*, Phys. Rev. A **81**, 033808 (2010).

[38] C. H. Monken, P. H. S. Ribereiro, and S. Pádua, *Optimizing the photon pair collection efficiency: A step toward a loophole-free bell's inequalities experiment*, Phys. Rev. A **57**, R2267 (1998).

CHAPTER 5

Photon pairs, double pairs, and quadruples in pulsed parametric down-conversion

We experimentally investigate the quantum state created by emission of four photons into the same optical mode as a result of stimulated parametric down conversion. The contribution from these four photons, which we call quadruplets, manifests itself as an extra peak in both single and coincidence count rates measured using bucket-type detectors with a small aperture placed in the far-field of the source. We observe a peak of extra coincidences in the collinear direction that grows quadratically with pump power, on a background of coincidence counts from single pairs created by spontaneous parametric down conversion that depends linearly on pump power. We attribute the extra coincidences in the collinear direction to quadruplet states with four indistinguishable photons emitted in the same mode. The contribution from this quadruplet state is superimposed on a signal due to double pair state, created by stimulated parametric down conversion of photon pairs into two distinguishable modes.

5.1 Introduction

Parametric down conversion (PDC) is a nonlinear optical process that can be used to create highly correlated quantum states of light [1]. At low pump power, the PDC process creates pairs of photons via a spontaneous process that splits the pump photon into two lower energy photons while conserving energy. The photons in each pair are strongly anti-correlated in momentum and frequency as a direct consequence of the underlying phase-matching condition and energy conservation. For higher pump powers, the probability to create multiple pairs increases and stimulated down-conversion gains importance. In this stimulated process, the photon pairs are exact copies of the initial photon pair, yielding a single quantum state that contains many indistinguishable particles [2].

When a continuous-wave laser is used in parametric down conversion, one produces independent photon pairs. Because the coherence time of the PDC light is much shorter than the coherence time of a typical laser [2], these pairs are mutually distinguishable. When a pulsed laser is used to pump the nonlinear crystal, two things change: (i) the instantaneous power can be so large that multiple photon pairs are generated during the pump pulse, and (ii) the coherence time of the laser can be comparable to the PDC bandwidth, so that there is little timing information that can lead to distinguishability. Further spectral filtering of the PDC light can then be used to erase all remaining timing information, reducing the number of temporal modes to 1 [2, 3]. A pulsed PDC experiment can thus yield states with an even number of photons, all in the same temporal mode. The questions we are addressing here are the following: (a) how do we distinguish a four photon event where all four photons are emitted into the same optical mode from an event that creates two exact copies of a photon pair that has its constituent photons in two distinct optical modes and (b) what are the characteristic features of an event where all four-photons couple to one and the same optical mode.

Traditionally, an experimental situation is used where the two photons in a pair follow different paths [4–6] as it allows to label the two photons in each pair. For instance, polarization-entangled states can be created via a type-II non-collinear PDC process, that introduces a polarization label for each photon [5]. The possibility of stimulated emission of pairs has been considered in this configuration either by using a strong laser pulse [3, 7, 8]

or by multiple passes of the laser pulse through the crystal [9]. In these cases, the process is stimulated by the presence of a single photon from a spontaneously emitted pair in each arm.

In this Chapter, we investigate a different situation, namely one that can be created when all photons are produced in the same optical mode. In this case, the creation of a second pair is stimulated by the presence of *both* photons of the initial pair in the same optical mode. This enhances the stimulated pair emission rate in that chosen spatial mode compared to the case in which the original pair is emitted into two different modes. The resulting quantum state then contains an even number of photons, condensed into the quantum state of indistinguishable photons labeled by the collinear direction of the PDC process. We report on the experimental observation of extra coincidence counts related to such a quantum state in a collinear PDC process in a periodically poled KTP (PPKTP) crystal. The contribution of the quadruplet state is superimposed on a signal of double-pair photon states created by stimulated emission of photon pairs into different spatial modes. A careful analysis of the experimental data using the known phase-matching conditions in the crystal allows to quantify the relative strength of the two second-order processes.

5.2 Quantum states generated by pulsed parametric down-conversion

Frequency-degenerate parametric down-conversion where photons are emitted into multiple discrete spatial modes can be described via an interaction Hamiltonian of the form [10]

$$\hat{H}_{\text{int}} = \tfrac{1}{2} i\hbar\kappa \sum_{j=-\infty}^{\infty} (\hat{a}^{\dagger}_{q_j}\hat{a}^{\dagger}_{-q_j} - \hat{a}_{q_j}\hat{a}_{-q_j}), \tag{5.1}$$

where $\hat{a}^{\dagger}_{q_j}$ and $\hat{a}^{\dagger}_{-q_j}$ are creation operators that create a photon pair in modes labeled by the transverse momenta q_j and $-q_j$, respectively. The parameter κ contains the strength of the nonlinearity and the amplitude of the classical pump field. To keep the notation simple, we limit the current discussion to down-conversion events that occur into two (discrete) spatial modes, labeled by q and $-q$. The corresponding Hamiltonian is given by [10]

$$\hat{H}_{\text{int}} = i\hbar\kappa(\hat{a}^{\dagger}_{q}\hat{a}^{\dagger}_{-q} - \hat{a}_{q}\hat{a}_{-q}), \tag{5.2}$$

Note that this expression contains an extra factor of 2 to account for the fact that the full Hamiltonian (Eq. 5.1) contains two terms that involve spatial modes labeled by q and $-q$. The product of the two creation operators in Eq. 5.2 creates a photon pair that is anti-correlated in transverse momentum. This anti-correlation in momentum follows directly from the phase-matching conditions for frequency degenerate down-conversion (for a plane wave pump and a crystal that is infinite in the transverse dimension). We compare this Hamiltonian to the Hamiltonian that corresponds to a process when the two photons are produced in the same mode, labeled by $q = 0$. This process leads to [10]

$$\hat{H}_{\text{int}} = i\hbar\kappa \left(\frac{\hat{a}_0^{\dagger 2}}{2} - \frac{\hat{a}_0^2}{2} \right), \tag{5.3}$$

where $\hat{a}_0^{\dagger 2}$ is the creation operator of a photon pair, emitted into the same mode labeled by $q = 0$.

The relevant quantum states, that contain contributions of multiple pairs, are obtained by having the time-evolution operator of the Hamiltonian acting on the vacuum state, i.e. by calculating $\exp(-i\hat{H}_{\text{int}}t/\hbar)|0\rangle$, where t is the interaction time. The resulting expressions can be evaluated by using disentangling expressions [10–12]. The wavefunction of the quantum states generated in a pair of modes with transverse momenta q and $-q$ ($q \neq 0$) is given by

$$|\Psi_q\rangle = \sum_n \frac{(\tanh(\kappa t))^n}{\cosh(\kappa t)} |n_q; n_{-q}\rangle, \tag{5.4}$$

where n is the number of photon pairs created. We denote the multi-photon state with n photons in both the spatial mode with transverse momentum q and $-q$ by $|n_q; n_{-q}\rangle$. Similarly, when both the signal and idler photons are created into the mode with transverse momentum $q = 0$, a superposition state of even numbers of photons is created. This state is given by

$$|\Psi_0\rangle = \sum_n \frac{(\tanh(\kappa t))^n}{\sqrt{\cosh(\kappa t)}} \frac{\sqrt{(2n)!}}{n!} \left(\frac{1}{2}\right)^n |2n_{q=0}\rangle, \tag{5.5}$$

where $|2n_{q=0}\rangle$ is a state with $2n$ photons in the spatial mode with transverse momentum $q = 0$. In this Chapter, we are interested in distinguishing the double-pair state $|2_q; 2_{-q}\rangle$ with 2×2 distinguishable photons from the quadruplet state $|4_{q=0}\rangle$ that contains four indistinguishable photons.

In most experiments the single pass gain is small, i.e. $\kappa t \ll 1$, and the quantum states Eq. 5.4 and Eq. 5.5 can be approximated by a Taylor expansion. This results in

$$|\Psi_q\rangle \approx (1 - \frac{(\kappa t)^2}{2})|0\rangle + \kappa t|1_q; 1_{-q}\rangle + (\kappa t)^2|2_q; 2_{-q}\rangle \tag{5.6}$$

$$|\Psi_0\rangle \approx (1 - \frac{(\kappa t)^2}{4})|0\rangle + \frac{\kappa t}{\sqrt{2}}|2_{q=0}\rangle + \sqrt{\frac{3}{8}}(\kappa t)^2|4_{q=0}\rangle \tag{5.7}$$

The difference in the two quantum states reflects the difference in the stimulated emission of pairs. For the non-collinear geometry the probability to create a double pair P_4 is increased by a factor two relative to the Poissonian expression $P_4 = \frac{1}{2}{P_2}^2$ [2, 3], i.e. $P_4 = {P_2}^2$. For the collinear geometry, the probability to create a double pair is $P_4 = \frac{3}{4}{P_2}^2$.

5.3 Quantum state detection schemes

Ideally, the detection of quantum states that contain four photons is done with four single photon detectors. A four-fold coincidence event where all detectors click simultaneously corresponds to a successful detection of a four-photon state. To implement such a scheme for the detection of the state $|\Psi_0\rangle$ requires the use of beamsplitters to distribute the four photons over the four detectors in a probabilistic way. A schematic diagram of a scheme that uses three beamsplitters and four detectors is depicted in Fig. 5.1a. If we assume that each of the beamsplitters has an equal 50/50 splitting ratio the probability for a photon to reach a particular detector is equal. The probability to create an event where each of the 4 photons arrives on a different detector is then given by $4!/4^4 = 0.09375$, while the probability to detect two photons with momentum $q \neq 0$ and two photon with $-q$ is $2!2!/4^4 = 0.015$. In order to select a particular transverse momentum of the photon, spatial filtering is required that will necessarily reduce the detection efficiency of the single photon counters. For detectors with an overall detection efficiency η, the total probability for registering a four photon event is $(4!/4^4)\eta^4$. This efficiency includes the collection efficiency and the spatial filtering of the photons. In a typical experiment [3] this efficiency is $\sim$1–3% and the probability to detect a four-fold coincidence is $\sim 10^{-9}$–10^{-7}. To generate four-photon states, a pulsed laser with a 80 MHz repetition rate is used. To keep the contribution

from states with more than four photons small, only a fraction of the laser pulses should create four photon states, limiting the generation rate of the state to $\sim 10^7$ s^{-1} and the four-fold coincidence rate to 0.01–1 s^{-1}. An experi-

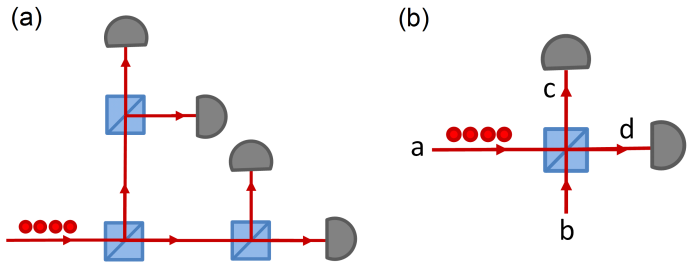

Figure 5.1: Detection schemes for a quantum state containing four photons using either 4 (a) or 2 (b) detectors.

mentally more viable approach is to use a single beamsplitter and two photon detectors as depicted in Fig. 5.1b. The coincidence count rates expected for this setup are much higher: the chance that both detectors are hit by at least one photon is now $> 99\%$, while the penalty for a limited detection efficiency is only η^2 instead of η^4. There are only two possibilities where one of the two detectors does not receive a photon while it is possible that both detectors register a photon from the two pairs produced by PDC. This leads to a coincidence rate proportional to η^2.

A complete calculation takes into account the quantum state and the probability that the detector clicks depending on the number of incident photons and depends on the exact experimental setup. In this section we consider pure number states (Fock states) as an input state to make the role of the beamsplitter and the finite efficiency of the detectors explicit. Approximate expressions of the count rates and coincidence rates relevant to the experiment are presented in section 5.4.1. The beamsplitter in Fig. 5.1b distributes the photons from the input port a over the two output ports c and d. The input state with n photons in port a and vacuum in port b is given by

$$|\Psi_{in}\rangle = |n\rangle_a |0\rangle_b. \tag{5.8}$$

The output state after the beamsplitter is easily computed for a symmetric

beamsplitter that has equal transmission and reflection coefficients. The output state after the beamsplitter is

$$|\Psi_{out}\rangle = \frac{1}{2^{n/2}} \sum_{k=0}^{n} i^{n-k} \sqrt{\frac{n!}{k!(n-k)!}} |n-k\rangle_c |k\rangle_d. \tag{5.9}$$

The photons at the output are detected by single photon counting avalanche photodiodes with a finite detection efficiency $\eta < 1$ that includes the finite collection efficiency as well as the non-unity internal quantum efficiency of the detectors. The probability that a detector clicks when n photons are incident on the detector is given by

$$p(n) = 1 - (1-\eta)^n, \tag{5.10}$$

where $(1-\eta)^n$ corresponds to the probability that the detector does not click. With the above equations the single count rate R_c on the detector that collects photons in output port c for an arbitrary state $|\Psi_{out}\rangle$ with n photons distributed over output ports c and d can be expressed as

$$R_c \propto \sum_{k=0}^{n} p(k) \left| \langle k|_c \sum_{l=0}^{n} \langle l|_d |\Psi_{out}\rangle \right|^2, \tag{5.11}$$

where the summation over the states $\langle l|_d$ traces out the photons in output port d and calculates the probability of a detection event in output port c. The count rates are proportional to this probability. A similar expression holds for the single count rate R_d for output port d. The coincidence rate is calculated by considering events where the two detectors click simultaneously

$$R_{cc} \propto \sum_{k=0}^{n} p(n-k)p(k) \left| \langle n-k|_c \langle k|_d |\Psi_{out}\rangle \right|^2. \tag{5.12}$$

These equations can be used to evaluate the single and coincidence rates in the experiment.

5.4 Experiment

In this section we describe our experimental scheme to investigate the multiple photon pairs generated in collinear parametric down-conversion. The experimental setup is schematically illustrated in Fig. 5.2.

Photon pairs are generated via type-I down-conversion in a 5 mm long periodically-poled $KTiOPO_4$ (PPKTP) crystal pumped by a pulsed laser that generates 2 ps long pulses at 413.2 nm. The pulses are created by frequency doubling of a pulsed Ti:Sapphire laser operating at a repetition rate of 80 MHz. The pulsed operation is essential as this strongly increases the probability to generate more than one photon pair in the time slot that is set by the pulse duration.

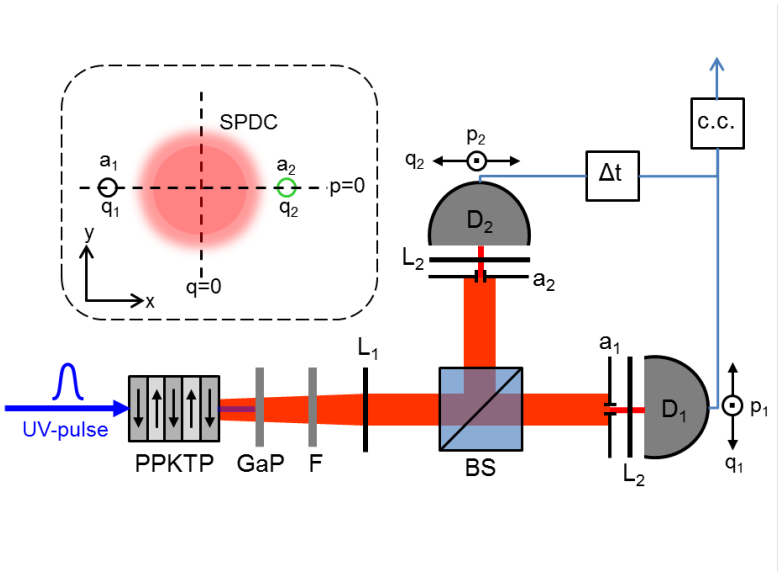

Figure 5.2: Schematic of the experimental setup to generate four-photon states via collinear, type-I SPDC obtained from a periodically poled KTP crystal (PPKTP). The pump light is blocked by an anti-reflection coated GaP wafer. A bandpass filter (F) with a bandwidth of 1 nm is used to collect frequency degenerate photon pairs at 826.4 nm. Down-converted photons are collected by the lens L_1 (f_1 = 150 mm) and split by a 50/50 beam splitter (BS). Apertures $a_1 = a_2 = 0.6$ mm in the far-field act as spatial-mode selectors and the transmitted photons are collected by the lens L_2 (f_2 = 11 mm) into a multi-mode fiber. Fiber-coupled single photon counting APDs D_1 and D_2 are used to detect the down-converted photons. The aperture, lens and fiber are placed on computer-controlled translation stages to provide photon detection while scanning the position of detectors in both horizontal (q) and vertical (p) directions. The inset shows the scanning configuration of either detector D_1 or D_2 in the far-field of the SPDC light.

The phase-matching in the crystal can be tuned by setting the crystal tem-

perature. For the crystal in this study, collinear phase-matching conditions for degenerate PDC of 826.4 nm light are reached at a temperature $T \approx 60^{\circ}$C. To detect the down-converted photons, we use a GaP wafer, anti-reflection coated at 826 nm, to fully block the 413.2 nm pump light. A narrow band-pass filter F (826.4 ± 1 nm) is used to select down-converted light close to frequency degeneracy. The photons are collected in the far-field by a lens L_1 with a focal length of 150 mm. The photons are then sent to two independent detection units via a beam splitter. Each of the detection unit is placed on a computer-controlled translation stage. The detection unit uses an aperture that spatially filters the down-converted photons. The unit as a whole can be regarded as a bucket-type detector, with a size equal to the aperture size. Photons that pass through the aperture are all collected by a f_1 = 11 mm lens into a multi-mode fiber (50 μm core diameter), and are registered by fiber-coupled single photon counting APDs.

The photons in a single pair generated by type-I PDC are anti-correlated in transverse momentum in the far-field. Therefore, these photons can be detected as coincidence counts when the two detectors are pointing in directions symmetrically around the collinear direction, i.e. corresponding to opposite transverse momenta ($q_1 = -q_2$). When pumping the PPKTP crystal with a picosecond pulse, stimulated parametric down-conversion may occur, yielding a second photon pair that is identical to the first pair. These stimulated events can be monitored by using a beam splitter and two detectors in the far-field positioned in such a way that they collect photons traveling in the same direction. In this configuration, where the transverse momenta of the two photons are identical, one does not measure single pairs. Hence, a coincidence measurement with $q_1 = q_2 \neq 0$ is sensitive to this correlated double-pair state created by stimulated emission, and is insensitive to single pairs, which are, as argued before, anti-correlated in their transverse momenta.

Computer-controlled actuators permit scanning the detectors in the angular position (q, p) in the far-field, where q and p refer to transverse momentum in the horizontal (x) and vertical (y) direction, respectively. The values of q and p are normalized to the wave-vector of the down-converted light and thus correspond to a far-field angle. In this Chapter we do not vary the detector position in the p-direction other than for alignment purposes. In addition, one-dimensional scans with improved signal-to-noise ratio are created for scanning configurations where both detectors D_1 and D_2 observe the

same position in the far-field ($q_1 = q_2$) or where the detectors move in opposite directions ($q_1 = -q_2$) during a scan. Coincidence counts are registered by a fast AND gate with a time window of 1.5 ns. We correct the measured coincidence rates for accidental coincidences by subtracting the coincidence rate between subsequent pulses. To measure these coincidences, we introduce a time delay of 12 ns (time between successive pulses of the laser) between the detectors using an electronic delay unit. Hence, the corrected coincidence rate can be obtained from the experimental data as $R_{cc} \equiv R_{cc}^{0\text{ ns}} - R_{cc}^{12\text{ ns}}$.

5.4.1 Calculation of single and coincidence rates

In this section we evaluate the single and coincidence rates expected in the experiment with two detectors for the states produced by PDC, using Eqns. 5.4 and 5.5 for the quantum state and Eqns. 5.8- 5.12 to incorporate the redistribution of photons by the beamsplitter and the finite detection efficiency. In the experiment the photons are both spectrally and spatially filtered using a bandpass filter and an aperture. Ideally, this allows to select a single spatial and temporal mode at the expense of the detection efficiency η.

We distinguish between the case when the photons are all emitted into the same $q = 0$ mode and when the photons from each pair are emitted in modes labeled by q and $-q$. For a pulsed laser, the single and coincidence count rates can be estimated by using the repetition rate R_p of the pulsed laser as the proportionality constant. The single count rates $R_s(q)$ and $R_s(0)$, for detection in a single mode, can be approximated for small parametric gain κt and for small detection efficiency $\eta \ll 1$ as

$$R_s(q) \approx R_p \left(\frac{(\kappa t)^2}{2}\eta + (\kappa t)^4 (\frac{\eta}{6} - \frac{\eta^2}{4}) \right) + \mathcal{O}((\kappa t)^6) \tag{5.13}$$

$$R_s(0) \approx R_p \left(\frac{(\kappa t)^2}{2}(\eta - \frac{1}{4}\eta^2) + (\kappa t)^4 (\frac{\eta}{6} - \frac{5}{12}\eta^2 + \mathcal{O}(\eta^3)) \right) + \mathcal{O}((\kappa t)^6), \tag{5.14}$$

where we have neglected all contributions due to quantum states produced by PDC that contain more than four photons.

In the experiment, we correct for accidental coincidences due to unrelated pairs by measuring the coincidence rate for events between subsequent laser pulses. This measured rate is expected to be equal to the accidental rate caused by two spontaneously emitted pairs within the same laser pulse. This

rate measured for different modes q and q' is given by:

$$R_{cc}^{12ns}(q,q') \approx R_p \frac{(\kappa t)^4}{4}\eta^2 + \mathcal{O}((\kappa t)^6). \tag{5.15}$$

and should be compared to the coincidence rate due to two photons emitted into the same mode with $q \neq 0$.

$$R_{cc}(q,q) \approx R_p \frac{(\kappa t)^4}{2}\eta^2 + \mathcal{O}((\kappa t)^6) \tag{5.16}$$

This rate is exactly twice the coincidence rate from spontaneously emitted pairs, consistent with the notion that the contributions due to stimulated and spontaneous emission of photon pairs should be equal for a single optical mode [2, 3]. For multiple modes the probability of stimulated pair emission in a specific mode is reduced. The ratio of the coincidence rate $R_{cc}(q,q)$ over the accidental coincidence rate $R_{cc}^{12ns}(q,q')$ is an experimental measure of the relative importance of stimulated emission. This ratio can be expressed as $1+\chi$, where χ can be interpreted as a visibility between 0 and 1 that is inversely proportional to the number of modes involved in the PDC process [2, 3], as long as no significant amount of events with more than four photons are generated.

Similarly, we find the coincidence rate for the two anti-correlated modes labeled by transverse momenta q and $-q$

$$R_{cc}(q,-q) \approx R_p \left(\frac{(\kappa t)^2}{4}\eta^2 + \frac{7(\kappa t)^4}{12}\eta^2 + \mathcal{O}(\eta^3) \right) + \mathcal{O}((\kappa t)^6) \tag{5.17}$$

as well as the coincidence rate for the $q = 0$ mode

$$R_{cc}(q=0) \approx R_p \left(\frac{(\kappa t)^2}{4}\eta^2 + \frac{5(\kappa t)^4}{6}\eta^2 + \mathcal{O}(\eta^3) \right) + \mathcal{O}((\kappa t)^6) \tag{5.18}$$

Based on the expressions for the single count rate, and the coincidence rate for the q and $-q$ modes, both the detector efficiency η and the single-pass gain $(\kappa t)^2$ can be estimated based on measured count rates, yielding

$$\eta \approx \frac{2R_{cc}(q,-q)}{R_s(q)} \tag{5.19}$$

and

$$(\kappa t)^2 \approx \frac{R_s(q)^2}{N_p R_{cc}(q,-q)}, \tag{5.20}$$

respectively, where the effect of the symmetric beamsplitter is incorporated in the expressions. For a typical experimental configuration with 0.6 mm detector aperture, and a 1 nm bandpass filter we obtain a detection efficiency $\eta \approx 0.02$. The single-pass gain $(\kappa t)^2$ is estimated as 0.34. This gain estimated from the experimental single and coincidence rates should be interpreted as the total gain for all modes involved. For a geometry with a 1 mm aperture, We have verified that a more lengthy calculation with an asymmetric beamsplitter and two detectors with unequal efficiency yields similar results. These results have been omitted here as they only complicate the notation.

5.4.2 Observation of a single-mode four-photon state

Figure 5.3 shows the coincidence rate R_{cc}, corrected for accidentals, as a function of the angular positions q_1 and q_2 of two detectors for nearly-collinear (a) (T=56 ^{o}C, $\varphi = -1.4$ rad) and collinear (b) (T=60 ^{o}C, $\varphi = 0.1$ rad) down-conversion, where φ is the phase-mismatch. The diameter of the detector apertures is set to 1 mm, and is a compromise between spatial resolution and count rate. The images in Fig. 5.3 clearly show large coincidence rates along the anti-diagonal direction ($q_1 = -q_2$), originating from single photon pairs. The false colour images are plotted on a logarithmic scale in order to make the contribution from double pairs visible. This contribution can be found along the diagonal direction ($q_1 = q_2$) in Fig. 5.3 (a) and (b) and is a result of stimulated emission of a photon pair in parametric down-conversion [3].

The consistency of the double-pair state shown in Fig. 5.3 with the experimental results reported in Chapter 4 can be checked by considering the ratio of the extra coincidences due to double pairs and the accidental coincidence rate. For the data in Fig. 5.3(b) we find a coincidence rate R_{cc}^{0ns} of 11760$\pm$50 s^{-1} for q_1 = q_2 = 10 mrad and a corresponding accidental rate R_{cc}^{12ns}=10570$\pm$50 s^{-1}. In Fig. 5.3, we plot the corrected coincidence rate $R_{cc} = R_{cc}^{0ns} - R_{cc}^{12ns}$. The visibility for this data in a non-collinear direction is $\chi \approx 0.11 \pm 0.01$ and is independent of angle. The value found here is consistent with the results of Chapter 4.

In order to see the contributions from single pairs and double pairs with a higher signal-to-noise ratio, we perform experiments where we scan the detectors only in the anti-correlated ($q_1 = -q_2$) and correlated ($q_1 = q_2$) configurations. Fig. 5.4(a) shows the measured coincidence rate along the anti-

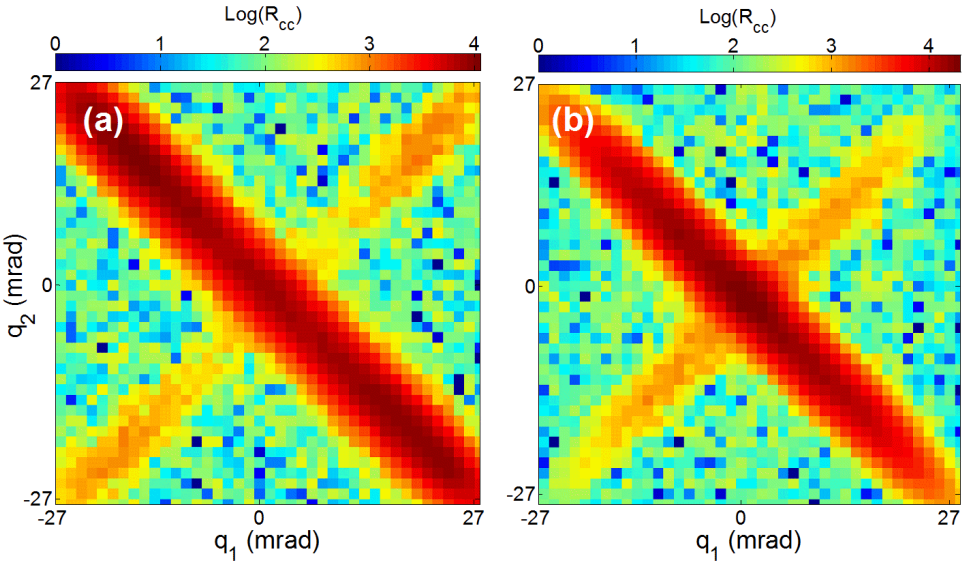

Figure 5.3: Measured (corrected) coincidence rate obtained for (a) nearly-collinear ($\varphi \approx -1.4$ rad) and (b) collinear ($\varphi \approx 0.1$ rad) down-conversion as a function of the angular position of the detectors q_1 and q_2. The coincidence rate (R_{cc}) on the diagonal ($q_1 = q_2$) and anti-diagonal ($q_1 = -q_2$) axes correspond to measurements of four-photon and two-photon events, respectively. The color scale indicates the number of corrected coincidence counts per second, plotted on a logarithmic scale.

correlated direction as a function of q_1 (bottom axis) and $q_2 = -q_1$ (top axis) for various pump powers. Starting at a pump power of 25 mW, a narrow feature in the center becomes apparent. This feature grows rapidly as the pump power is increased. This narrow peak lies at $q = 0$, and can therefore be identified with coincidences in the same spatial mode. We attribute the broad feature to single photon pairs with one photon each in two distinct spatial modes, labeled by transverse momenta q and $-q$. The center peak on the curve indicates extra coincidence counts as a result of four photons emitted into a single spatial mode. We refer to this contribution as quadruples.

The measured coincidence rate due to single pairs, for detectors in an anti-correlated ($q_1 = -q_2$) configuration, can be calculated from the phase-matching conditions in the crystal. To describe the contribution from quadruplets, we add an extra Gaussian peak in the center. The total coincidence rate

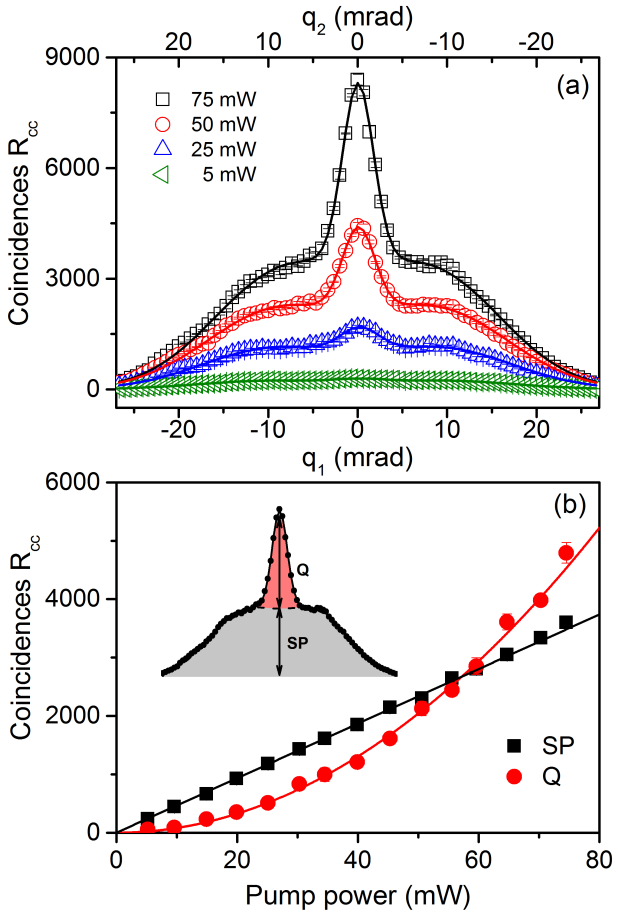

Figure 5.4: (a) Measured coincidence rates R_{cc} in the far-field for collinear pulsed SPDC ($\varphi \approx 0.1$) as a function of the detector angular positions q_1 and q_2 when the detectors are scanned in the anti-correlated configuration ($q_1 = -q_2$). We show the experimental data for different pump powers (5-75 mW) together with fits to the data (solid lines) based on Eq. 5.21. (b) Measured coincidence rates R_{cc} at $q_1 = q_2 = 0$ due to double pairs DP (red circles) and single pairs SP (black square) as a function of pump power. Solid lines correspond to linear and quadratic fits to the data. The inset shows how we separate the contribution due to single pairs (SP) from those due to quadruplets (Q) for the 75 mW data.

$R_{cc}(q)$ is then given by

$$R_{cc}(q) \propto R_Q \exp(-(\frac{q}{w_Q})^2) + C \int_\Omega d\Omega \exp(-\frac{1}{2}(\frac{\Omega}{\sigma})^2) \operatorname{sinc}^2(\frac{1}{4}Lk_p q^2 + \varphi + \frac{1}{2}D\Omega L), \tag{5.21}$$

where R_Q is the coincidence rate associated with the quadruplet state with w_Q the angular width of the $q = 0$ mode in the far field. The single-pair contribution is characterized by the integral over Ω, where Ω is the detuning of the pump frequency relative to the center frequency of the pump [13]; k_p is the wavenumber of the pump. The spectral intensity distribution of the pump is assumed to be Gaussian with a standard deviation σ. The influence of the phase-mismatch at a particular frequency Ω is given by the sinc function and is a function of the crystal length L, the collinear phase-mismatch φ and the fixed group velocity dispersion $D = 1.5$ ps/mm [13, 14]. The solid lines in Fig. 5.4(a) are fits of Eq. 5.21 to the data and allow us to separate the single pair (SP) and quadruplet (Q) contributions.

Figure 5.4(b) shows the measured coincidence count rates R_{cc} of single pairs (SP) and quadruplets (Q) as a function of pump power extracted from the data in Fig. 5.4(a). These two contributions are indicated in the inset (for the 75 mW data). The coincidence rate for single-pairs is proportional to the pump power i.e. $R_{SP} = \alpha P$. The coincidence rate due to quadruples shows a purely quadratic dependence on pump power $R_Q = \beta P^2$. The linear and quadratic fits to the data are shown by the solid lines in Fig. 5.4(b). The coefficients α and β are defined in the center of the figure, i.e. for a transverse momentum $q = 0$, to ensure that we compare parametric processes in the same optical mode that are characterized by the same single-pass gain. Parametric down-conversion of single pairs corresponds to a first order process and the count rate thus depends linearly on pump power. The quadruples increase quadratically and are thus a result of a quadratic term in the Hamiltonian that represents the creation of quantum states with four photons. The quadratic dependence on pump power confirms that this is indeed a stimulated PDC process, i.e. a stimulated process based on the second-order nonlinear susceptibility $\chi^{(2)}$ rather than a process based on $\chi^{(4)}$.

In order to obtain a more complete picture of the extra contribution from quadruplet photons, we measure the coincidences for a range of phase-mismatch values by varying the temperature of the PPKTP crystal. We set temperature values in the range $52 - 64^\circ C$ to obtain non-collinear PDC light with a phase-mismatch in the range $\varphi = -2.4$ to $\varphi = 1.2$ rad. Figure 5.5 shows the measured coincidence rate along the anti-correlated ($q_1 = -q_2$) direction. Data are shown for phase-mismatch values equal to $\varphi = 1.2$ rad (a), $\varphi = 0.1$ rad (b), $\varphi = -1.4$ rad (c) and $\varphi = -2.4$ rad (d). Note that the vertical

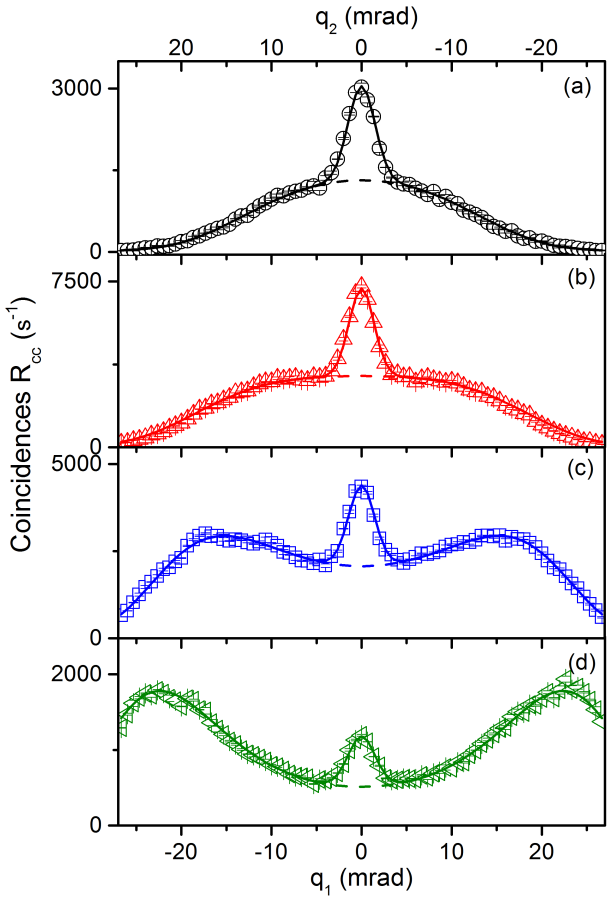

Figure 5.5: Measured coincidence rates R_{cc} as a function of the detector angular positions q_1 and q_2 when the detectors are scanned in opposite directions ($q_1 = -q_2$) (see inset of Fig. 5.2) for a phase mismatch of (a) $\varphi = 1.2$ rad (T=64^{o}C) (b) $\varphi = 0.1$ rad (T=60^{o}C) (c) $\varphi = -1.4$ rad (T=57^{o}C) (d) $\varphi = -2.4$ rad (T=52^{o}C). Solid and dashed lines represent fits to the data (see text).

scales in Fig. 5.4 are different. The maximum coincidence rates are achieved for a phase-mismatch $\phi = 0$ rad. From the figure, it is clear that the contribution from quadruples, i.e. four photons in the same mode, remains visible as a peak (in the center), despite the fact that the phase-matched single-pair contribution moves to larger angles. The solid lines through the data correspond to fits of Eq. 5.21 to the data. The dashed lines indicate the contribution from

$\varphi \approx$	1.2 rad	0.1 rad	-1.4 rad	-2.4 rad
α ($s^{-1}mW^{-1}$)	17.5 ± 0.5	46.9 ± 0.3	19.8 ± 0.2	6.8 ± 0.3
β ($s^{-1}mW^{-2}$)	0.31 ± 0.01	0.82 ± 0.01	0.29 ± 0.01	0.12 ± 0.01

Table 5.1: Parameters α and β that indicate the linear and quadratic increase in the coincidence rate due to single pairs and quadruplets as a function of pump power. The values of α and β for phase-mismatch values $\varphi \approx 0.1$ rad and $\varphi \approx -1.4$ rad are based on a fit of the measured coincidence rate at q=0 as a function of power. The values for a phase-mismatch of 1.2 rad and -2.4 rad are estimates based on experimental data taken at 75 mW only.

single pairs only, calculated by setting $R_Q = 0$ in Eq. 5.21.

The fitting parameters α and β that characterize the linear and quadratic increase of the coincidence rate R_{cc} at $q = 0$ are given in Table 5.1 for four different values of the phase-mismatch. The width of the central peak is approximately 4.5 mrad FWHM in both cases and comparable to the aperture diameter in the far field $\sim$ 4 mrad. Both α and β peak at phase-mismatch φ_0 of zero, where we expect the single-pass gain to be maximum. Both fit parameters vary by more than a factor 6 over the range of phase-mismatch values explored in the experiment. However, the dimensionless ratio $\alpha/(\beta P)$ is comparable for all values of the phase-mismatch and varies between 0.75 and 0.90 for a power of 75 mW. This can also be observed directly in Fig. 5.5 as the height of the central peak is comparable to the background at $q = 0$, independent of the phase-mismatch.

5.4.3 Quadruples vs. double pairs

The double photon pairs created via pulsed parametric down-conversion are either independent spontaneous pairs or stimulated pairs. Stimulated emission of pairs may occur for transverse momenta $q \neq 0$ creating a double-pair state, or for transverse momentum $q = 0$ creating a quadruplet state. This latter contribution gives rise to the Gaussian peak in the center of Fig. 5.3, while double-pair states at $q \neq 0$ are responsible for the signal along the diagonal ($q_1 = q_2 \neq 0$) in Fig. 5.3. The quantum correlations with the double-pair state correspond to a four-photon state $|2_q, 2_{-q}\rangle$. In this case, the four photons are distributed among two spatial modes and the correlations are similar to our earlier observations for a large negative phase-mismatch in Chapters 3-4.

Stimulated photon pairs with zero photon momenta result in a single-mode four-photon quadruplet state $|4_{q=0}\rangle$. The distinctive feature of the quadruplet state is that all four photons are emitted in the same spatial mode.

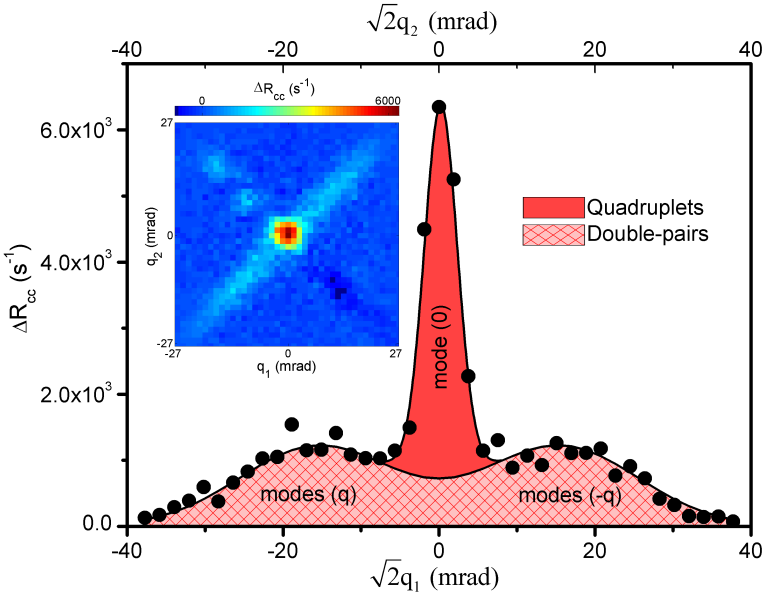

Figure 5.6: Coincidence rates for double photon pairs after subtraction of the single-pair coincidences from the data in Fig. 5.3(b). Correlated double-pairs are observed for two spatial modes (modes(q),($-q$)) away from the center. A clear Gaussian shape peak is observed in the center when photons are produced in the same spatial-mode (mode (0)). These are labeled as quadruplets. The coincidence rate is registered while the two detectors are scanned together in the correlated configuration ($q_1 = q_2$). Inset: Complete joint spatial distribution of quadruplets and double twins obtained after substraction of the coincidences of single photon pairs from Fig. 5.3(b).

To illustrate and quantify the quadruplet contribution in the images shown in Fig. 5.3, we remove the contribution from single photon pairs along the anti-diagonal using the fit procedure based on Eq. 5.21. With the single-pair contribution removed, only contributions from double-pair states along the diagonal and the quadruplet state in the center remain. In order to remove the single-pair contribution we fit the measured coincidences in Fig. 5.3(b) ($\varphi = 0.1$ rad) in the anti-correlated configuration $q_1 = -q_2$ to Eq. 5.21 setting $R_Q = 0$. We repeat this procedure for lines parallel to the line

$q_1 = -q_2$ and subtract the fit from the data. Figure 5.6 shows the result after this procedure. The main figure shows a cross section along the diagonal. A two-dimensional false color image of the data after subtraction of the single pair contribution is shown in the inset.

The data in Fig. 5.6 shows coincidences resulting from a stimulated PDC process only. Two contributions can be distinguished, those resulting from double pairs and those from quadruples, separately indicated in Fig. 5.6. The quadruples give rise to the Gaussian central feature, while the double-pairs give the broad underlying feature. The peak demonstrates that the measured coincidence rate in Fig. 5.3 is not a simple addition of two contributions due to single pairs along the anti-diagonal $(q, -q)$ and double pairs along the diagonal (q, q) due to stimulated pair emission. Because the stimulated emission process creates an exact copy of the spontaneously emitted pairs the underlying background as a function of q due to double pairs is described in the same way as single pairs, and the data in Fig. 5.6 can again be fitted by Eq. 5.21.

We emphasize that theoretical predictions of the coincidence rate that are outlined in sections 5.2, 5.3 and 5.4.1 are unable to predict the observed peak at $q = 0$ given the values of the gain parameter κt and detection efficiencies η. This conclusion remains true for an asymmetric beamsplitter and/or detectors with unequal detection efficiencies. It is possible to produce a peak if we modify Eqn. 5.10 to increase the probability to produce a click for a larger number of photons incident on the detector. This would then imply that it is more likely for photons in a state with four photons in the same mode to pass through the aperture.

In Fig. 5.6, contributions from quadruples and double pairs are visible. This raises the question whether one can design an experiment where the broad feature due to double pairs is absent. The answer is negative because, even for a collinear phase mismatch $\varphi = 0$, multiple spatial modes are involved in the PDC process [15]. The number of Schmidt modes calculated in Ref. [15] has a clear minimum but for a realistic phase-matching function ($\mathrm{sinc}(\Delta kL/2)$), the minimum number of modes is greater than one. Hence, the double-pair state and the quadruplet state are always observed simultaneously.

5.5 Conclusion

In this chapter, we have explored the experimental signature of a four-photon state where all photons are emitted in the same spatial mode. This state appears in our experiment superimposed on a signal of single pairs and four-photon state of double-pairs created into different spatial modes. By a careful analysis of the far-field structure of the coincidences associated with these different type of events, the various processes can be disentangled.

The coincidence rate observed in the experiment is described by the intensity distribution for pulsed parametric down-conversion, with an extra Gaussian peak at the center. This extra peak is due to the contribution of the four-photon state. The measured coincidences for this state show a purely quadratic dependence on pump power, while the single-pair contribution depends linearly on pump power. We stress that the accepted theoretical description of parametric down-conversion [10] is unable to explain our observation of the extra peak in the coincidences.

Bibliography

[1] D. C. Burnham and D. L. Weinberg, *Observation of simultaneity in parametric production of optical photon pairs*, Phys. Rev. Lett. **25**, 84 (1970).

[2] H. D. Riedmatten, V. Scarani, I. Marcikic, A. Acn, W. Tittel, H. Zbinden, and N. Gisin, *Two independent photon pairs versus four-photon entangled states in parametric down conversion*, J. Mod. Opt. **51**, 1637 (2004).

[3] A. J. H. van der Torren, S. C. Yorulmaz, J. J. Renema, M. P. van Exter, and M. J. A. de Dood, *Spatially entangled four-photon states from a periodically poled potassium-titanyl-phosphate crystal*, Phys. Rev. A **85**, 043837 (2012).

[4] C. K. Hong, Z. Y. Ou, and L. Mandel, *Measurement of subpicosecond time intervals between two photons by interference*, Phys. Rev. Lett. **59**, 2044 (1987).

[5] P. G. Kwiat, A. M. Steinberg, and R. Y. Chiao, *Observation of a 'quantum eraser': A revival of coherence in a two-photon interference experiment*, Phys. Rev. A **45**, 7729 (1992).

[6] I. Marcikic, H. de Riedmatten, W. Tittel, V. Scarani, H. Zbinden, and N. Gisin, *Time-bin entangled qubits for quantum communication created by femtosecond pulses*, Phys. Rev. A **66**, 062308 (2002).

[7] H. S. Eisenberg, G. Khoury, G. A. Durkin, C. Simon, and D. Bouwmeester, *Quan-*

tum entanglement of a large number of photons, Phys. Rev. Lett. **93**, 19 (2004).

[8] A. Lamas-Linares, J. C. Howell, and D. Bouwmeester, *Stimulated emission of polarization-entangled photons*, Nature **412**, 887 (2001).

[9] A. Lamas-Linares, C. Simon, and D. B. J.C. Howell, *Experimental quantum cloning of single photons*, Science **296**, 712 (2002).

[10] S. M. Barnett and P. M. Radmore, *Methods in theoretical quantum optics*, Oxford University Press, Oxford, 1997.

[11] M. J. Collett, *Exact density-matrix calculations for simple open systems*, Phys. Rev. A **38**, 2233 (1988).

[12] D. F. Walls and G. J. Milburn, *Quantum optics*, Springer-Verlag, Berlin, 1994.

[13] T. E. Keller and M. H. Rubin, *Theory of two-photon entanglement for spontaneous parametric down-conversion driven by a narrow pump pulse*, Phys. Rev. A **56**, 1534 (1997).

[14] S. C. Yorulmaz and M. J. A. de Dood, *Characterization of pulsed parametric down-conversion in PPKTP crystals*, Proc. SPIE **8440**, 84400G (2012).

[15] C. K. Law and J. H. Eberly, *Analysis and interpretation of high transverse entanglement in optical parametric down conversion*, Phys. Rev. Lett. **92**, 127903 (2004).

Summary

In classical optics, light is described as a wave phenomenon and the famous Young's double slit experiment is often quoted as landmark demonstration of the wave nature of light. A fully quantum-mechanical description of light should involve both the wave nature of light as well as the notion of quantized light particles. Both these effects are captured by the introduction of photons as quanta of light. Among others, the field of quantum optics investigates the number distributions of and correlations between photons. These two concepts are important in the context of stimulated emission of photon pairs studied in this thesis.

In particular, we investigate the number distribution of, and the correlations between photons that are created by the nonlinear process of parametric down-conversion. At low intensities of the pump laser, this nonlinear process produces single pairs via a spontaneous process. Once the pump intensity is increased the probability to emit more than one pair at a time increases i.e. a stimulated parametric down-conversion process gains importance, affecting the number distribution of the photon pairs. In experiments on stimulated down-conversion, both the number of optical modes available to the pair generation process and the number of modes collected in the detection process are important. The number of available modes in the down-conversion process is controlled via the size of the pump beam and can be minimized by a careful choice of the combination of crystal length and pump beam size. The number of modes in the detection process can be reduced by using a small aperture in the optics used to collect the pairs, at the expense of a strong reduction in count rate. The experiments in this thesis that aim to observe and explore stimulated pair emission are thus carefully designed to keep the number of modes involved in the generation and the detection process small.

Spontaneous and stimulated parametric down-conversion

Spontaneous parametric down-conversion (SPDC) occurs in a non-linear medium (crystal) where the interaction with light induces spontaneous splitting of a pump photon into, two highly correlated twin photons. These photons are created into optical modes that can be labeled by transverse momenta $\overrightarrow{q}$ and $-\overrightarrow{q}$ as shown in Fig.1. The physical properties of these photons are correlated via energy and momentum conservation dictated by the phase-matching conditions of the nonlinear mixing process.

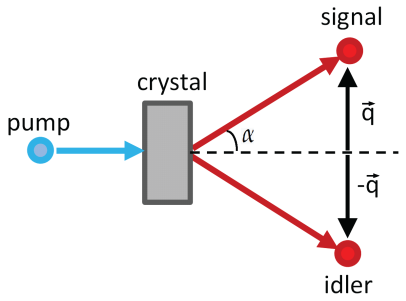

Figure 1: Schematic drawing of the SPDC process, where a blue pump photon is split by the nonlinear crystal into two identical (frequency degenerate) signal and idler photons. $\overrightarrow{q}$ and $-\overrightarrow{q}$ indicate the transverse momenta of the two photons emitted by the crystal. Note that the drawing is not to scale; the opening angle α is typically a few degrees only.

If the nonlinear medium is pumped by a single-frequency continuous-wave laser, photon pairs are created spontaneously and all pairs are mutually independent. This independence arises because the coherence time of the down-converted photons ($\ll$ 1 ps) is much shorter than the coherence time of the laser ($\gtrsim$ 0.1 μs). To achieve correlations between pairs, i.e., to lift the independence, one should make these coherence times comparable. This is rather simply achieved by using a pulsed laser as a source (coherence time 1 ps). Moreover, since the peak power of the pulsed laser is typically many orders of magnitude larger than that of a cw laser, the probability of stimulated events is also increased by a large amount. **Chapter 2** characterizes a pulsed parametric down-conversion (PDC) setup based on periodically-poled KTP crystals.

Measuring the contribution from stimulated emission

Observing stimulated emission of pairs requires a careful design of the experiment so that the number of relevant optical modes is limited. Two aspects play a role here: first, the number of modes that the pairs from the source are emitted into, and second the number of modes that are involved in the detection process. The first aspect is addressed by a proper choice of beam waist and crystal length to limit the number of spatial modes in the generation process to values between $\sim$1 and 10.

To understand the role of the number of modes involved in the detection process it is important to note that we use only two single photon detectors to detect the stimulated events. In a non-collinear down-conversion geometry these detectors are used to detect two photons emitted in the same direction (the other two auxiliary photons will give rise to similar correlations and are not detected). Because the detectors cannot distinguish between a single and a double photon we insert a beam-splitter in the optical path. A coincidence event where both detectors click simultaneously then signifies an event with two pairs that can either be in the same mode (and thus belong to a stimulated pair), or they can be in different modes (and thus belong to two simultaneously emitted independent photons emitted through the spontaneous process). This latter process is of minor interest to us and its contribution should be kept small. This can be achieved by using an aperture in front of the detectors to favor a particular spatial mode and the relative importance of stimulated pairs while reducing the absolute count rate on the detector. **Chapter 3** introduces mode selection by spatial and spectral filtering as well as an experimental technique to distinguish stimulated photon pairs from the independent spontaneous pairs. The detectors measure a contribution due to photons emitted into the same spatial mode. Subtracting the measured count rates into different modes yields the amount of four-photon correlations.

Figure 2 illustrates the down-conversion process that creates four-photon states and the coincidence measurement done by using a beam splitter and two detectors. A time delay applied to one of the two detectors provides a means to compare coincidence count rates for photons emitted in the same laser pulse to the coincidence count rate for photons emitted independently (spontaneously) by two distinct laser pulses. This technique is used through-

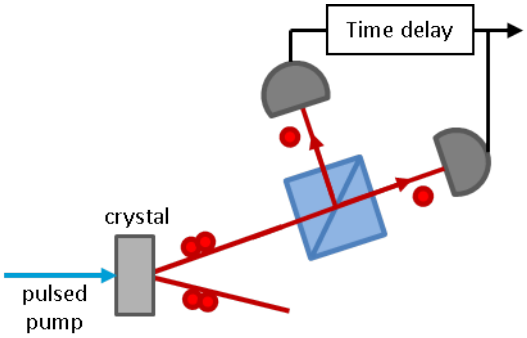

Figure 2: Scheme for coincidence measurements in a non-collinear stimulated down-conversion process, where two signal-idler photon pairs are created in the same pulse. An adjustable time-delay enables to distinguish coincidences in the same pulse and coincidences between subsequent pulses.

out this thesis to distinguish stimulated emission of four photons from the spontaneous emission of double photon pairs.

Visibility of four-photon events

The ratio of stimulated and spontaneous coincidence counts defines the visibility of four-photon events where all photons are in the same quantum state. This ratio is a direct measure of the number of optical modes relevant to the down-conversion process. **Chapter 4** presents the characterization of this visibility parameter in experiments using different focussing conditions, crystal lengths and spatial-temporal filtering. A universal expression for the visibility of the four-photon state is introduced that quantifies the influence of the size of the pump beam used in the creation of the stimulated PDC light.

Chapter 5 focuses on a *collinear* parametric down conversion, which is illustrated in Fig.3. In a collinear geometry, all four photons are emitted into the same optical mode, which changes the nature of the stimulated down-conversion process. In this case, all photons become indistinguishable and a special quantum state is created. The measurements in this chapter comprise a first experimental study that reveals a remarkable peak of excess coincidences in the collinear direction. This peak is due to four-photon stimulated emission, but is not predicted by the standard theory of squeezed states. We exclude asymmetries in the beam splitter and/or detectors as an explanation

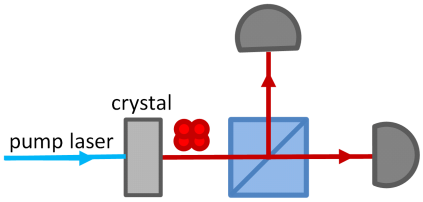

Figure 3: Schematic drawing of the collinear stimulated down-conversion process. Indistinguishable four photons are created into the same optical mode.

for this effect. The effect can be explained if we assume that the transmission of photons through an aperture is enhanced by the number of photons in the state.

Samenvatting

In de klassieke optica wordt licht beschreven als een golfverschijnsel, en het beroemde dubbelspleet-experiment van Young wordt vaak gezien als een mijlpaal in het aantonen van het golfkarakter van licht. Een volledig quantummechanische beschrijving van licht moet zowel dit golfkarakter omvatten alsook de notie van gequantiseerde lichtdeeltjes. Het vakgebied quantumoptica omvat onder andere het onderzoek naar de kansverdeling van de aantallen fotonen (de aantalverdeling) en correlaties tussen fotonen. Deze twee concepten zijn belangrijk voor het onderzoek naar gestimuleerde emissie van fotonparen dat beschreven wordt in dit proefschrift.

Meer in het bijzonder onderzoeken we de aantalverdeling en correlaties van fotonen die gecreëerd worden door het niet-lineaire proces van parametrische down-conversie opstelling. Bij lage intensiteit van de pomplaser produceert dit proces individuele paren via een spontaan proces. Als de pompintensiteit verhoogd wordt neemt de kans op emissie van meer dan één paar tegelijk toe. Het gestimuleerde proces wordt daarmee belangrijker, wat de aantalverdeling van fotonen beïnvloedt. In onderzoek naar gestimuleerde down-conversie zijn zowel het aantal toestanden (modes) dat beschikbaar is voor de fotonen als het aantal toestanden dat beschikbaar is in de detectie belangrijk. Het aantal beschikbare modes in het down-conversieproces kan worden gecontroleerd door de grootte van de pumpbundel te variëren, en kan geminimaliseerd worden door een nauwkeurige keuze van de lengte van het kristal en de afmeting van de pomp. Het aantal toestanden in het detectieproces kan worden beperkt door kleine diafragma's te plaatsten voor de detectoren waarmee de paren worden gedetecteerd. De prijs die hiervoor wordt bepaald is een sterke vermindering in de telsnelheid. De experimenten in dit proefschrift, die gericht zijn op het waarnemen van gestimuleerde down-conversie, zijn daarom zorgvuldig ontworpen om het aantal toestan-

den in het conversie en detectie proces precies klein genoeg te maken zodat het effect kan worden waargenomen zonder daarbij de telsnelheid onnodig laag te maken.

Spontane en gestimuleerde down-conversie

Spontane parametrische down-conversie (spontaneous parametric down-conversion (SPDC)), vindt plaats in een niet-lineair krisral. De wisselwerking van intens licht met een dergelijk kristal kan ervoor zorgen dat één van de pompfotonen uiteenvalt in twee sterk gecorreleerde tweelingfotonen. Deze fotonen worden gecreëerd in optische toestanden die kunnen worden aangeduid door gebruik te maken van de loodrechte impuls-component $\overrightarrow{q}$ en $-\overrightarrow{q}$, zoals aangegeven in figuur 1. De fysische eigenschappen van deze fotonen zijn gecorreleerd via zowel behoud van energie als impuls. Dit laatste wordt bewerkstelligd door de conditie dat alle bijdragen uit het niet-lineare process in fase zijn zodat er constructieve interferentie optreedt (phase-matching).

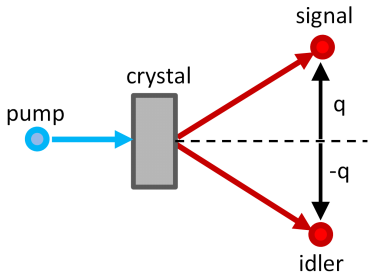

Figuur 1: Schematische weergave van het SPDC-proces, waarbij een blauw pompfoton wordt opgesplitst door het niet-lineaire kristal in paren van fotonen. $\overrightarrow{q}$ en $-\overrightarrow{q}$ geven de transversale component van de impuls aan voor beide fotonen. De tekening is niet op schaal; in het werkelijke experiment is de openingshoek slechts enkele graden.

Als het niet-lineaire proces aangedreven wordt door een continue laser worden alle fotonparen spontaan gegenereerd en zijn zij allemaal onderling onafhankelijk. Deze onafhankelijkheid onstaat omdat de coherentietijd van de down-conversiefotonen ($\ll 1$ ps) veel kleiner is dan de coherentietijd van de laser ($\gtrsim 0.1$ μs). Om correlaties tussen de paren te bereiken - dat wil zeggen: om hun onafhankelijkheid op te heffen - moeten deze twee tijden vergelijkbaar gemaakt worden. Dit is relatief eenvoudig te bereiken door een ge-

pulste laser als bron te gebruiken, met een coherentietijd van ongeveer 1 ps. Bovendien is het piekvermogen van zo'n laser typisch ordes van grootte hoger dan dat van een continue laser. Hierdoor wordt de kans op gestimuleerde emissie sterk verhoogd. In hoofdstuk 2 wordt een gepulste parameterische down-conversieopstelling gebaseerd op een periodiek gepoold KTP-kristal gekarakteriseerd.

De bijdrage van gestimuleerde emissie

Om de gestimuleerde emissie waar te nemen is een zorgvuldig ontwerp van het experiment nodig om ervoor te zorgen dat het totaal aantal beschikbare toestanden beperkt is. Twee aspecten spelen hierbij een rol: enerzijds is er het aantal toestanden waarin de paren door de bron uitgezonden kunnen worden, anderzijds is er het aantal toestanden dat bij het detectieproces betrokken is. De eerste kwestie wordt opgelost door de juiste keuze van bundeldiameter en kristallengte, waardoor het aantal ruimtelijke toestanden in het emissie proces beperkt wordt tussen de $\sim$1 en 10.

Om de rol van het aantal toestanden in de detectie te begrijpen is het cruciaal dat we ons realiseren dat wij slechts twee één fotondetectoren gebruiken om de gestimuleerde paren te detecteren. In een niet-colineaire down-conversie geometrie worden deze detectoren gebruikt om twee fotonen te detecteren die in dezelfde richting uitgezonden worden. De twee bijbehorende fotonen die de andere kant op gaan worden niet gedetecteerd. Omdat de detectoren geen onderscheid kunnen maken tussen enkele en dubbele fotonen plaatsen we een bundelsplitser in het optisch pad. Als beide detectoren tegelijk afgaan dan wordt deze gebeurtenis geregistreerd en spreken we van een coincidentie. Door deze gelijktijdige gebeurtenissen waar te nemen kunnen we afleiden dat de beide fotonen hetzij in dezelfde toestand zaten, en daarom bij een gestimuleerd paar behoren, hetzij in een verschillende toestand zaten, en daarom bij twee onafhankelijk geproduceerde spontane paren behoren. Dit laatste proces is voor dit onderzoek weinig relevant en de bijdrage ervan aan de totale telsnelheden moet bij voorkeur laag gehouden worden. Dit kan bereikt worden door een diafragma voor de detectoren te plaatsen, waarmee een bepaalde ruimtelijke toestand voorgetrokken kan worden. Hierdoor wordt zowel de absolute telsnelhied als de fractie van detectiegebeurtenissen die behoren bij onafhankelijke paren verlaagd. **Hoofdstuk 3** introduceert

deze toestandsselectie door ruimtelijke en spectrale filtering alsook een experimentele techniek om gestimuleerde en spontane emissie van paren in het experiment van elkaar te onderscheiden. De detectoren meten een bijdrage die veroorzaakt wordt door fotonen in dezelfde toestand. Door de gemeten telsnelheid van fotonen in verschillende toestanden hiervanaf te trekken kan de totale bijdrage van vierfotonprocessen vastgesteld worden.

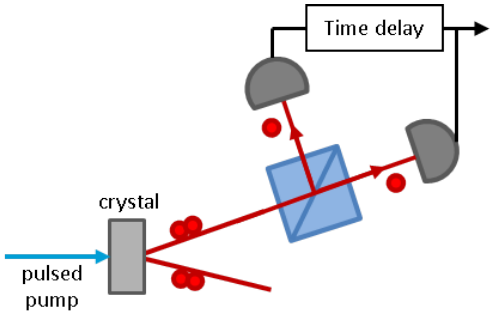

Figuur 2: Schematische weergave van coincidentie metingen van fotonen in een niet-colineair down-conversieproces, waarbij twee fotonparen in dezelfde puls gegenereerd worden. Een instelbare tijdsvertraging stelt ons in staat om gebeurtenissen in dezelfde puls te vergelijken met gebeurtenissen tussen twee opéénvolgende pulsen.

Figuur 2 geeft het down-conversieproces weer dat vierfotontoestanden genereert. Het laat zien hoe de coincidentie metingen gedaan worden door middel van een bundelsplitser en twee detectoren. In een van beide detectoren wordt een tijdsvertraging aangebracht om de telsnelheid van coincidenties voor gestimuleerde fotonparen in dezelfde laserpuls te vergelijken met de telsnelheid van coincidenties voor onafhankelijke paren in afzonderlijke pulsen. Deze techniek wordt in het hele proefschrift gebruikt om gestimuleerde vierfotontoestanden te onderscheiden van spontaan gegenereerde dubbele paren.

Zichbaarheid van de vierfotonbijdrage

De verhouding tussen de bijdrage door gestimuleerde en spontane gebeurtenissen definieert de zichbaarheid van de vierfotonbijdrage en is een directe meting van het aantal optische toestanden dat meedoet in het downconversieproces. **Hoofdstuk 4** bevat de karakterisatie van deze zichtbaarheidsparameter in experimenten waarbij verschillende focuscondities, kristallengtes

en ruimtelijk-temporele filters gebruikt worden. Een universele uitdrukking voor de zichtbaarheid van de vierfotontoestand wordt geïntroduceerd. Deze uitdrukking kwantificeert de invloed van de afmeting van de pompbundel die gebruikt wordt om het SPDC-licht te maken, ten opzichte van de grootte van het diafragma dat gebruikt wordt om de fotonen te detecteren.

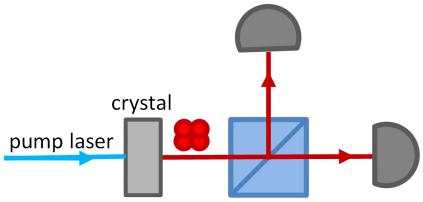

Figuur 3: Schematische weergave van het colineaire down-conversieproces. Ononderscheidbare fotonen worden gecreëerd in dezelfde optische toestand.

Hoofdstuk 5 richt zich op een colinear parametrisch down-conversieproces, dat geïllusteerd wordt in figuur 3. In een colineare geometrie worden alle fotonen in dezelfde optische toestand uitgezonden, waardoor de eigenschappen van het gestimuleerde proces veranderen. In dit geval worden alle fotonen ononderscheidbaar en wordt er een speciale quantumtoestand gecreëerd. De metingen in dit hoofdstuk vormen een eerste experimentele studie die laat zien dat er in de colineare richting onverwachte, extra, coincidenties worden waargenomen. Deze piek ontstaat door gestimuleerde emissie van vier fotonen, maar wordt niet voorspeld door de standaard theorie van gedrongen toestanden (squeezed states). Op basis van berekening sluiten we uit dat asymetrie in de bundelsplitser en detectoren een dergelijk groot effect kan verklaren. Het effect kan wel verklaard worden als we aannemen dat de transmissie van fotonen door een diafragma vergroot wordt naarmate er grotere aantallen fotonen in dezelfde toestand zitten.

Curriculum Vitae

Saime Çiğdem Yorulmaz

9 March 1983	Born in Denizli, Turkey
1997-2001	Secondary Education , Mehmet Akif Ersoy Lisesi, Denizli, Turkey
2001-2007	B.Sc. Physics, Bilkent University, Ankara, Turkey
2005	Research internship at Princeton University, New Jersey, USA
2007-2009	M.Sc. Physics, Koç University, Istanbul, Turkey
	Thesis: *Controlled deformation and Raman lasing in microdroplets standing on a superhydrophobic surface*
	Supervisor: Dr. A. Kiraz
2009-2013	Ph.D. research at Leiden University, the Netherlands
	Thesis: *Beyond photon pairs*
	Supervisors: Dr. M. J. A. de Dood and Prof. dr. E. R. Eliel
	Teaching assistant in Physics Research Laboratory course

List of publications

- **S. C. Yorulmaz**, M. P. van Exter and M. J. A. de Dood, *Photon pairs, double pairs, and quadruples in pulsed parametric down-conversion*, in preparation. (Chapter 5 of this thesis)

- **S. C. Yorulmaz**, M. P. van Exter and M. J. A. de Dood, *The role of spatial and temporal modes in pulsed parametric down-conversion*, Optics Express **22**, 5913-5926 (2014). (Chapter 4 of this thesis)

- A. J. H. van der Torren, **S. C. Yorulmaz**, J. J. Renema, M. P. van Exter, and M. J. A. de Dood, *Spatially entangled four-photon states from a periodically-poled potassium-titanyl-phosphate crystal*, Phys. Rev. A **85**, 043837 (2012). (Chapter 3 of this thesis)

- **S. C. Yorulmaz**, M. J. A. de Dood, *Characterization of parametric down-conversion in periodically-poled KTP crystals with a picosecond pump*, Proc. of SPIE 8440, 84400G, (2012). (Chapter 2 of this thesis)

- **S. C. Yorulmaz**, M. Mestre, M. Muradoglu, B. E. Alaca, and A. Kiraz, *Controlled observation of nondegenerate cavity modes in a microdroplet on a superhydrophobic surface*, Opt. Commun. **282**, 3024-3027 (2009).

- A. Kiraz, **S. C. Yorulmaz**, M. Yorulmaz, and A. Sennaroglu, *Raman lasing near 650 nm from pure water microdroplets on a superhydrophobic surface*, Photon. Nanostruct.: Fundam. Appl. **7**, 186-189 (2009).

- M. Mestre, Y. Karadag, **S. C. Yorulmaz**, M. Gundogan, and A. Kiraz, *Photothermal tuning and size locking of salt-water microdroplets on a superhydrophobic surface*, Int. J. Optomechatronics **3** (4), 303-318 (2009).

- A. Kiraz, Y. Karadag, **S. C. Yorulmaz**, and M. Muradoglu, *Reversible photothermal tuning of a salty water microdroplet*, Phys. Chem. Chem. Phys. **11**, 2597-2600 (2009).
- A. Kiraz, **S. C. Yavuz**, Y. Karadag, A. Kurt, A. Sennaroglu, and H. Cankaya, *Large spectral tuning of liquid microdroplets standing on a superhydrophobic surface using optical scattering force*, Appl. Phys. Lett. **91**, 231102 (2007).
- A. Kiraz, Y. Karadag, **S. C. Yorulmaz**, and M. Muradoglu, *Large spectral tuning of liquid microdroplets by local heating with a focused infrared laser*, Proc. of SPIE 7038, 70381I (2008).

Acknowledgement

First and foremost I would like to express my gratitude to my co-promotor Dr. Michiel de Dood, for his patient guidance, enthusiastic encouragement and especially strong support during my PhD. I would like to thank my promotor Prof. Eric Eliel for the helpful critics and for the guidance to stay on track. I wish to thank Dr. Martin van Exter for many enlightening discussions and suggestions to improve this thesis.

I would also like to extend my thanks to Prof. Gerard Nienhuis and Dr. Wolfgang Löffler for scientific discussions. I wish to thank Alexander van der Torren and Karlien Sambell for assistance with the experiment. I am thankful to Fred Schenkel from the Fine Mechanics Department, Arno van Amersfoort and Ren Overgauw from the Electronics Department for their technical support. I would also like to acknowledge all the members of Quantum Optics group; it has been a great pleasure to work with them. My special thanks are extended to Flavio and Jelmer for being my Paranimfen. I am also thankful to Jelmer for the Dutch translation of the thesis summary. I am grateful for the financial support by the foundation for Fundamental Research on Matter (FOM). I would like to thank Annette Bor, Maria Teuwissen, Joost Weber and Henriette van Leeuwen for all the administrative assistance during my PhD period.

I wish to express my sincere appreciation to my parents, parents in law and my family members for their kind support and enthusiasm. Above all, I owe my deepest gratitude to Mustafa and my little princess Elif for their unconditional love.